CHAPTEER III
RESULTS AND DISCUSSION

3.1 Flow Curves

Flow curve is the plot of the wall shear stress, τ_w, versus the apparent strain rate, $\dot{\gamma}_a$, obtained by the capillary rheometer. Figures 3.1-3.6 show flow curves of three grades of LLDPE (L2020F, L2009F and M3204RU) melts and three grades of HDPE (H5690S, H5604F and H6205JU) melts. The flow curves were obtained from a capillary length of 25.10 mm, a diameter of 0.75 mm and l_c/d_c=33.36. In each flow curve, we divided the flow curve into several regimes; each regime is identified by either an extrudate skin texture or an oscillation in load required to extrudate the melt through the capillary.

For LLDPE (L2009F) shown in Figure 3.1, there are 4 regimes identifiable. Regime I corresponds to an extrudate with a smooth skin, it ends at the apparent strain rate of 265 (1/s) and the critical wall shear stress of $2.38*10^6$ dyn/cm^2. Regime II can be seperated from the regime I by the appearance of a sharkskin surface, which has some order and regularity with short wavelength surface distortion. It terminates at the apparent strain rate of 667 (1/s) and the critical wall shear stress of $3.47*10^6$ dyn/cm^2. Regime III is called an oscillating regime because the load required to push the barrel piston at a constant speed fluctuates. Here, the stress becomes double valued, and the extrudate alternates in periodic fashion between a sharkskin and a smooth surface section. The polymer chains are disentangled periodically from each other and the slip occurs at the polymer/metal interface, resulting in two

unstable velocity profiles at the same apparent strain rate. Regime III terminates at the apparent strain rate of 1620 (1/s) and the critical wall shear stress of $4.45*10^6$ dyn/cm^2. Regime IV covers the portion of the flow curve when a melt fracture, which has a random surface roughness , occurs.

For other materials, we have identified regimes according to the skin textures as shown in Figures 3.2-3.10. The regimes identified with skin textures and the critical wall shear stress ($\tau_{w,c}$) and the strain rate ($\dot{\gamma}_a$) of all materials are summarized in Table 3.2.1, Table 3.2.2 and Table 3.2.3 respectively.

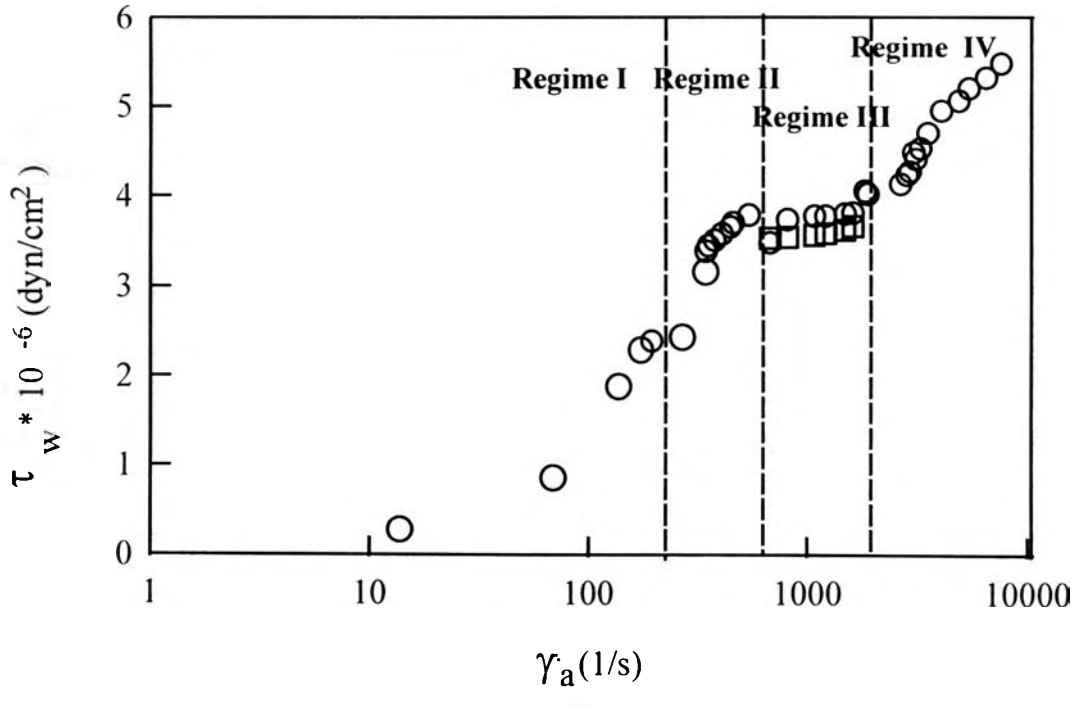

Figure 3.1 The wall shear stress, τ_w, as a function of the apparent strain rate, $\dot{\gamma}_a$, for LLDPE (L2009F) at temperature of 190 ^oC.

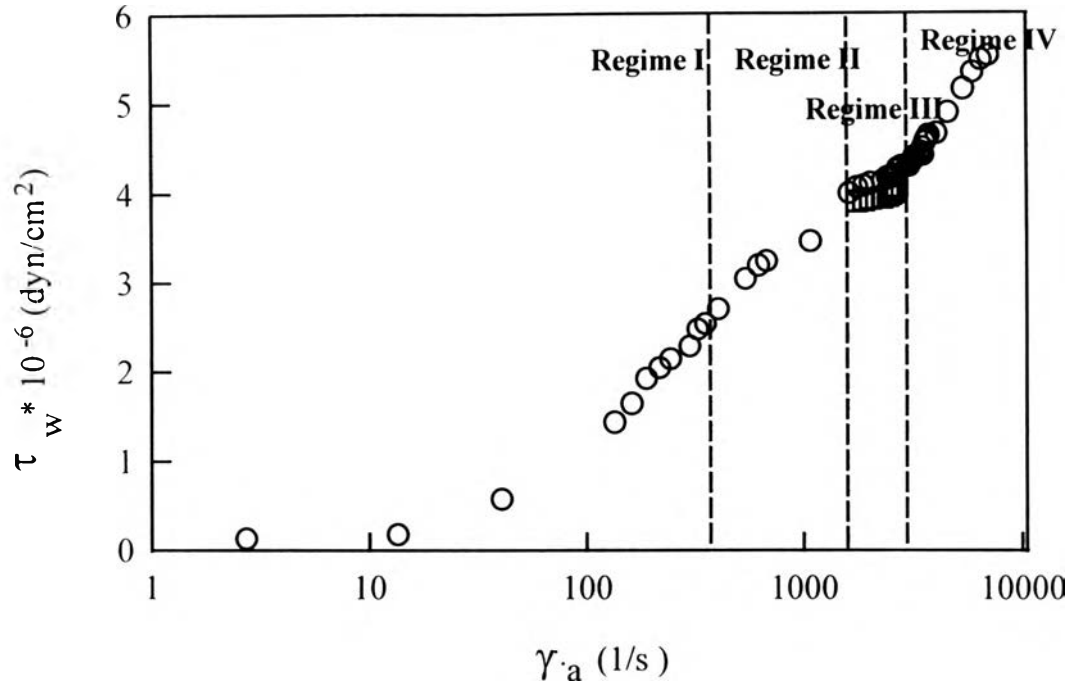

Figure 3.2 The wall shear stress, τ_w, as a function of the apparent strain rate, $\gamma_{\cdot a}$, for LLDPE (L2020F) at temperature of 190 ^oC.

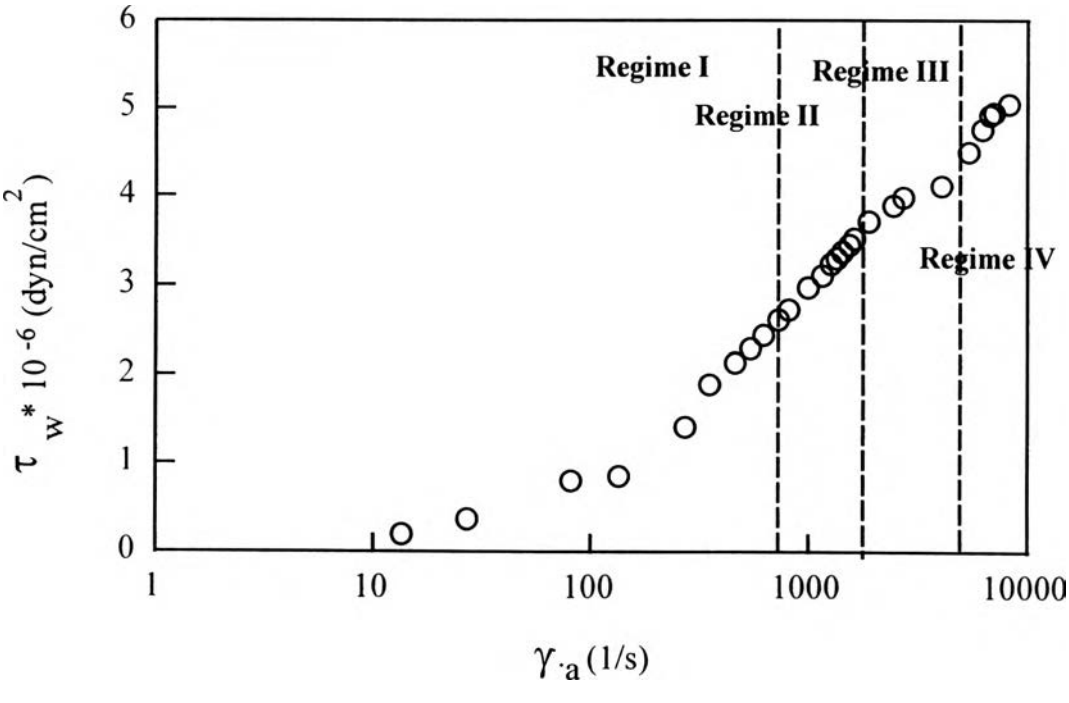

Figure 3.3 The wall shear stress, τ_w, as a function of the apparent strain rate, $\gamma_{\cdot a}$, for MDPE (M3204RU) at temperature of 190 ^oC.

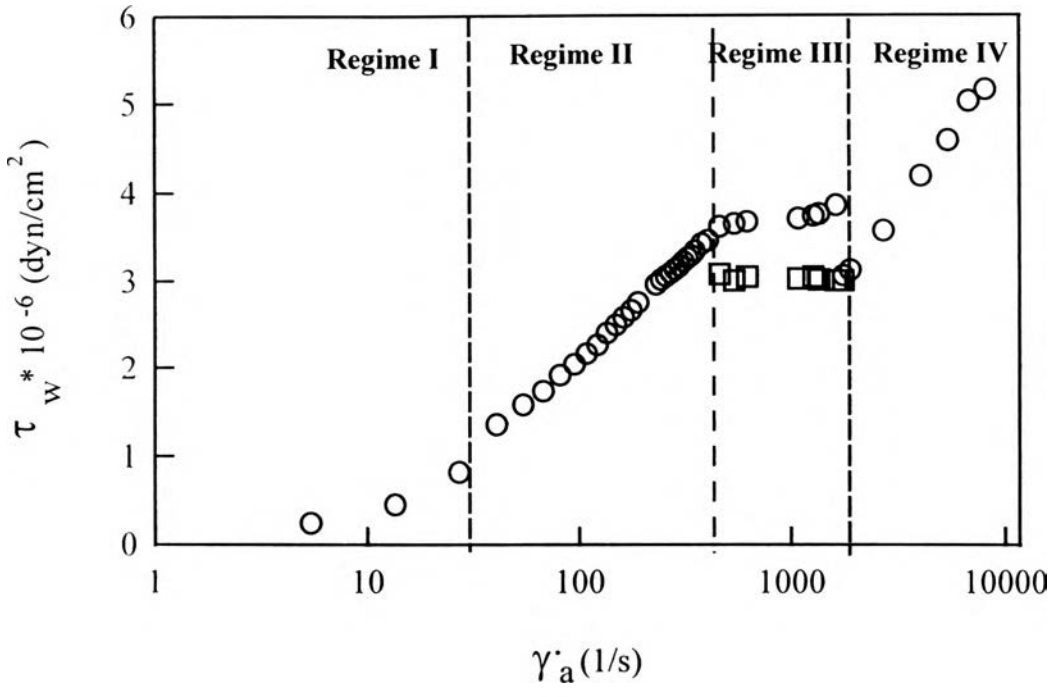

Figure 3.4 The wall shear stress, τ_W, as a function of the apparent strain rate, γ_a, for HDPE (H5690S) at temperature of 190 ^oC.

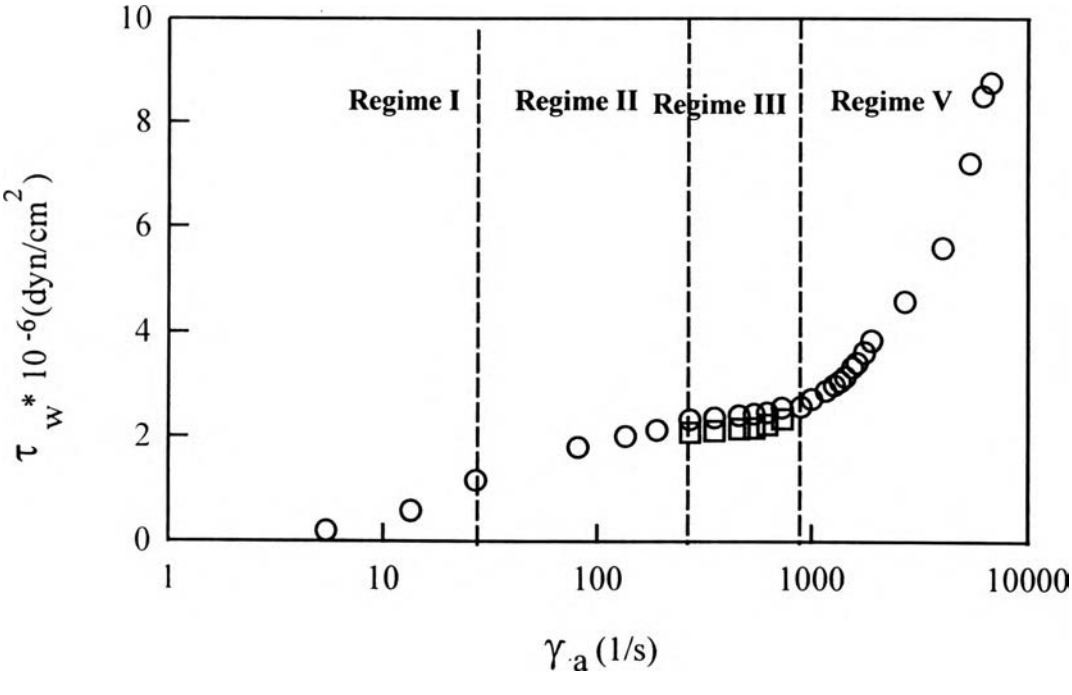

Figure 3.5 The wall shear stress, τ_W, as a function of the apparent strain rate, γ_a, for HDPE (H5604F) at temperature of 190 ^oC.

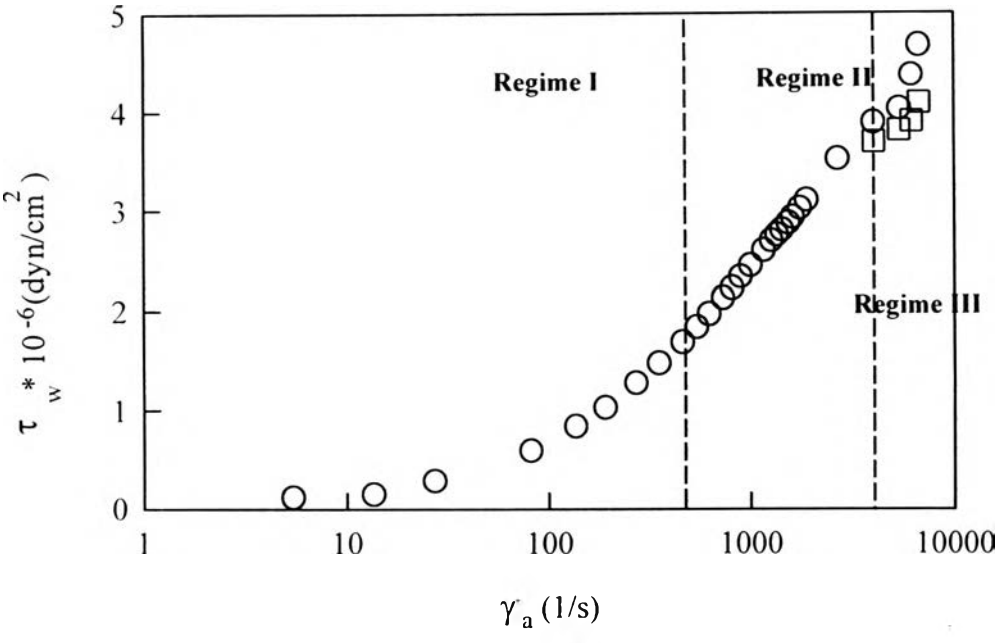

Figure 3.6 The wall shear stress, τ_W, as a function of the apparent strain rate, γ_a, for HDPE (H6205JU) at temperature of 190 ^oC.

3.2 Surface Textures

Now we shall attempt to describe each skin texture.

LLDPE (L2009F)

Figures 3.7-3.10 show photographic pictures of the capillary melt extrudates from the 4 regimes identified. The melt extrudate of regime I in Figure 3.7 has a surface which appears to be smooth. We noted that the melt flow was laminar and the melt viscosity was independent of strain rate and therefore no instability took place. A sharkskin texture appears in regime II as shown in Figure 3.8. Here we identified the sharkskin by its regular and high-frequency surface variations. The amplitude and the wavelength are small compared to the extrudate diameter or the capillary diameter. Figure 3.9 shows a mixture of a sharkskin segment and a smooth segment occurring in regime III.

The descriptions of the smooth and the sharkskin segments are similar to those given in the regime I and regime II respectively. Figure 3.10 shows the melt fracture extrudate of regime IV. The skin has an irregular or random roughness whose amplitude is comparable to the extrudate diameter.

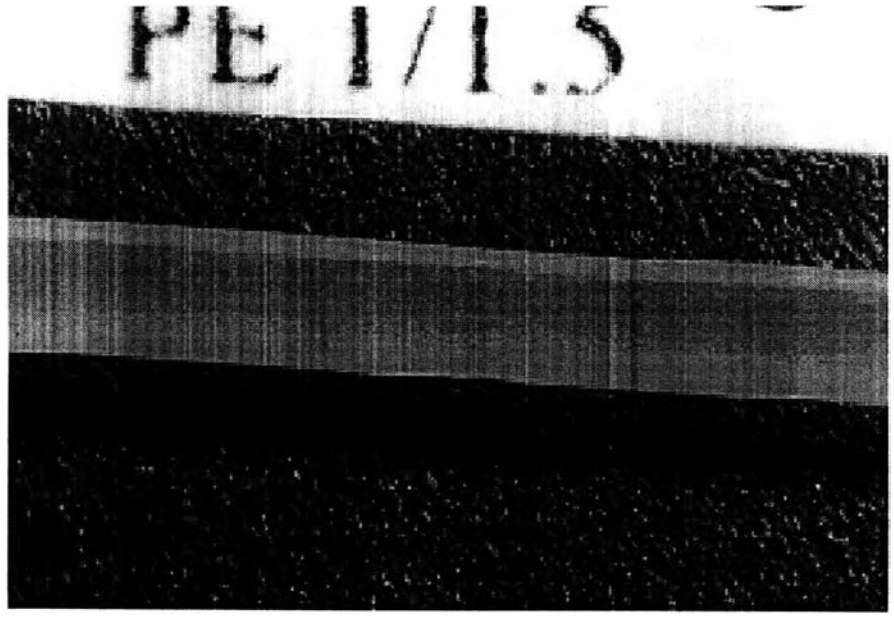

Figure 3.7 Stereomicroscope photography of the smooth extrudate of LLDPE (L2009F) at temperature of 190 ^{o}C.

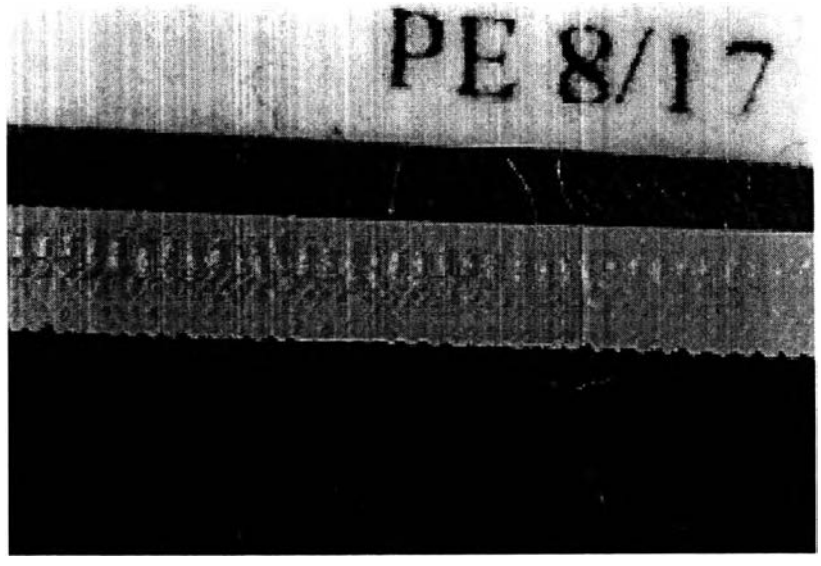

Figure 3.8 Stereomicroscope photography of the sharkskin extrudate of LLDPE (L2009F) at temperature of 190 ^{o}C.

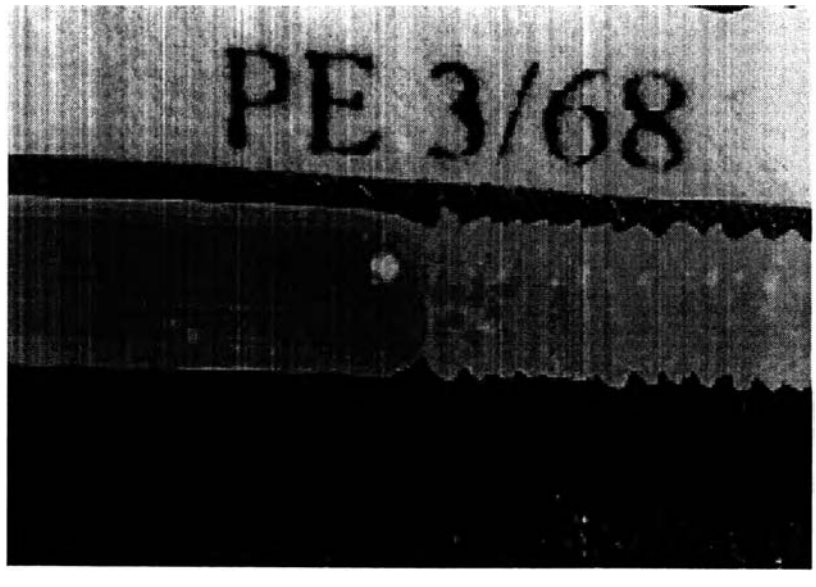

Figure 3.9 Stereomicroscope photography of the alternating surfaces between smooth and sharkskin of LLDPE (L2009F) at temperature of 190 ^{o}C.

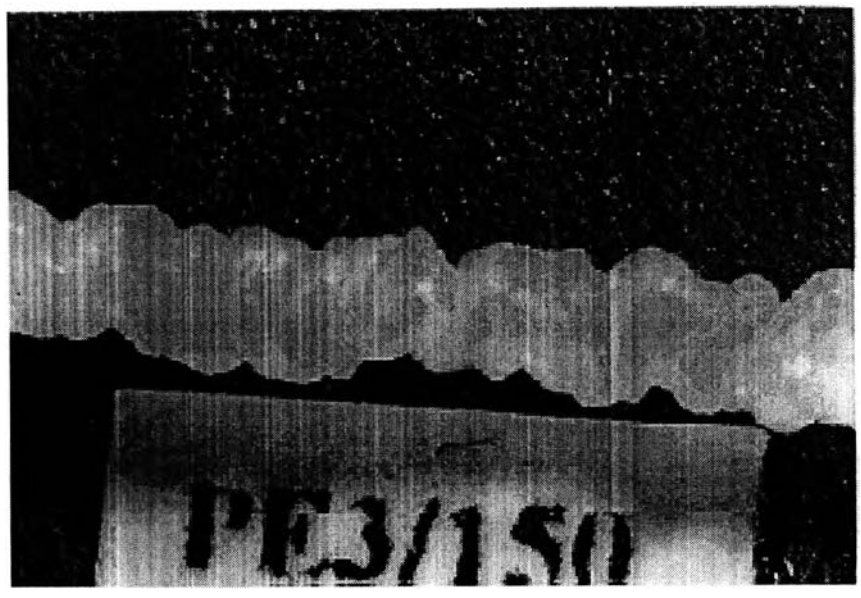

Figure 3.10 Stereomicroscope photography of the melt fracture of LLDPE (L2009F) at temperature of 190 ^{o}C.

Table 3.2.1 Surface textures in each regime for all materials studied

Materials	Regime I	Regime II	Regime III	Regime IV
L2009F	Smooth	Sharkskin	Oscillating	Melt fracture
L2020F	Smooth	Sharkskin	Oscillating	Melt fracture
M3204RU	Smooth	Sharkskin	Peeled orange	Melt fracture
H5690S	Smooth	Sharkskin	Oscillating	Melt fracture
H5604F	Smooth	Matteness	Oscillating	Melt fracture
H6205JU	Smooth	Matteness	Oscillating	-

Table 3.2.2 The critical wall shear stress ($\tau_{w,c}$) and the strain rate ($\dot{\gamma}_a$) for LLDPE (L2009F and M3204RU) and HDPE (H5690S and H6205JU) at temperature of 190°C

Regime	Critical Data	L2009F	M3204RU	H5604F	H6205JU
II Sharkskin	γ_a (1/s)	265	730	27	622
	$\tau_{w,c}$ (dyn/cm^2)	2.38E+06	2.83E+06	1.16E+06	2.97E+06
III Oscillating	γ_a (1/s)	677	2430	189	4060
	$\tau_{w,c}$ (dyn/cm^2)	3.47E+06	3.78E+06	2.13E+06	3.90E+06
IV Melt Fracture	γ_a (1/s)	3020	7040	893	-
	$\tau_{w,c}$ (dyn/cm^2)	4.45E+06	4.94E+06	2.59E+06	

Table 3.2.3 The critical wall shear stress ($\tau_{w,c}$) and the strain rate ($\dot{\gamma}_a$) for LLDPE (L2020F) and HDPE (H5690S) at temperatures between 150-230 °C

Materials	T (°C)	Critical Data	Regime II Sharkskin	Regime III Oscillating	Regime IV Melt Fracture
L2020F	230	γ_a (1/s)	520	1821	5420
		$\tau_{w,c}$ (dyn/cm^2)	2.81E+06	4.40E+06	4.80E+06
	210	γ_a (1/s)	417	1790	4780
		$\tau_{w,c}$ (dyn/cm^2)	2.75E+06	4.20E+06	4.67E+06
	190	γ_a (1/s)	325	1760	3520
		$\tau_{w,c}$ (dyn/cm^2)	2.61E+06	3.94E+06	4.45E+06
	170	γ_a (1/s)	274	1524	2710
		$\tau_{w,c}$ (dyn/cm^2)	2.45E+06	2.75E+06	4.32E+06
	150	γ_a (1/s)	253	1320	2010
		$\tau_{w,c}$ (dyn/cm^2)	2.32E+06	2.24E+06	4.02E+06
H5690S	230	γ_a (1/s)	270	622	5414
		$\tau_{w,c}$ (dyn/cm^2)	2.65E+06	3.91E+06	4.66E+06
	210	γ_a (1/s)	189	541	4060
		$\tau_{w,c}$ (dyn/cm^2)	2.61E+06	3.74E+06	3.93E+06
	190	γ_a (1/s)	83	459	2707
		$\tau_{w,c}$ (dyn/cm^2)	2.31E+06	3.51E+06	3.75E+06
	170	γ_a (1/s)	81	427	1353
		$\tau_{w,c}$ (dyn/cm^2)	2.28E+06	2.42E+06	2.75E+06
	150	γ_a (1/s)	70	351	1110
		$\tau_{w,c}$ (dyn/cm^2)	1.12E+06	2.08E+06	2.16E+06

3.3 Rheological Characterizations

In our experiment, the high density polyethylenes (HDPE) used were H5604F, H5690S and H6205JU , the linear low density polyethylenes (LLDPE) used were L2009F, L2020F and M3204RU. The physical properties of all materials studied are shown in Table 3.3.1

Table 3.3.1 Physical properties of all materials studied

Physical Properties	H5604F	H5690S	H6205JU	L2009F	L2020F	M3204RU
MFI (g/10min)	0.04	0.90	5.00	0.90	2.00	5.00
Density (g/cm^3)	0.95	0.95	0.96	0.92	0.92	0.93
M_w (g/mol)	133,000	107,000	98,000	87,000	60,700	33,000
M_n (g/mol)	2,200	8,900	7,300	4,080	2,400	2,700
M_w/M_n	60.45	12.02	13.42	21.31	25.29	12.22

3.3.1 The storage modulus (G') and the loss modulus (G'')

Using the parallel plate rheometer, we carried out 2 sets of measurement. The first measurement mode was Dynamic Strain Sweep which determined G' and G'' within a range of sinusoidal strains, each at a constant frequency. in order to determine the limits of linear viscoelasticity. The temperature was set at 230 °C, the frequency was set at 1 rad/s and the strain was varied from 0.01-100 s^{-1}. The number of points per decade was set at 7 and the nominal gap size was approximately 0.6 mm. The second measurement mode was Dynamic Frequency Temperature Sweep. This mode allows application of a sinusoidal strain over a range of frequencies while temperature is stepped between selectable temperature limits. The temperature was varied between 230-150 °C, the frequency was varied from 0.01-100 rad/s and soak time of 3 minutes was allowed before each measurement. The number of points per decade was set at 7 and nominal gap size was approximately 0.6 mm. From the experiment, we obtained the value of storage modulus, G', and the loss modulus, G'', as a function of the frequency, ω. Figures 3.11-3.16 show the storage modulus, G', as a function of the frequency, ω, and Figures 3.17-3.22 show the loss modulus, G'', as a function of the frequency, ω, for LLDPE (L2009F, L2020F and M3204RU) melts and HDPE (H5604F, H5690S and H6205JU) melts at different temperatures respectively.

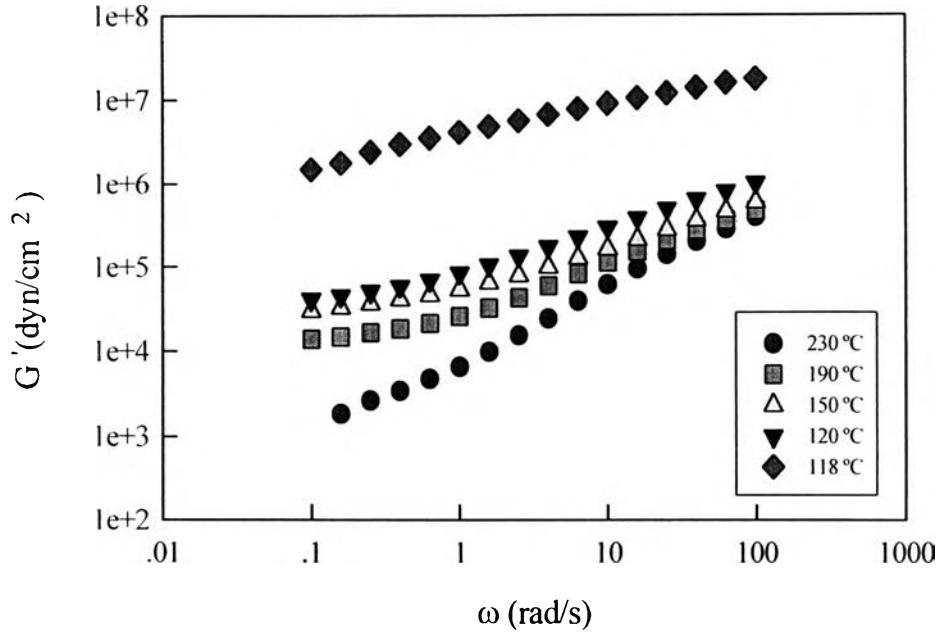

Figure 3.11 The storage modulus, G', as a function of the frequency, ω, of LLDPE (L2009F) melts at different temperatures.

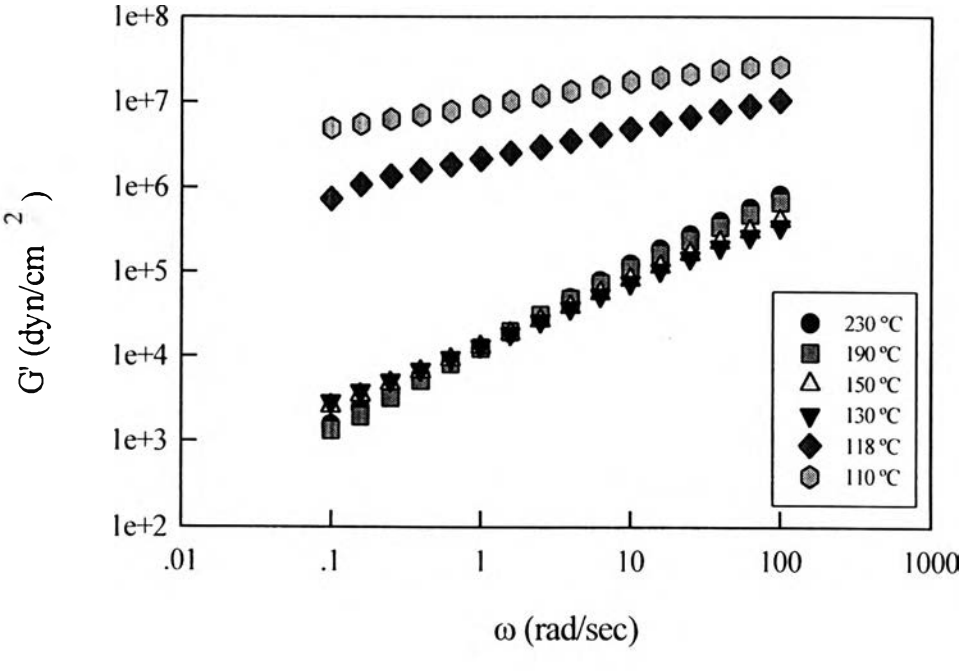

Figure 3.12 The storage modulus, G', as a function of the frequency, ω, of LLDPE (L2020F) melts at different temperatures.

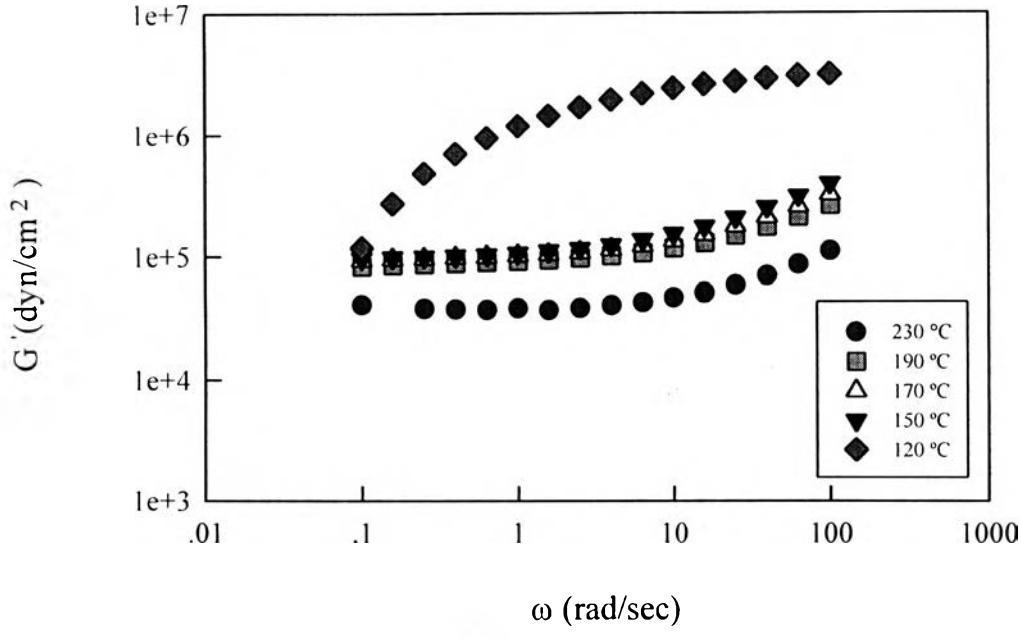

Figure 3.13 The storage modulus, G', as a function of the frequency, ω, of LLDPE (M3204RU) melts at different temperatures.

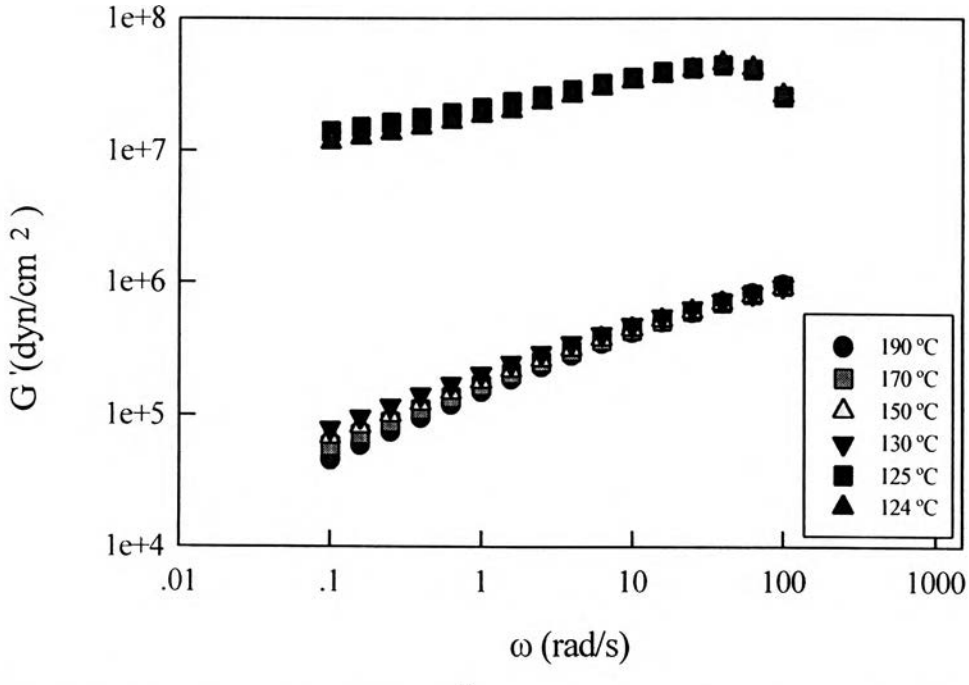

Figure 3.14 The storage modulus, G', as a function of the frequency, ω, of HDPE (H5604F) melts at different temperatures.

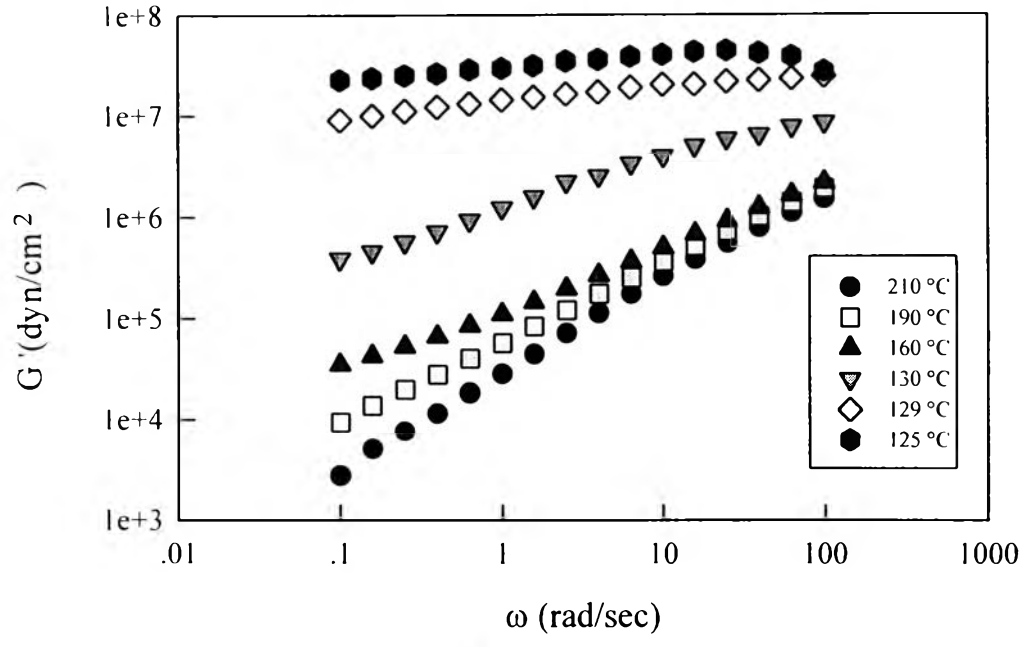

Figure 3.15 The storage modulus, G', as a function of the frequency, ω, of HDPE (H5690S) melts at different temperatures.

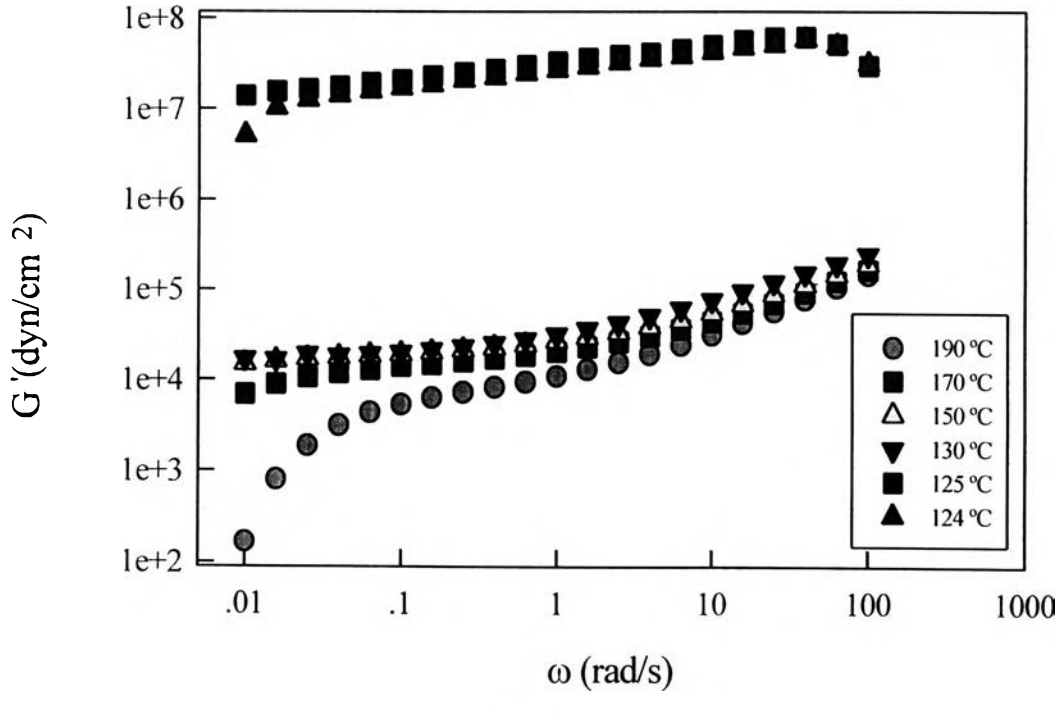

Figure 3.16 The storage modulus, G', as a function of the frequency, ω, of HDPE (H6205JU) melts at different temperatures.

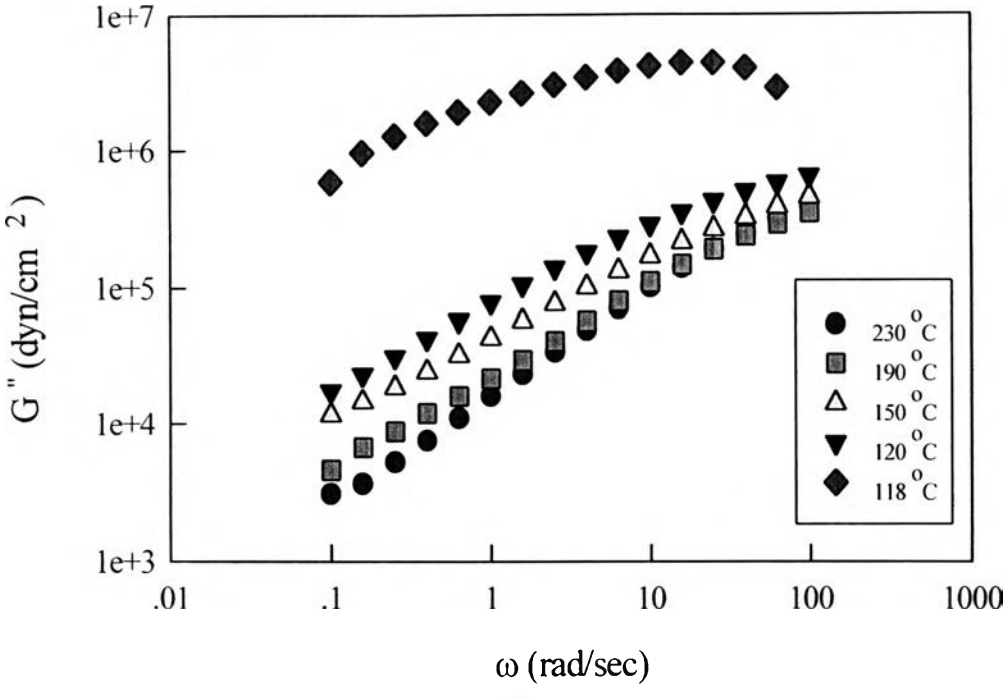

Figure 3.17 The storage modulus, G", as a function of the frequency, ω, of LLDPE (L2009F) melts at different temperatures.

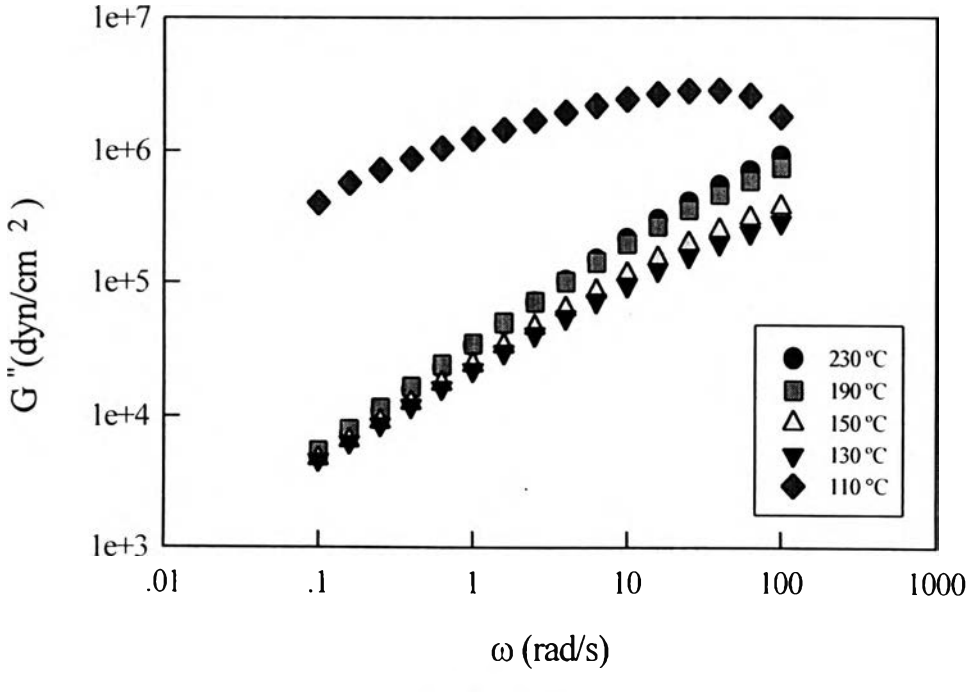

Figure 3.18 The storage modulus, G", as a function of the frequency, ω, of LLDPE (L2020F) melts at different temperatures.

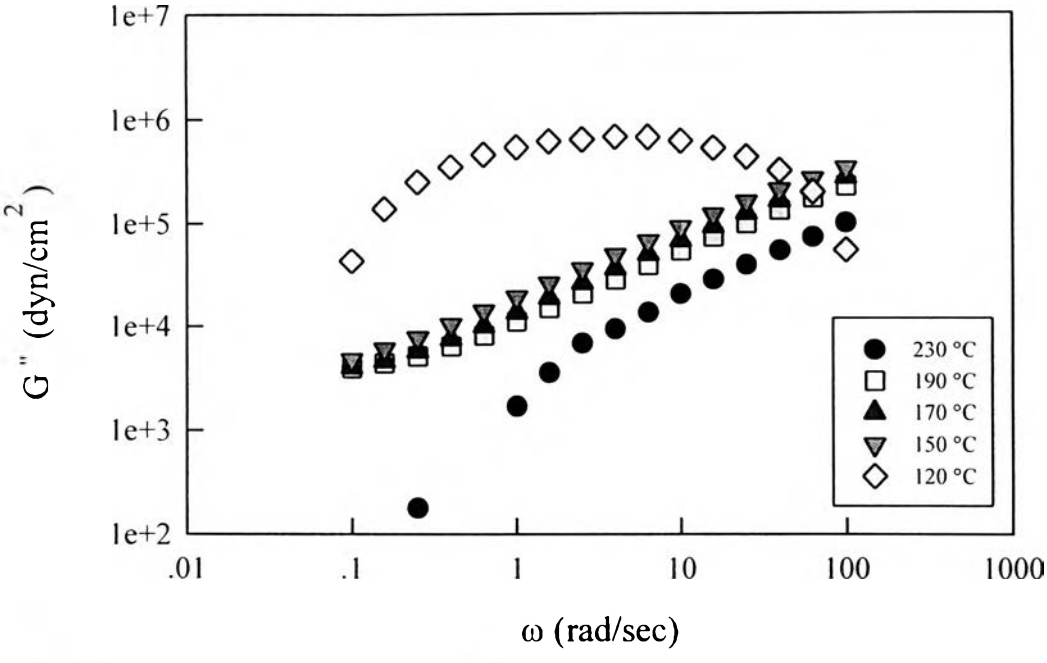

Figure 3.19 The storage modulus, G", as a function of the frequency, ω, of LLDPE (M3204RU) melts at different temperatures.

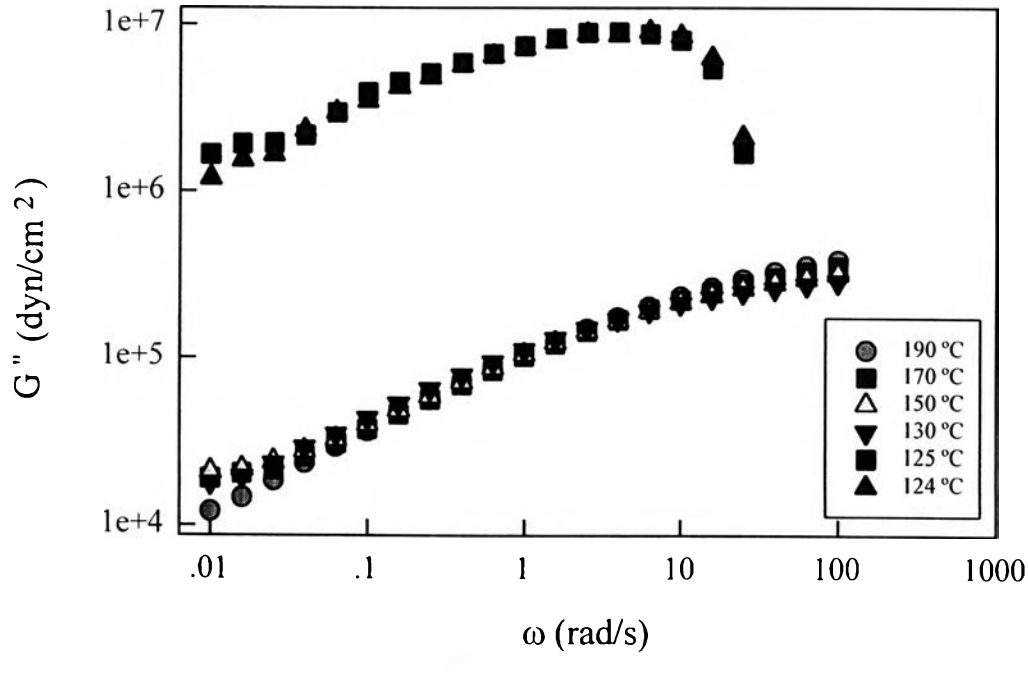

Figure 3.20 The storage modulus, G", as a function of the frequency, ω, of HDPE (H5604F) melts at different temperatures.

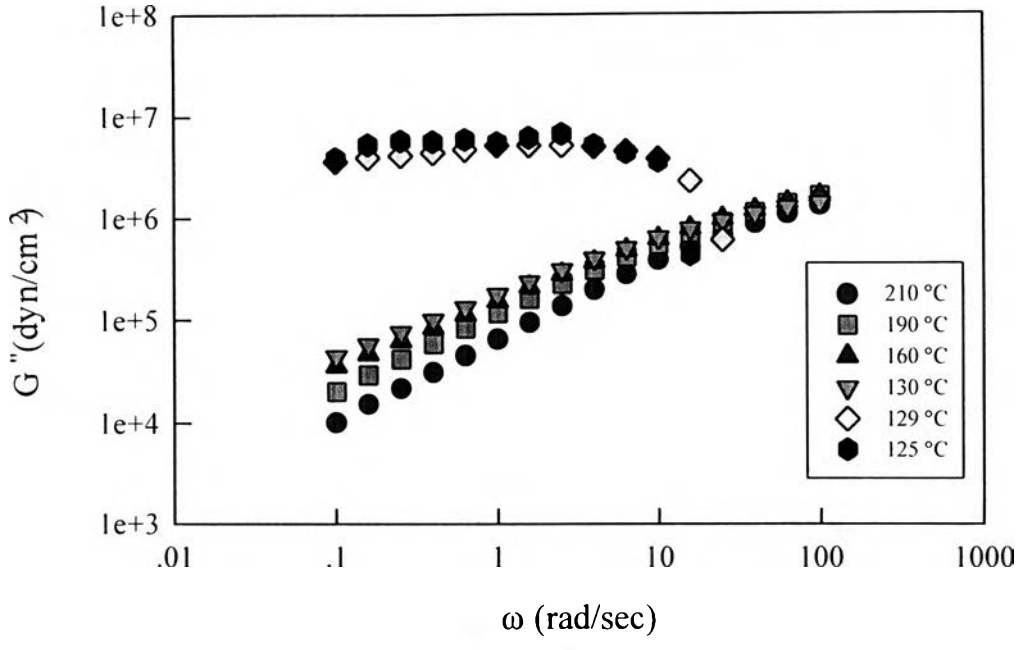

Figure 3.21 The storage modulus, G'', as a function of the frequency, ω, of HDPE (H5690S) melts at different temperatures.

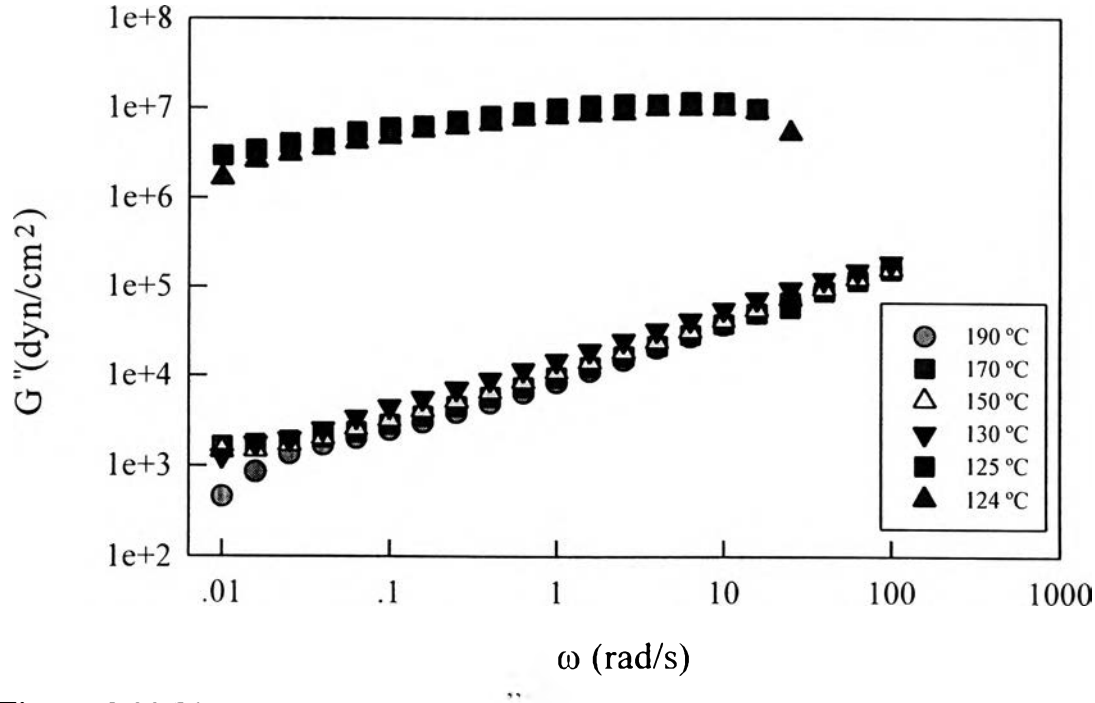

Figure 3.22 The storage modulus, G'', as a function of the frequency, ω, of HDPE (H6205JU) melts at different temperatures.

3.3.2 Master Curves

The master curve can be obtained through measurement of G' and G'' as a function of frequency at various temperatures. The storage modulus, G', and the loss modulus, G'', curves at different temperatures were shifted horizontally and vertically to form a single master curve at a fixed reference temperature. The shift factor is a measure of how material's frequency respond changes with temperature to its behavior at a reference temperature. By assuming the reference temperature of 190 °C we determined the horizontal shift factor (a_T) emperically. We took the constant values to calculate the shift factor (log a_T) which was used to generate the time-temperature master curve, using the vertical shift factor (b_T) according to equation (2.23). Figures 3.23 - 3.28 show the master curves of LLDPE (L2009F, L2020F and M3204RU) melts and HDPE (H5604F, H5690S and H6205JU) melts at the reference temperature of 190 ^oC, respectively. For other reference temperatures, the results are shown in the Appendix.

For LLDPE (L2009F and L2020F) shown in Figures 3.23 and 3.24, we obtained each value of G^o_N from the apparent value from the plateau by selected point of $G'(\omega)$ before $G''(\omega)$ falls in plateau region. Other G^o_N values were obtained from a fitting equation, in the case which we can not see the plateau directly. The G^o_N values of all materials studied are summarized and tabulated in Table 3.3.2. We note that, the order magnitude of G^o_N is consistent with the reported values ($G^o_N = 2.29*10^7$ dyn/cm^2) of polyethylene by Ferry (1980).

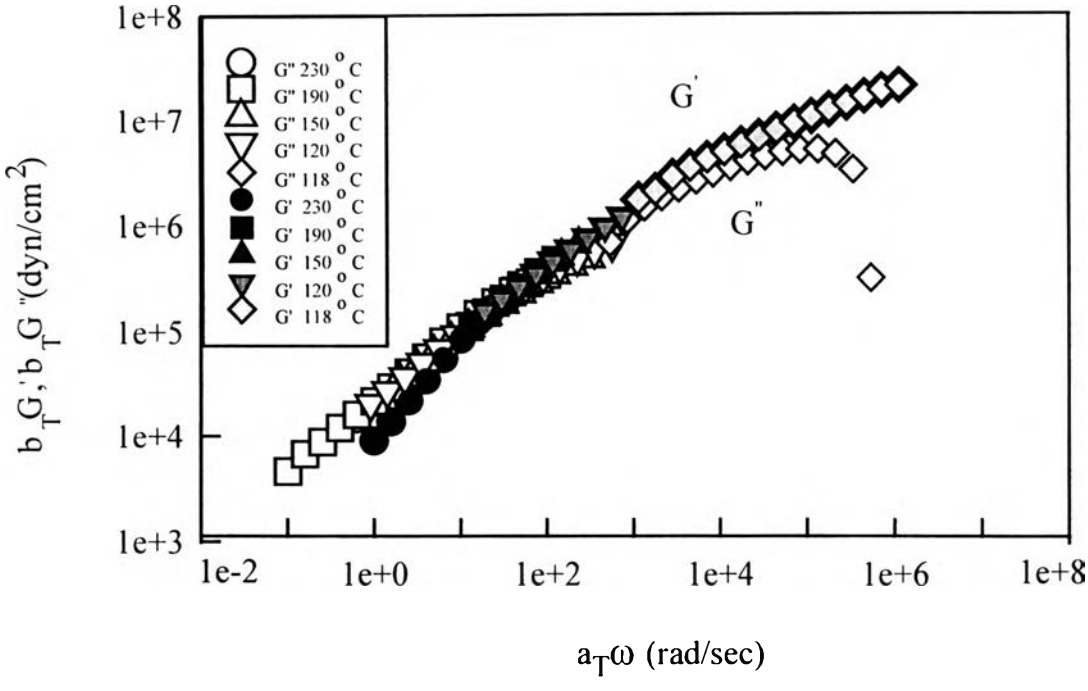

Figure 3.23 Master curve of LLDPE (L2009F) melts at reference temperature of 190 °C.

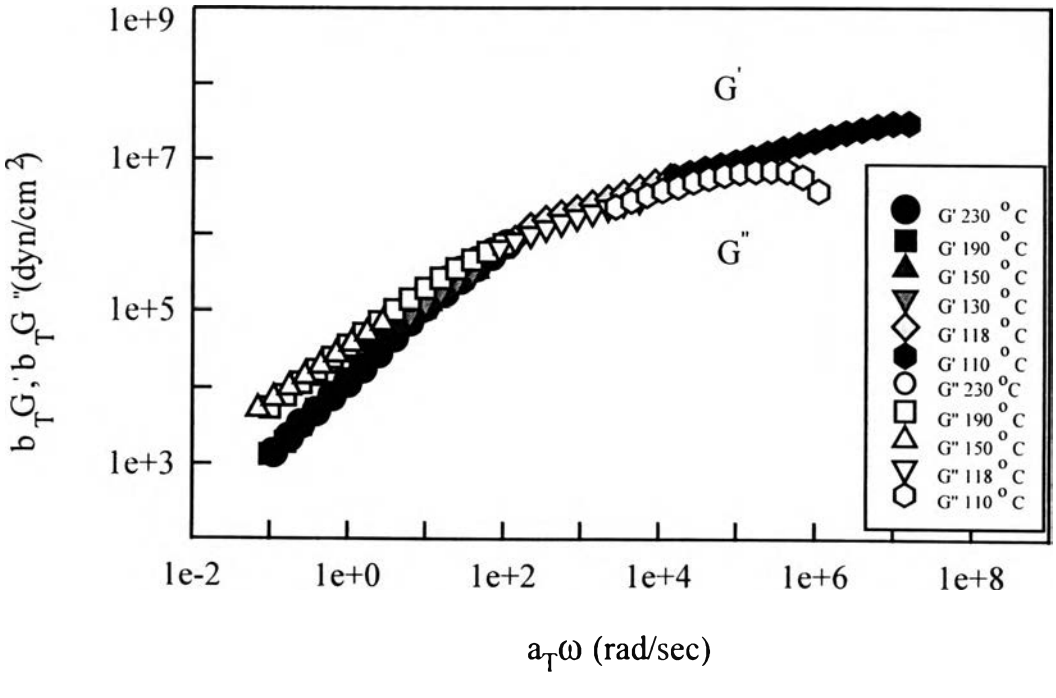

Figure 3.24 Master curve of LLDPE (L2020F) melts at reference temperature of 190 °C.

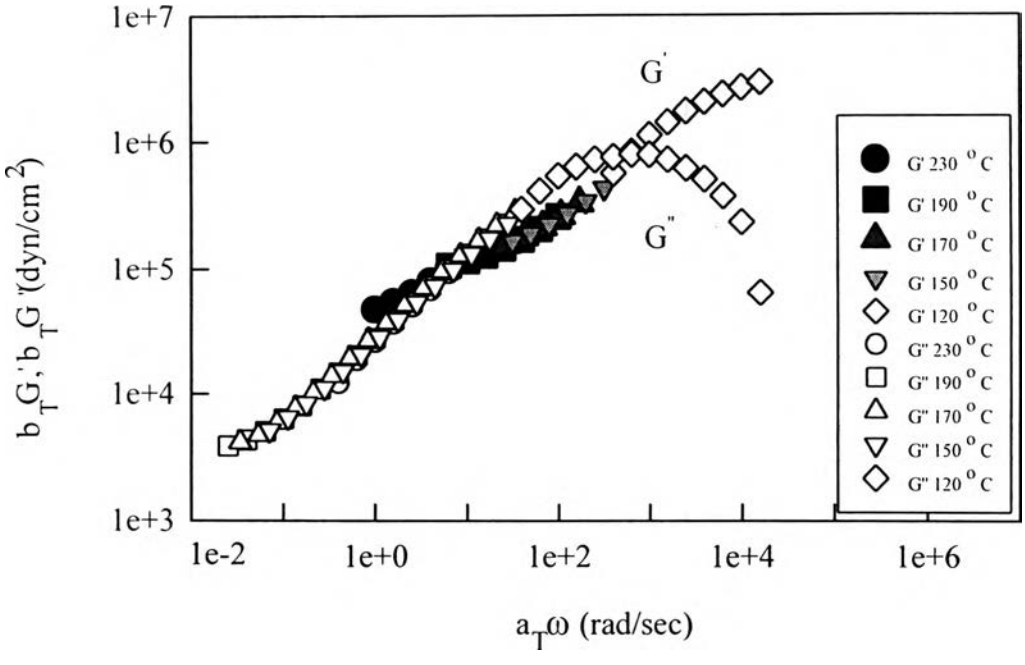

Figure 3.25 Master curve of LLDPE (M3204RU) melts at reference temperature of 190 °C.

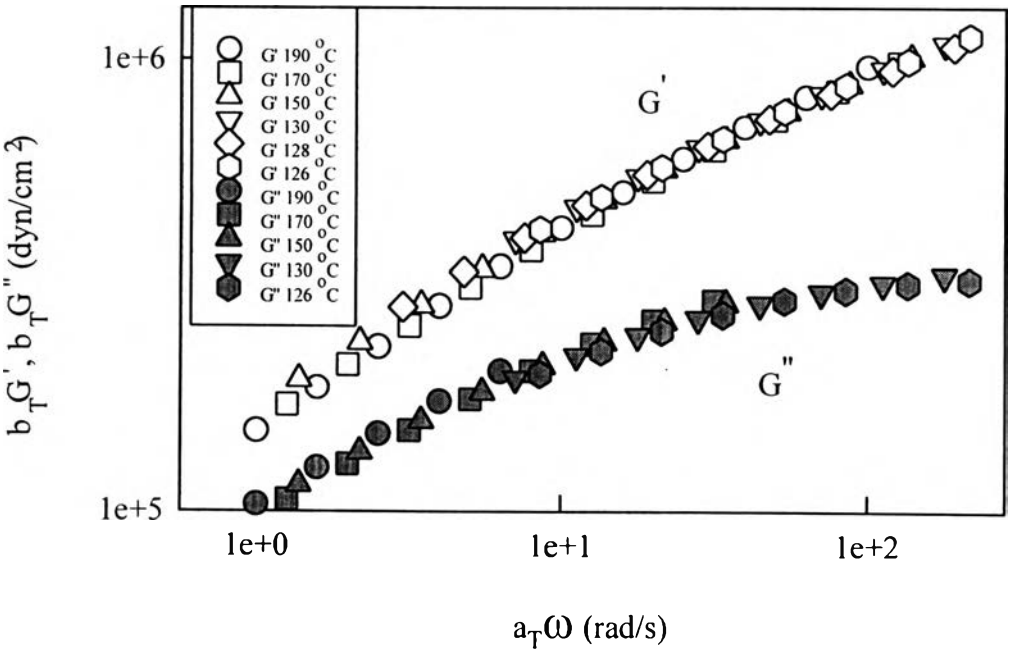

Figure 3.26 Master curve of HDPE (H5604F) melts at reference temperature of 190 °C.

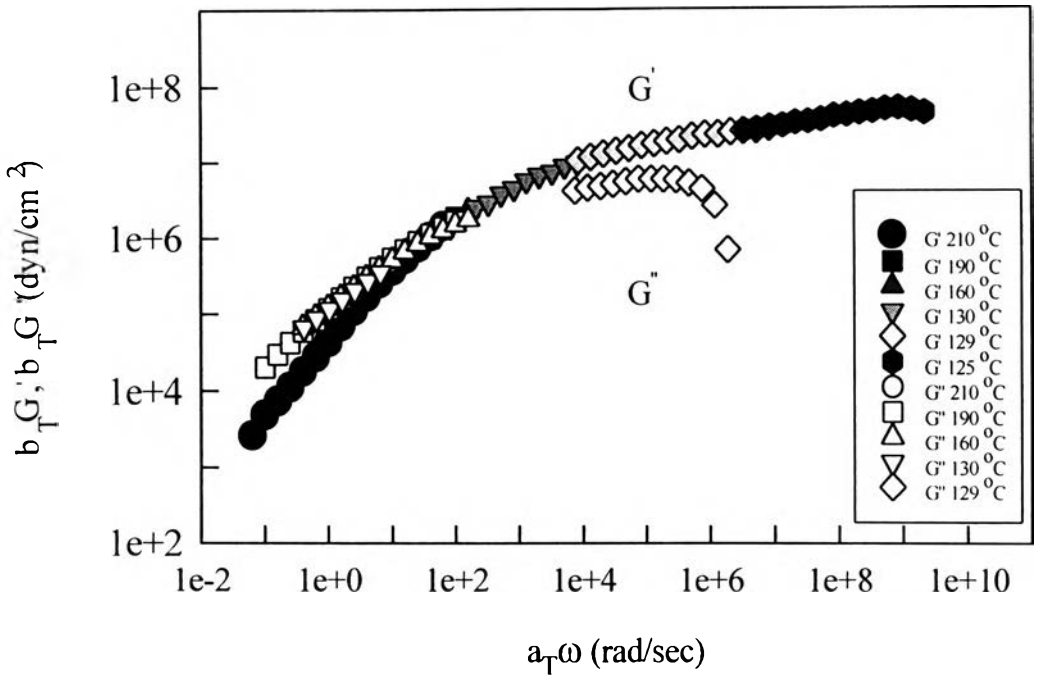

Figure 3.27 Master curve of HDPE (H5690S) melts at reference temperature of 190 °C.

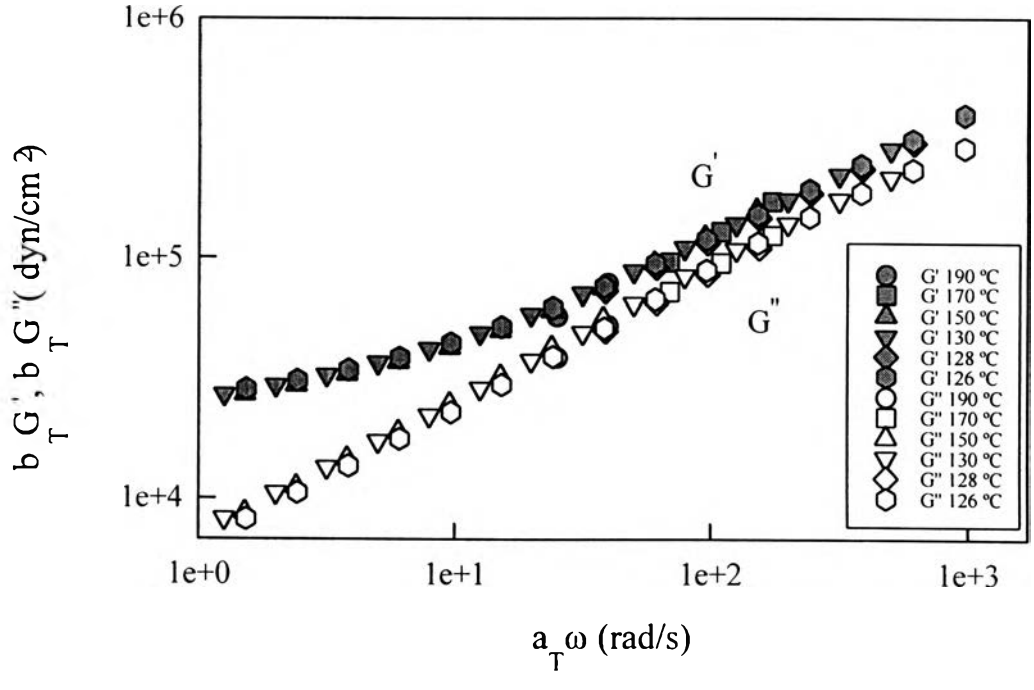

Figure 3.28 Master curve of HDPE (H6205JU) melts at reference temperature of 190 °C.

3.3.3 Cox-Merz Rule

Cox-Merz (1985) compared the complex viscosity, η^*, vs. frequency obtained from the parallel plates rheometer with the steady state viscosity vs. strain rate obtained from the capillary rheometer. Their rule suggests that the two viscometric functions would collapse to form a single curve.

3.3.3.1 Effect of Temperature. Figures 3.29-3.33 show the plots of η vs. $\dot{\gamma}_a$, and η^* vs. ω, for LLDPE (L2020F) melt at temperatures between 150-230 °C respectively. Figures 3.34-3.38 show the plots of η vs. $\dot{\gamma}_a$ and η^* vs. ω for HDPE (H5690S) melts at temperatures between 150-230 °C respectively. The values of zero complex viscosity, η^*_o, for LLDPE (L2020F) and HDPE (H5690S) at temperatures between 150-230 °C are summarized and tabulated in Table 3.3.2. Each η^*_o was determined from extrapolation of η^* vs. ω curve toward ω = 0.01 rad/s. The zero complex viscosity, η^*_o, decreases with temperature. This result is consistent with published data by Ferry (1980).

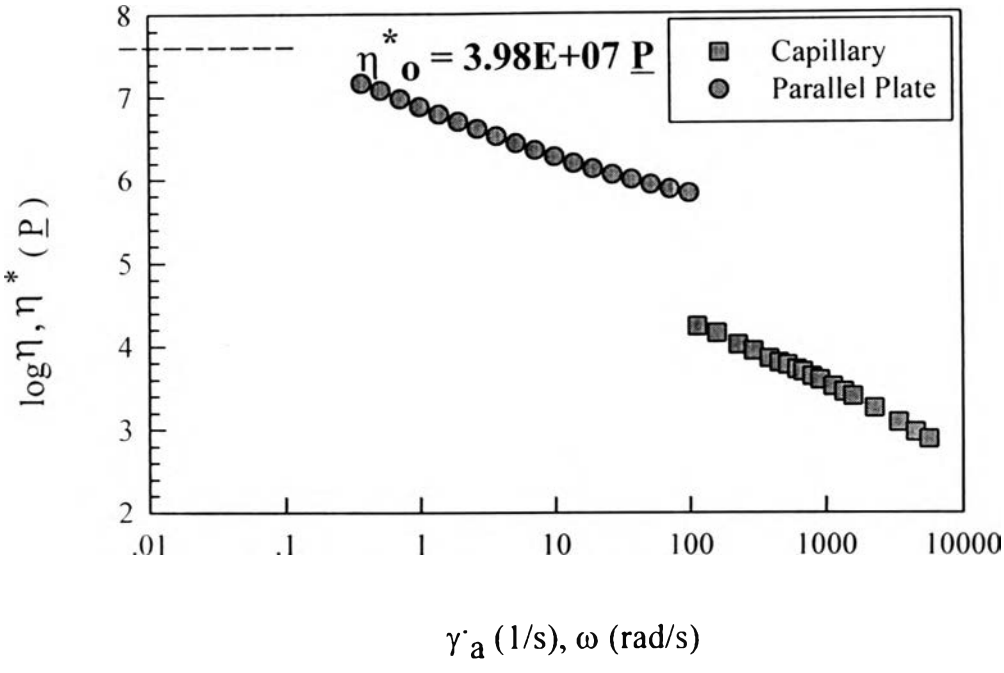

Figure 3.29 The viscosity as a function of the apparent strain rate and frequency of LLDPE (L2020F) melts by Cox-Merz rule at temperature of 150 °C.

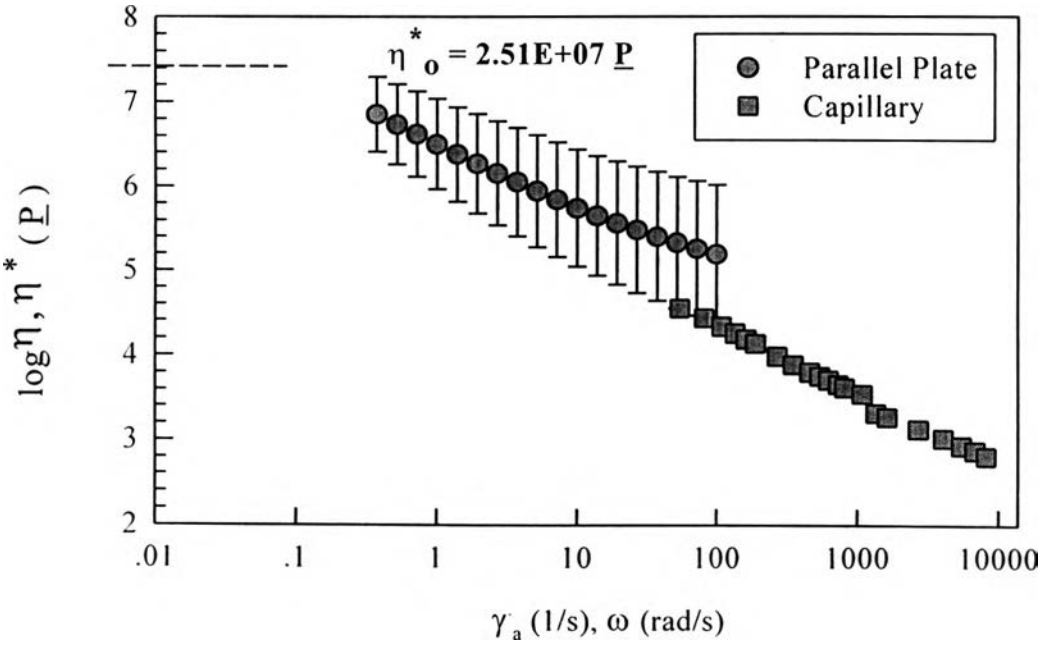

Figure 3.30 The viscosity as a function of the apparent strain rate and frequency of LLDPE (L2020F) melts by Cox-Merz rule at temperature of 170 °C.

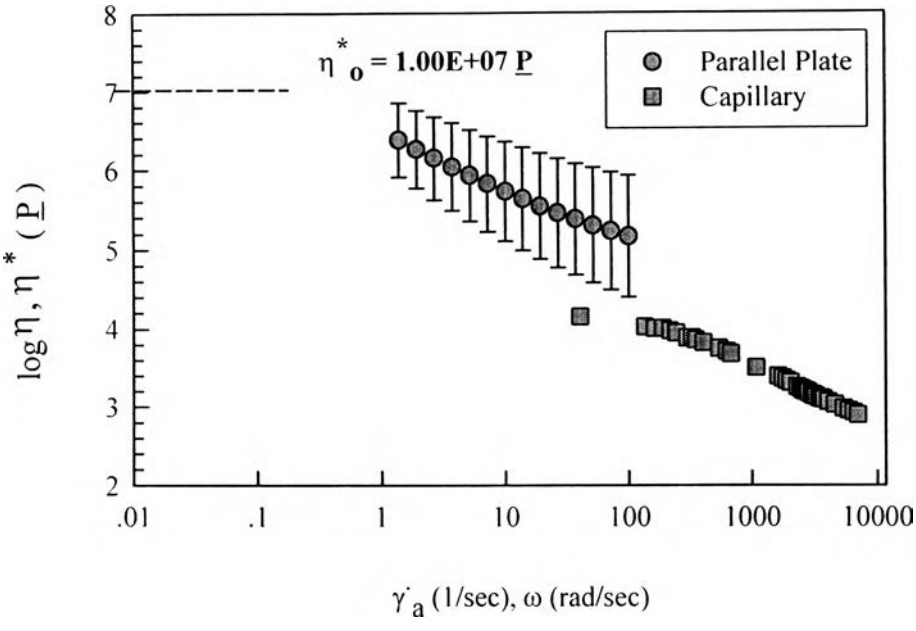

Figure 3.31 The viscosity as a function of the apparent strain rate and frequency of LLDPE melts (L2020F) melts by Cox-Merz rule at temperature of 190 °C.

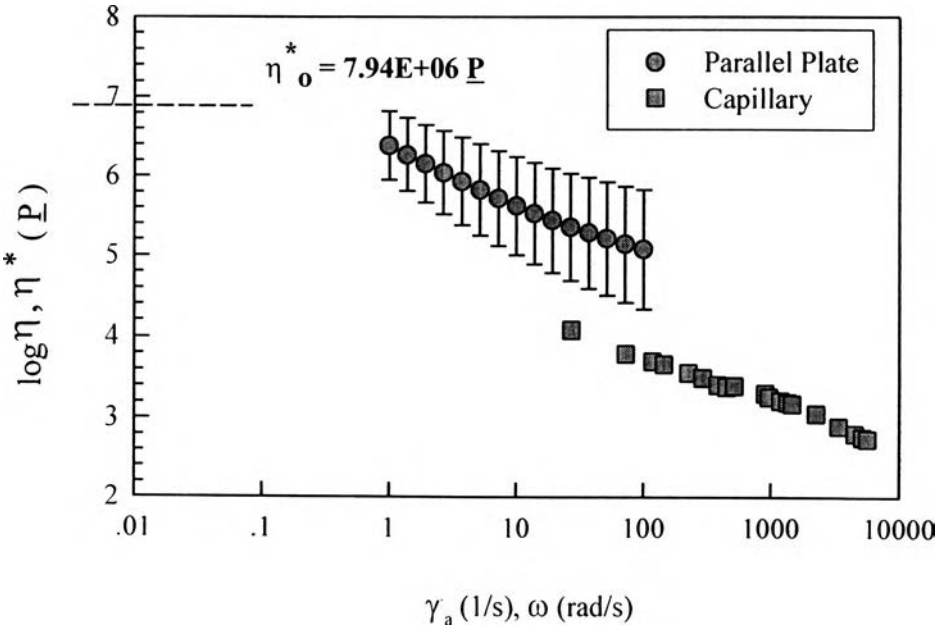

Figure 3.32 The viscosity as a function of the apparent strain rate and frequency of LLDPE (L2020F) melts by Cox-Merz rule at temperature of 210 °C.

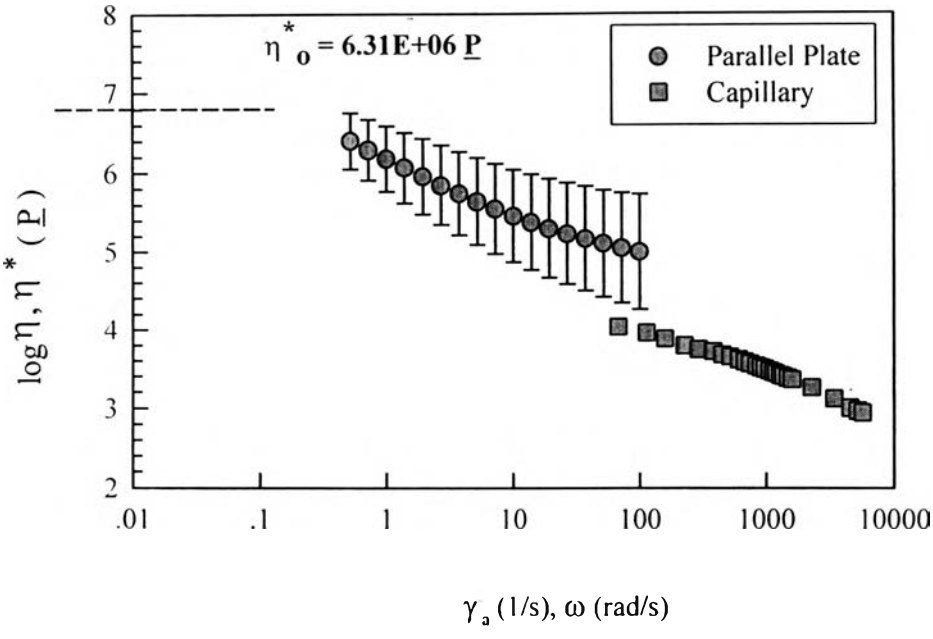

Figure 3.33 The viscosity as a function of the apparent strain rate and frequency of LLDPE (L2020F) melts by Cox-Merz rule at temperature of 230 °C.

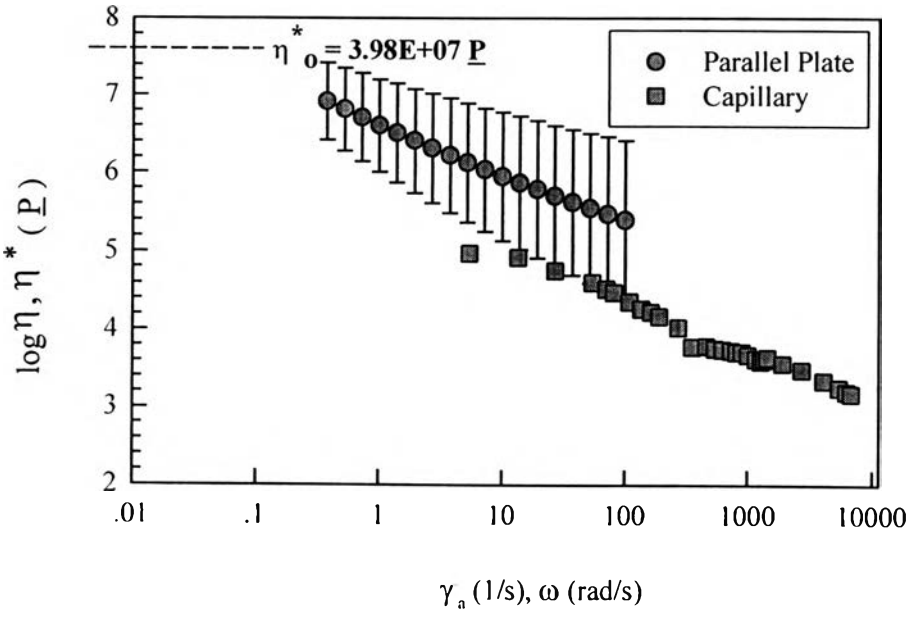

Figure 3.34 The viscosity as a function of the apparent strain rate and frequency of HDPE (H5690S) melts by Cox-Merz rule at temperature of 150 °C.

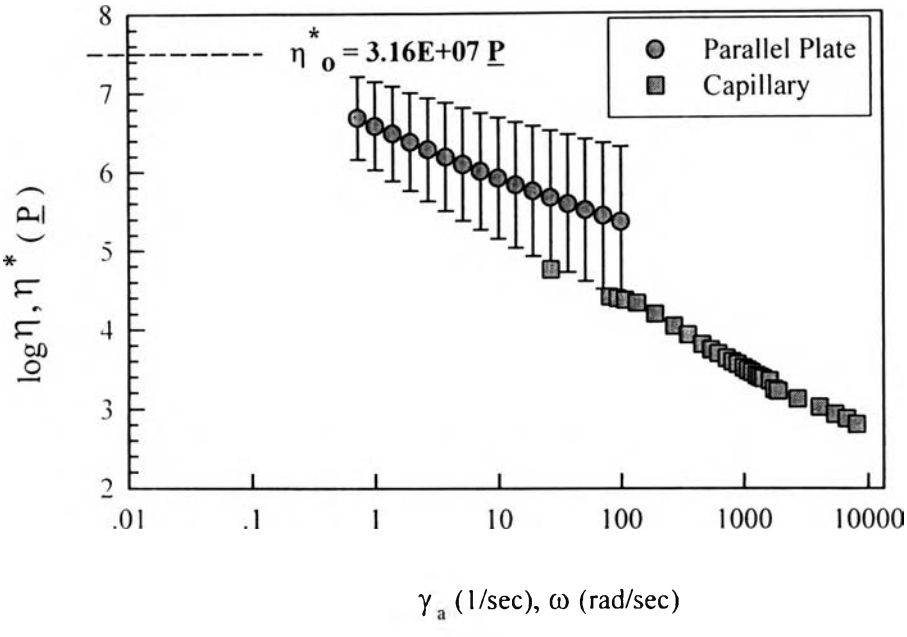

Figure 3.35 The viscosity as a function of the apparent strain rate and frequency of HDPE (H5690S) melts by Cox-Merz rule at temperature of 170 °C.

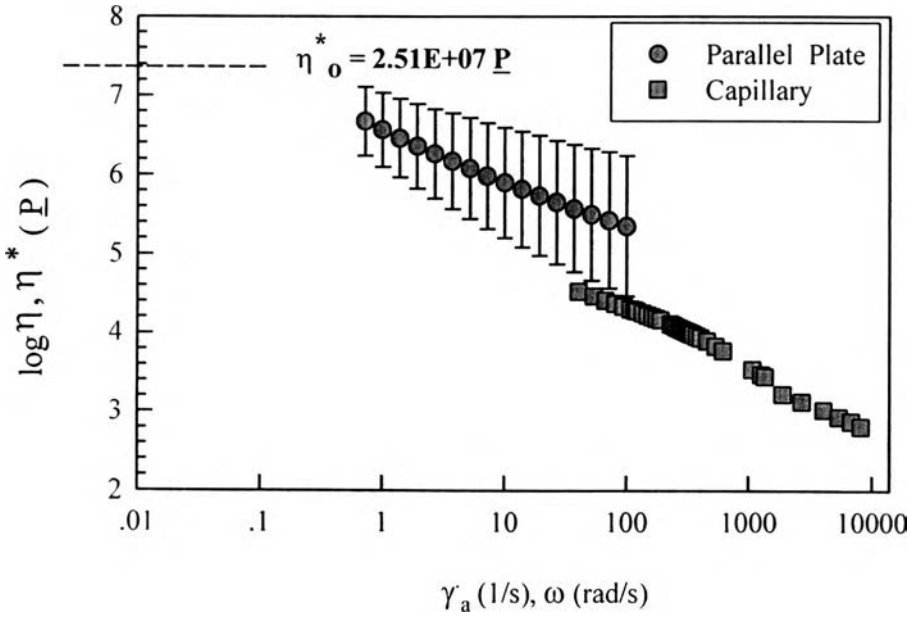

Figure 3.36 The viscosity as a function of the apparent strain rate and frequency of HDPE (H5690S) melts by Cox-Merz rule at temperature of 190 °C.

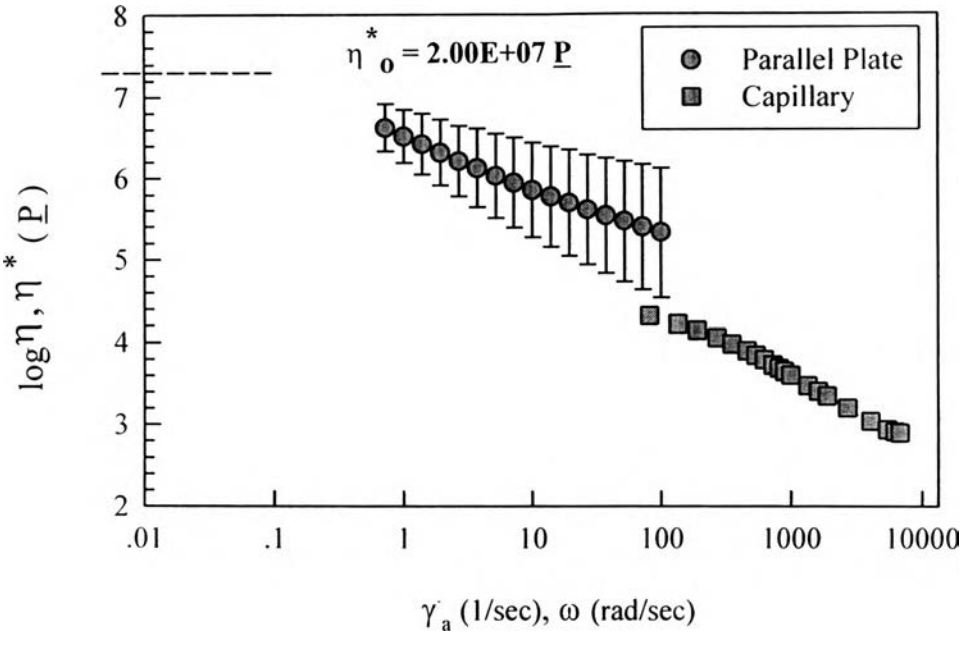

Figure 3.37 The viscosity as a function of the apparent strain rate and frequency of HDPE (H5690S) melts by Cox-Merz rule at temperature of 210 °C.

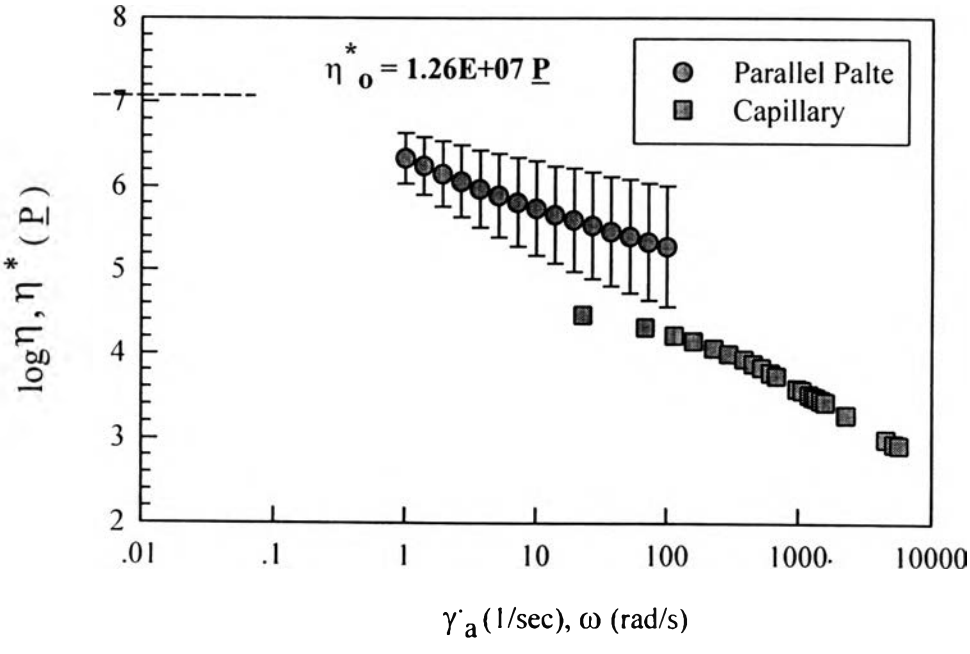

Figure 3.38 The viscosity as a function of the apparent strain rate and frequency of HDPE (H5690S) melts by Cox-Merz rule at temperature of 230 °C.

3.3.3.2 Effect of Molecular weight. Figures 3.39-3.41 show the plots of η vs. $\dot{\gamma}_a$ and η^* vs. ω for LLDPE (L2009F, L2020F and M3204RU) melt at temperature of 190 °C respectively. Figures 3.42-3.44 show the plots of η vs. $\dot{\gamma}_a$ and η^* vs. ω for HDPE (H5604F, H5690S and H6205JU) melt at temperature of 190 °C respectively. The values of zero complex viscosity, η^*_o, for LLDPE (L2009F, L2020F and M3204RU) melt and HDPE (H5604F, H5690S and H6205JU) melt at temperature of 190 °C are summarized and tabulated in Table 3.3.3. From the results, the zero complex viscosity, η^*_o, increases with molecular weight. This result is consistent with published data by Ferry (1980).

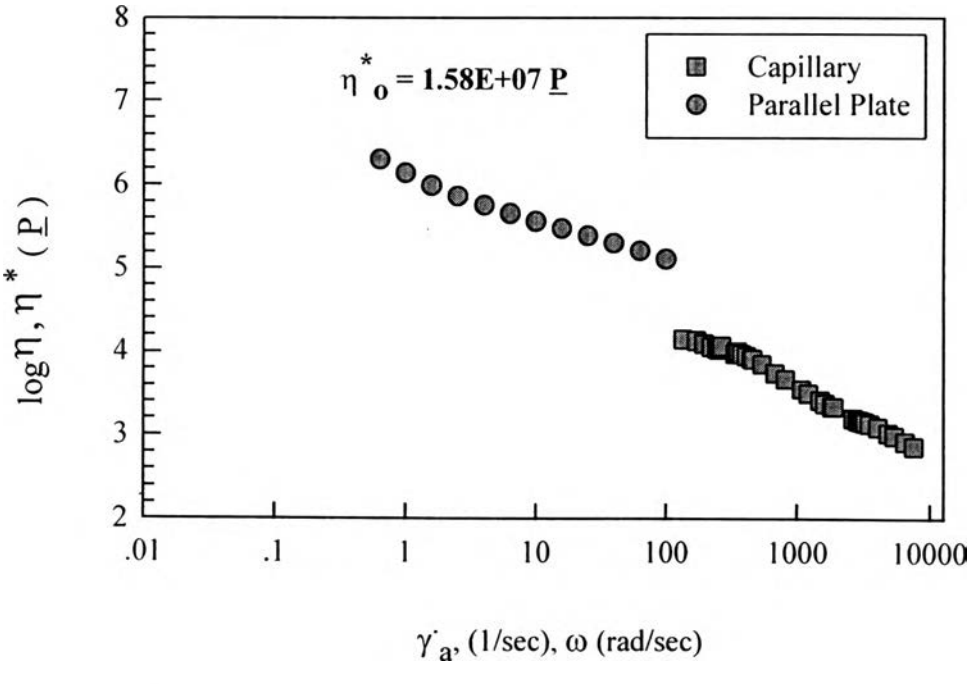

Figure 3.39 The viscosity as a function of the apparent strain rate and frequency of LLDPE (L2009F) melts by Cox-Merz rule at temperature of 190 °C.

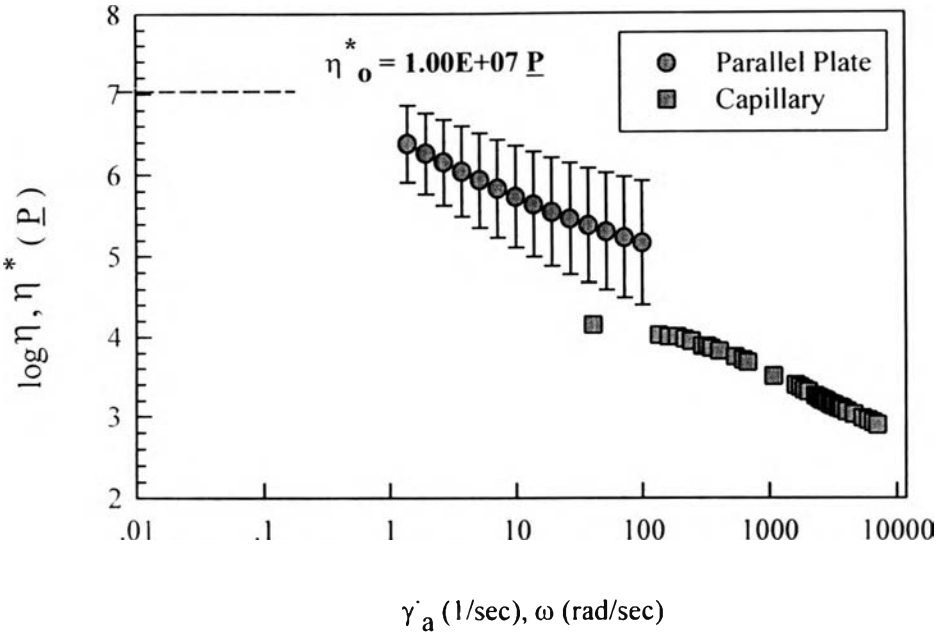

Figure 3.40 The viscosity as a function of the apparent strain rate and frequency of LLDPE (L2020F) melt by Cox-Merz rule at temperature of 190 °C.

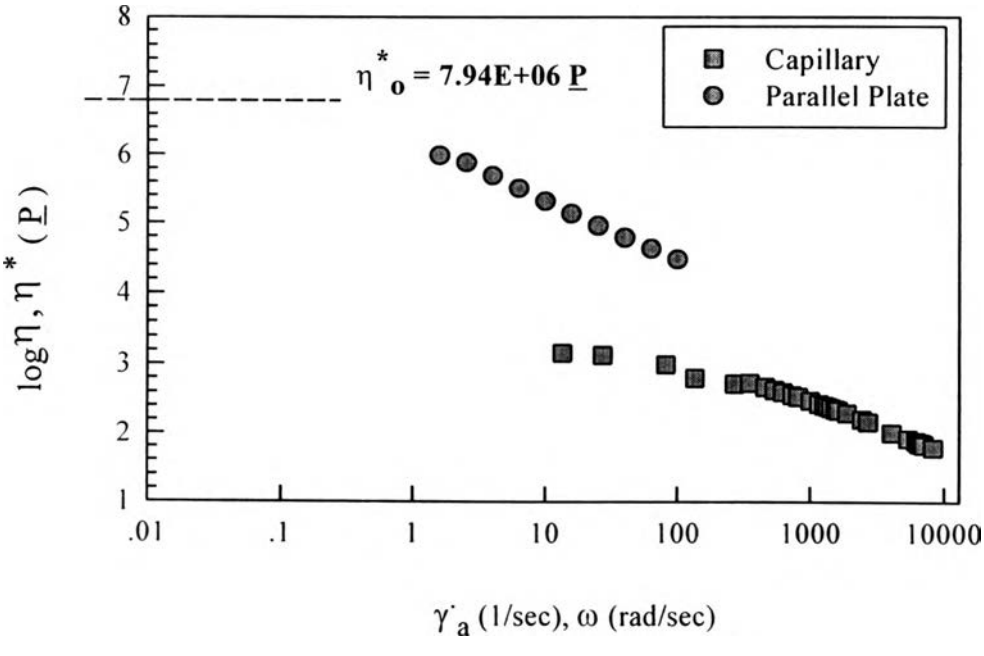

Figure 3.41 The viscosity as a function of the apparent strain rate and frequency of LLDPE (M3204RU) melt by Cox-Merz rule at temperature of 190 °C.

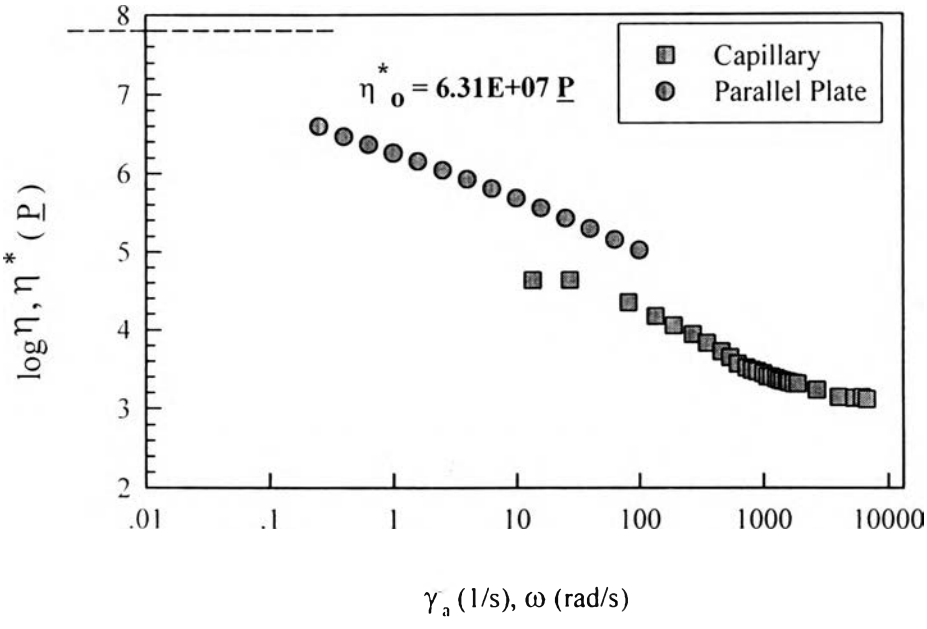

Figure 3.42 The viscosity as a function of the apparent strain rate and frequency of HDPE (H5604F) melt by Cox-Merz rule at temperature of 190 °C.

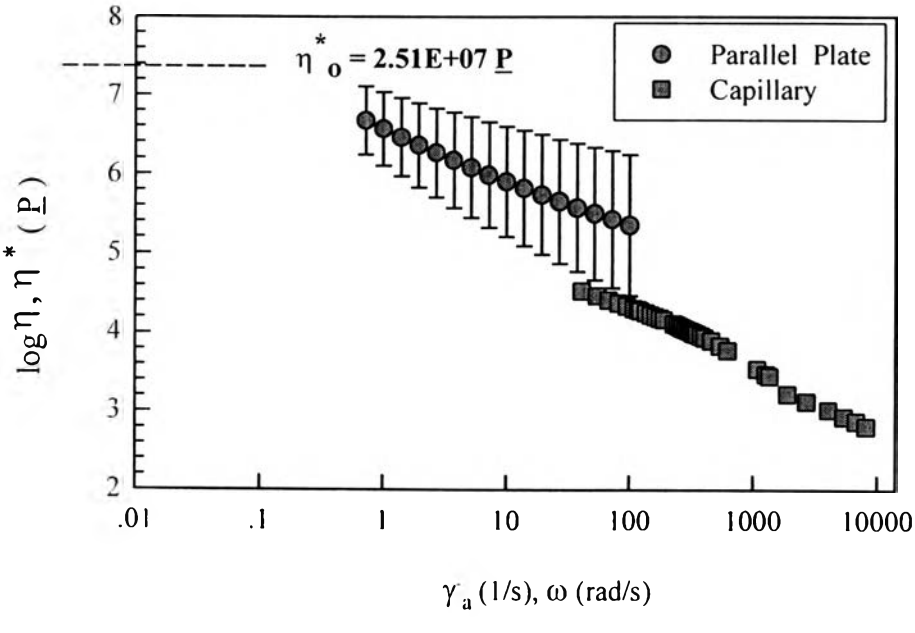

Figure 3.43 The viscosity as a function of the apparent strain rate and frequency of HDPE (H5690S) melt by Cox-Merz rule at temperature of 190 °C.

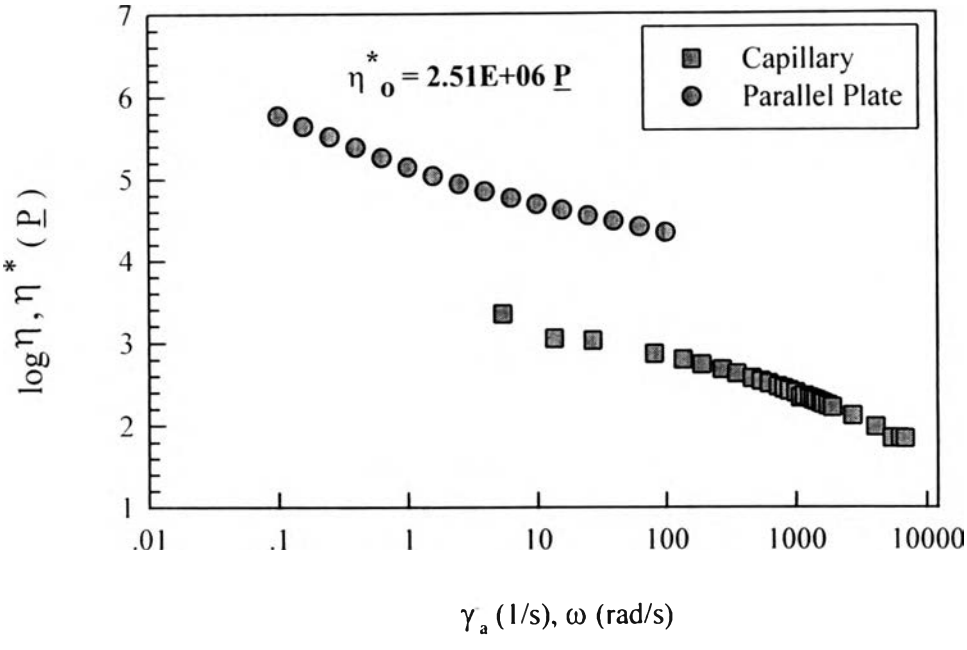

Figure 3.44 The viscosity as a function of the apparent strain rate and frequency of HDPE (H6205JU) melt by Cox-Merz rule at temperature of 190 °C.

3.3.4 Viscosity

The viscosity obtained from the parallel plate rheometer was determined from equation (2.24). From the results, we obtained the zero shear viscosity, η^*_o, by average from 2 experiments and extrapolate to the frequency equal to 0.01 rad/s.

3.3.4.1 Effect of Temperature. Figures 3.45-3.49 show the viscosity, η^*, as a function of the frequency, ω, for LLDPE (L2020F) melts at temperatures between 150-230 °C respectively. Figures 3.50-3.54 show the viscosity, η^*, as a function of the frequency, ω, for HDPE (H5690S) melts at temperatures between 150-230 °C respectively. The values of the zero shear viscosity, η^*_o, of LLDPE (L2020F) and HDPE (H5690S) are summarized and tabulated in Table 3.3.2. From the results, the zero shear viscosity, η^*_o,

decreases with temperature. This result is consistent with published data by Ferry (1980). We note that the order magnitude of η'_o, is consistent with reported values (10^5-10^6 P) of polyethylene by Byron (1924).

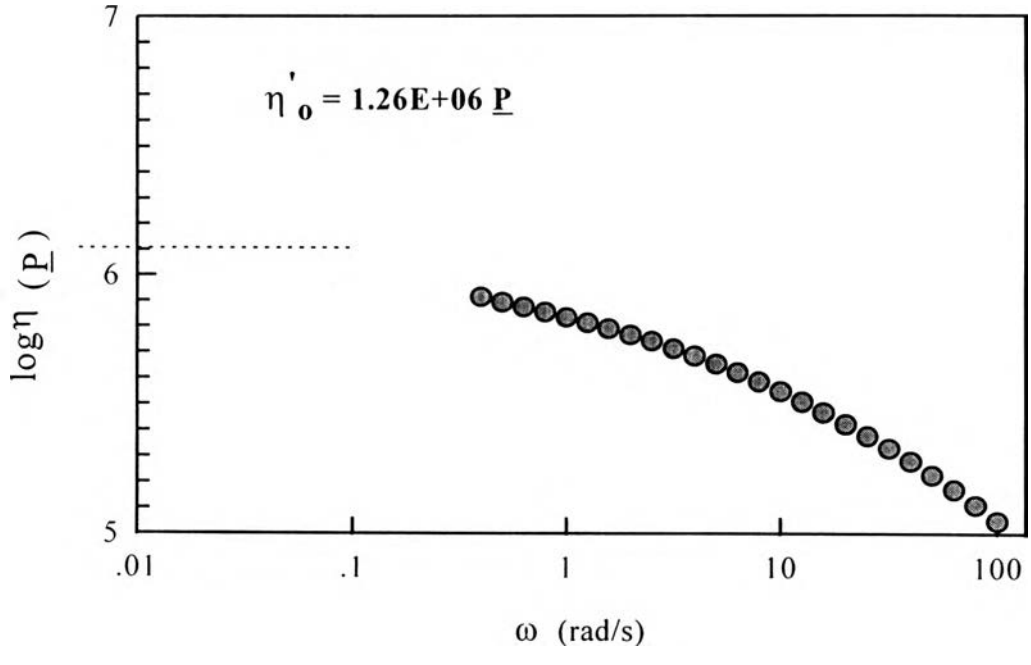

Figure 3.45 The viscosity as a function of the frequency of LLDPE (L2020F) melts at temperature of 150 °C.

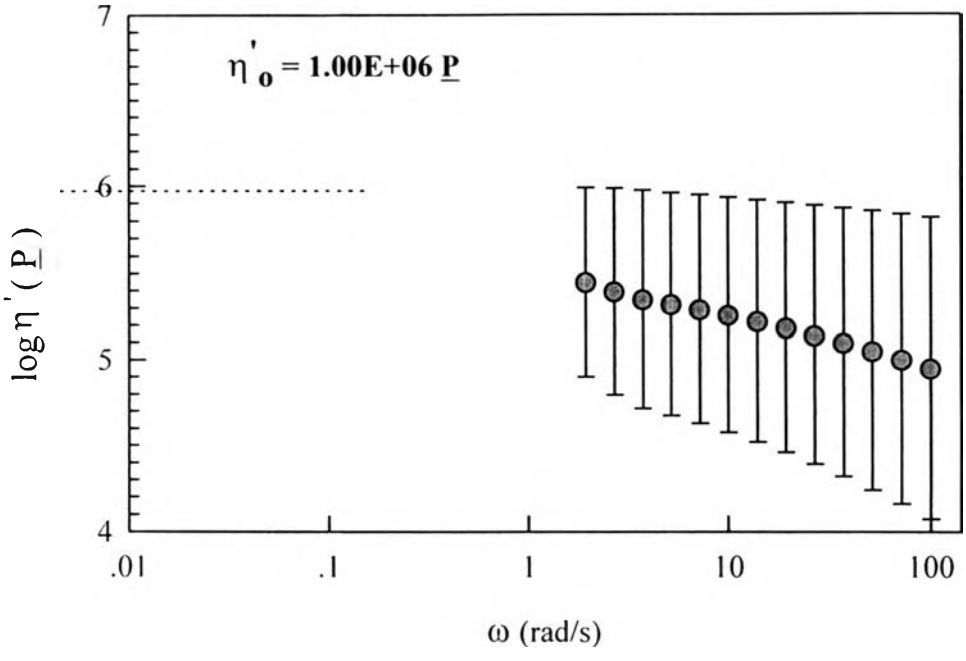

Figure 3.46 The viscosity as a function of the frequency of LLDPE (L2020F) melts at temperature of 170 °C.

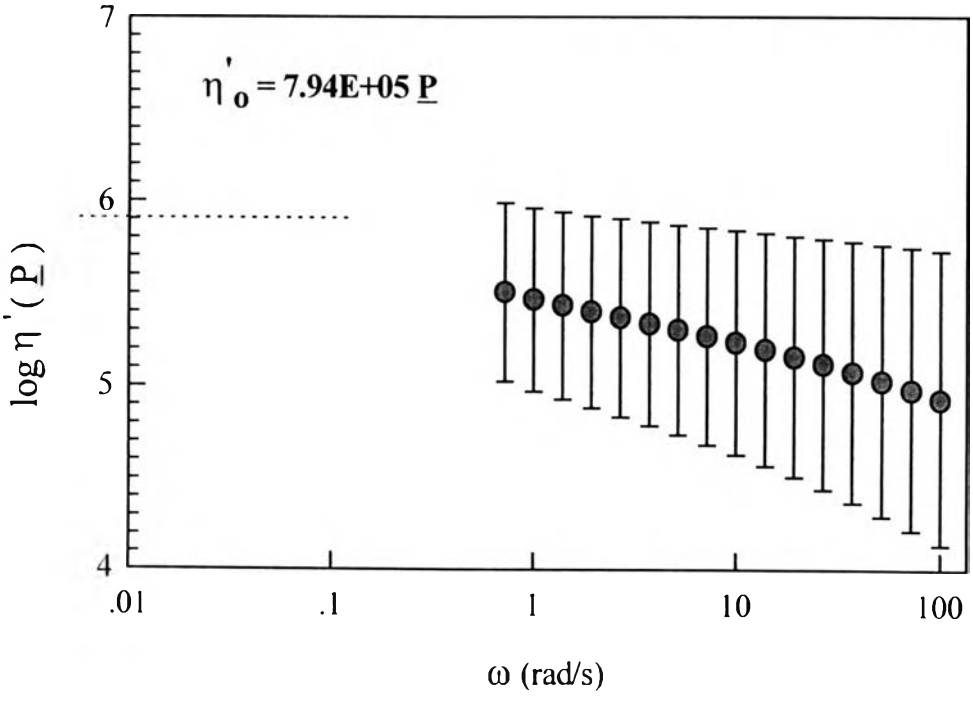

Figure 3.47 The viscosity as a function of the frequency of LLDPE (L2020F) melts at temperature of 190 °C.

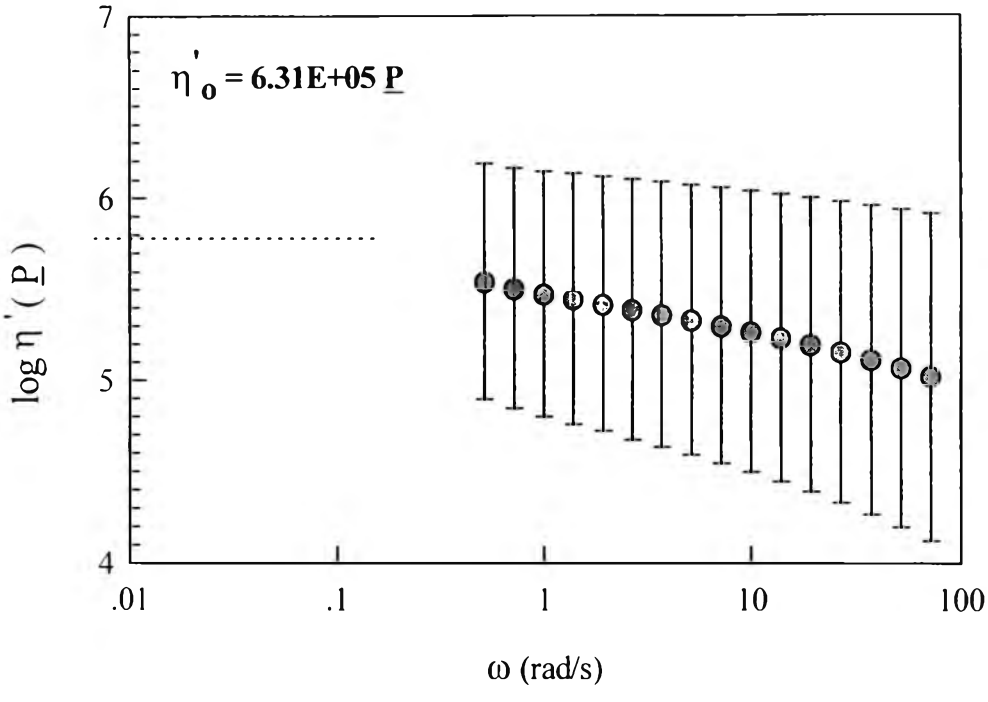

Figure 3.48 The viscosity as a function of the frequency of LLDPE (L2020F) melts at temperature of 210 °C.

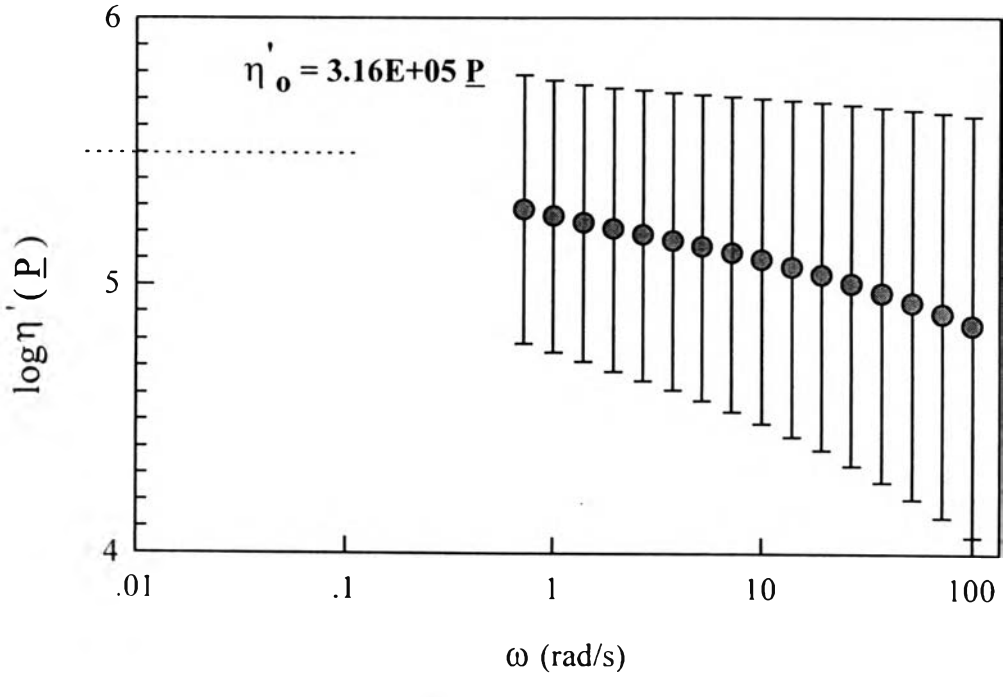

Figure 3.49 The viscosity as a function of the frequency of LLDPE (L2020F) melts at temperature of 230 °C.

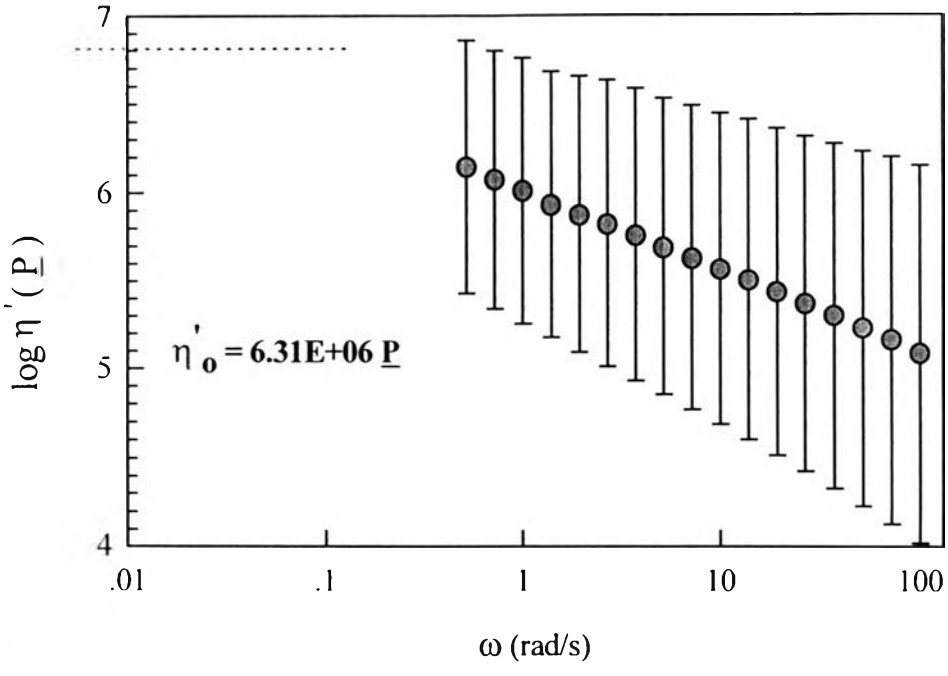

Figure 3.50 The viscosity as a function of the frequency of HDPE (H5690S) melts at temperature of 150 °C.

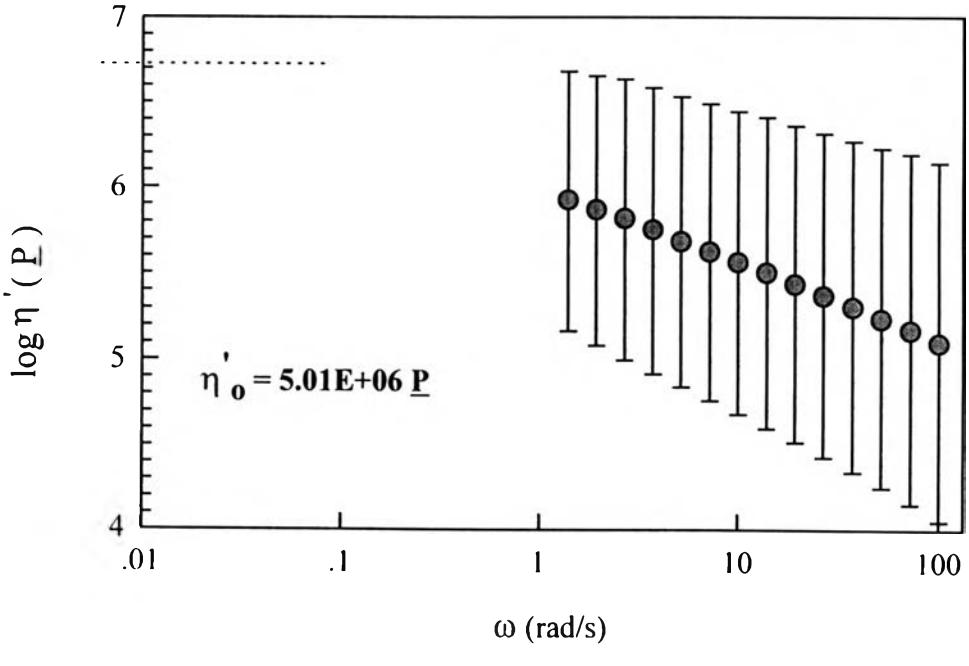

Figure 3.51 The viscosity as a function of the frequency of HDPE (H5690S) melts at temperature of 170 °C.

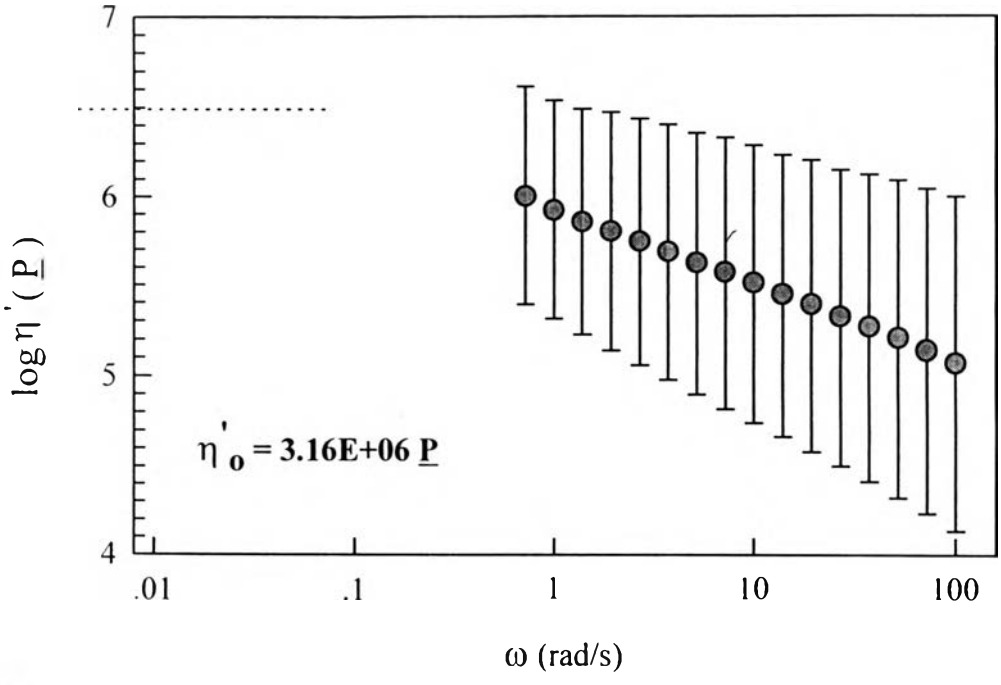

Figure 3.52 The viscosity as a function of the frequency of HDPE (H5690S) melts at temperature of 190 °C.

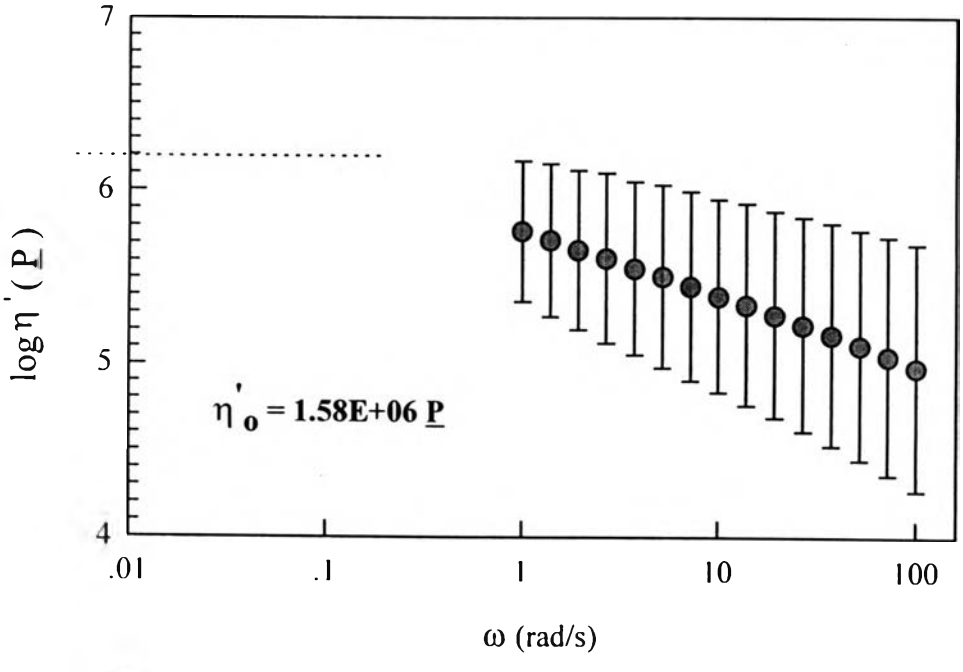

Figure 3.53 The viscosity as a function of the frequency of HDPE (H5690S) melts at temperature of 210 °C.

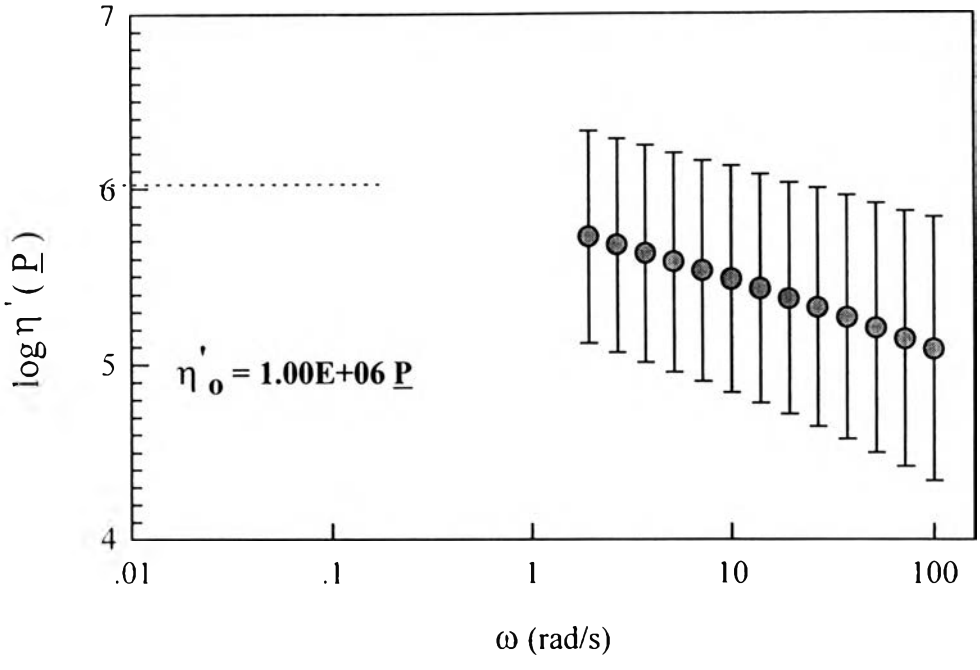

Figure 3.54 The viscosity as a function of the frequency of HDPE (H5690S) melts at temperature of 230 °C.

3.3.4.2 Effect of Molecular weight. Figures 3.55-3.57 show the viscosity, η', as a function of the frequency, ω, for LLDPE (L2009F, L2020F and M3204RU) melts at temperature of 190 °C. Figures 3.58-3.60 show the viscosity , η', as a function of the frequency, ω, for HDPE (H5604F, H5690S and H6205JU) melts at temperature of 190 °C. The values of zero shear viscosity of LLDPE (L2009F, L2020F and M3204RU) and HDPE (H5604F, H5690S and H6205JU) are summarized and tabulated in Table 3.3.3. From the results, the zero shear viscosity increases with molecular weight. This result is consistent with published data by Ferry (1980).

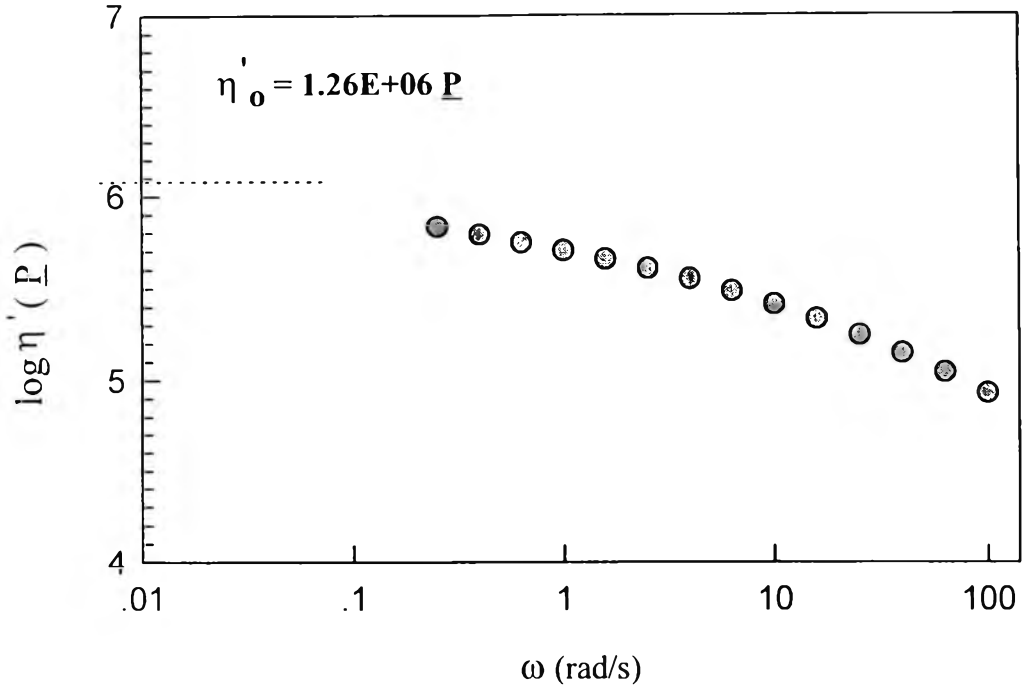

Figure 3.55 The viscosity as a function of the frequency of LLDPE (L2009F) melts at temperature of 190 °C.

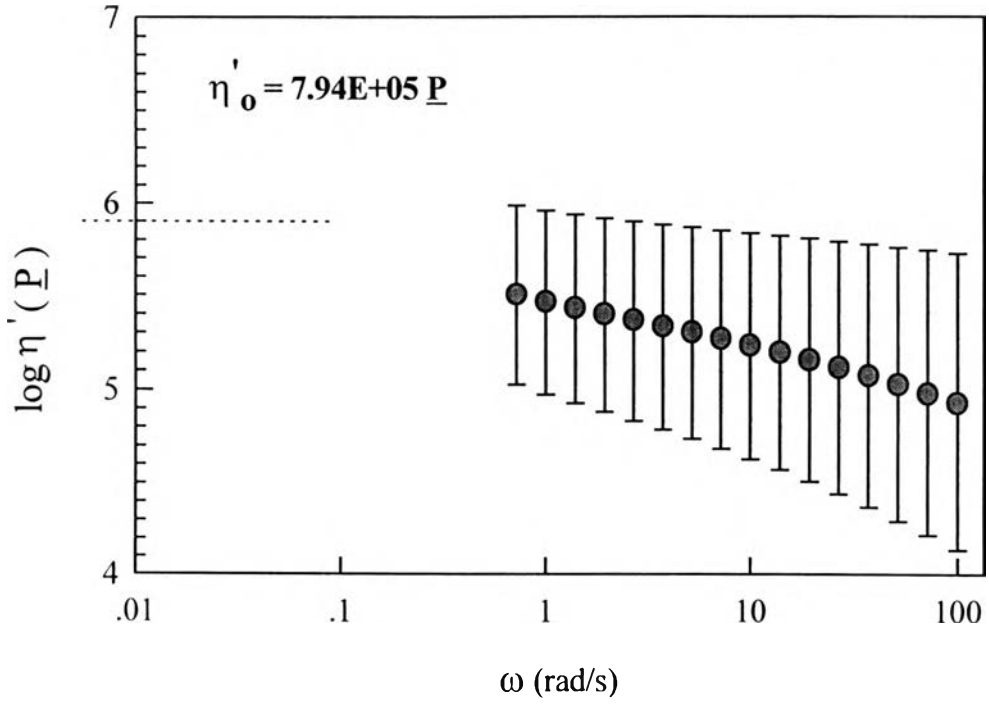

Figure 3.56 The viscosity as a function of the frequency of LLDPE (L2020F) melts at temperature of 190 °C.

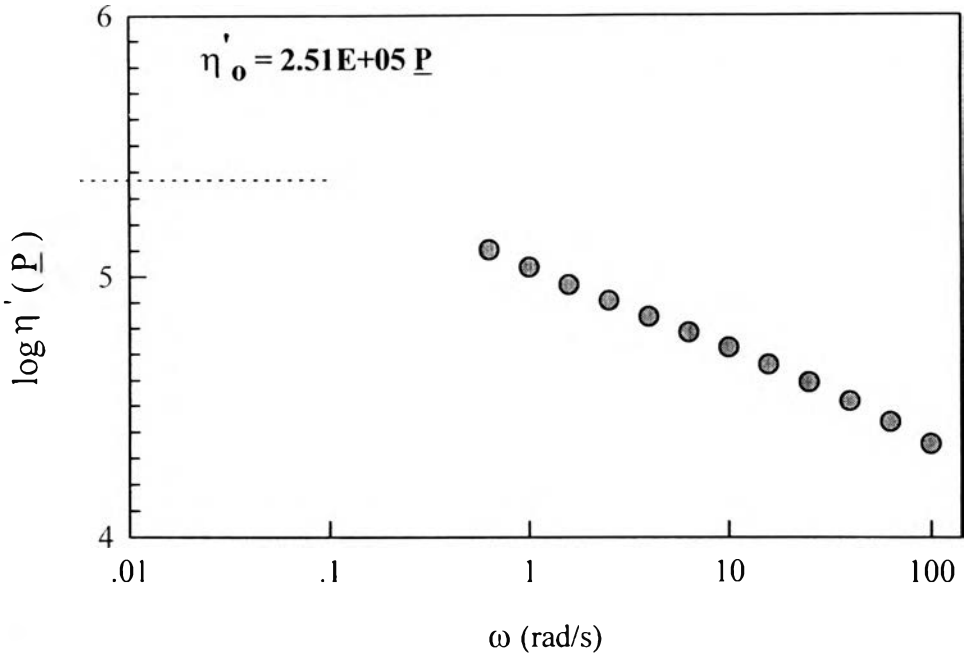

Figure 3.57 The viscosity as a function of the frequency of LLDPE (M3204RU) melts at temperature of 190 °C.

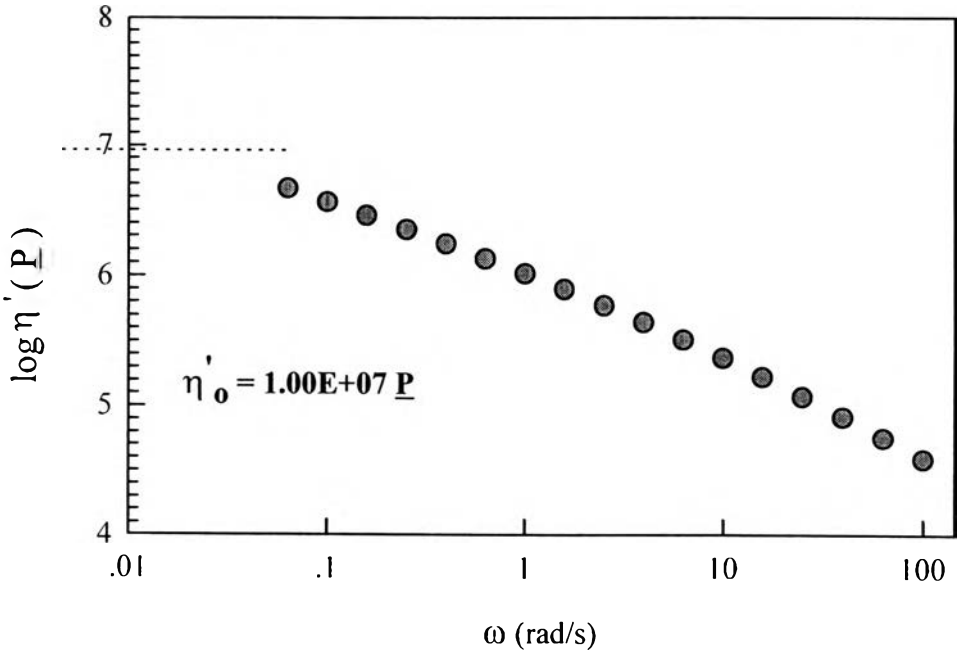

Figure 3.58 The viscosity as a function of the frequency of HDPE (H5604F) melts at temperature of 190 °C.

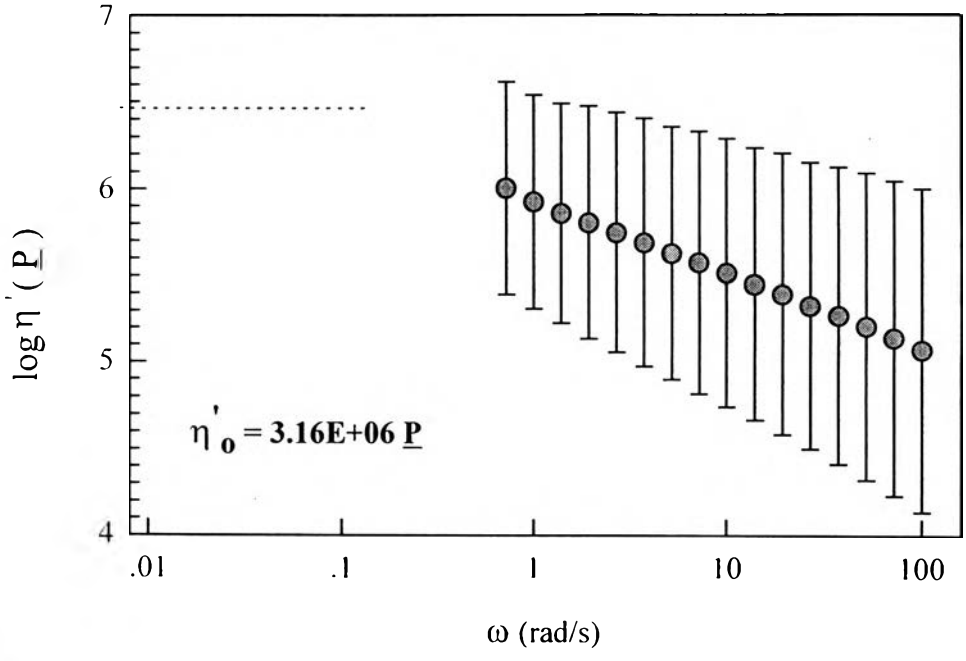

Figure 3.59 The viscosity as a function of the frequency of HDPE (H5690S) melts at temperature of 190 °C.

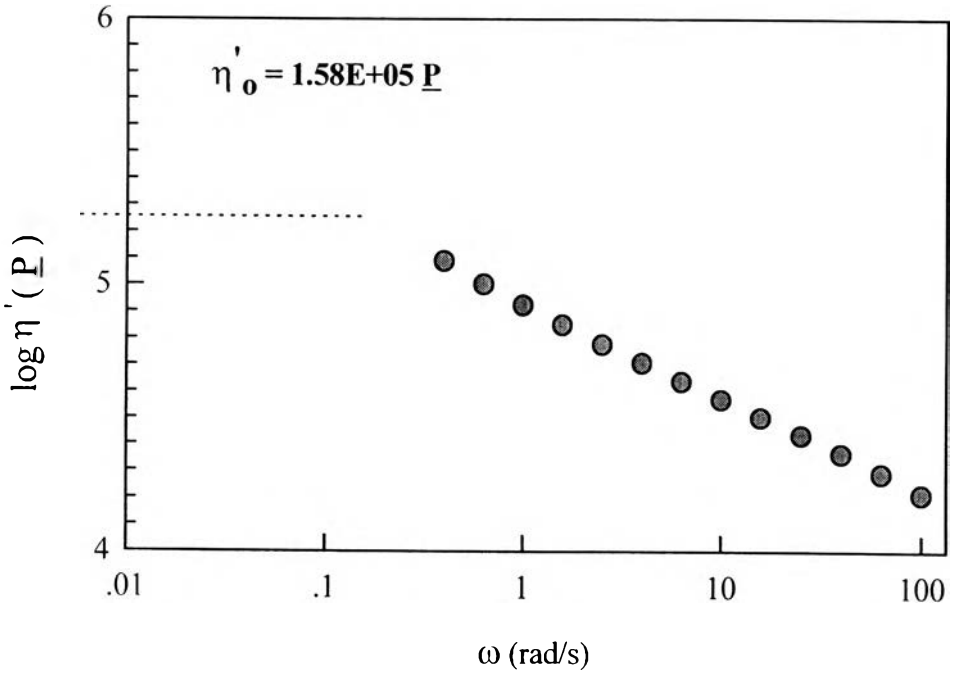

Figure 3.60 The viscosity as a function of the frequency of HDPE (H6205JU) melts at temperature of 190 °C.

3.3.5 The stress at the onset of the slip velocity (τ^*)

3.3.5.1Effect of Temperature. Figures 3.61-3.64 show the stress at the onset of the slip velocity for LLDPE (L2020F) melts at temperatures between 170-230 °C. Figures 3.65-3.67 show the stress at the onset of the slip velocity for HDPE (H5690S) melts at temperatures between 190-230 °C. The values of the stress at the onset of the slip velocity for LLDPE (L2020F) and HDPE (H5690S) are summarized in Table 3.3.2. From the results, the stress at the onset of the slip velocity decreases with temperature.

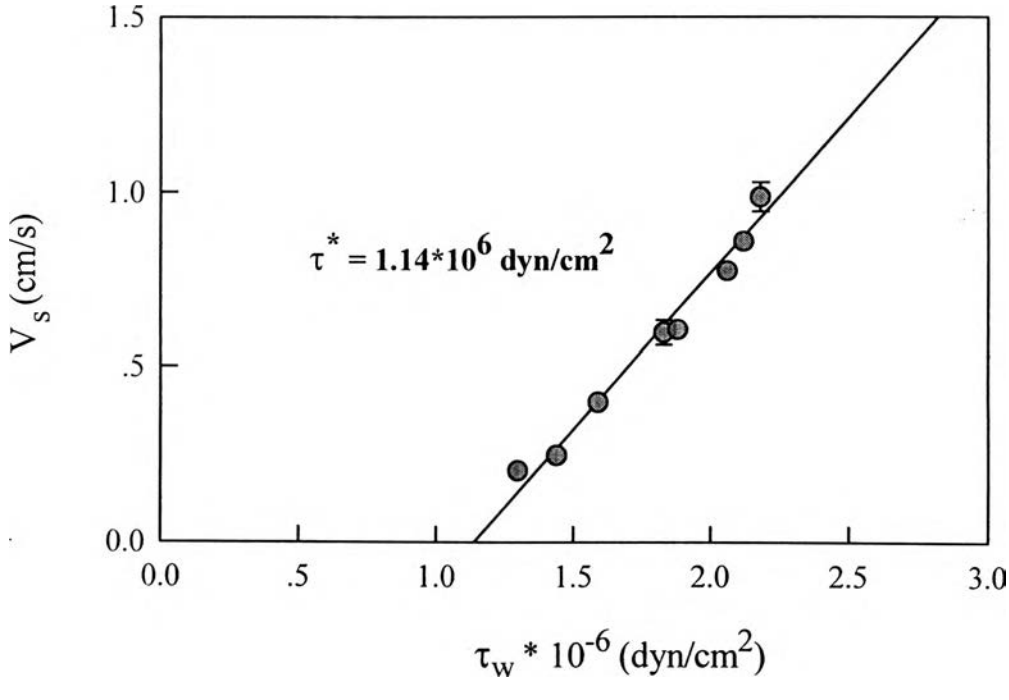

Figure 3.61 The slip velocity, V_S, as a function of the wall shear stress, τ_w, for LLDPE (L2020F) melts at temperature of 170 °C.

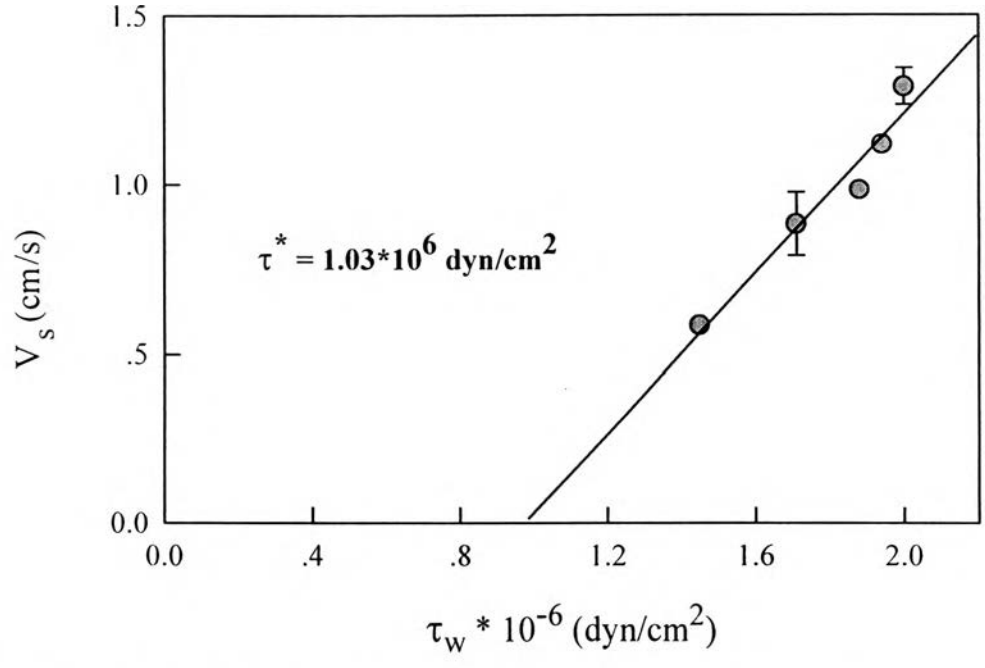

Figure 3.62 The slip velocity, V_S, as a function of the wall shear stress, τ_w, for LLDPE (L2020F) melts at temperature of 190 °C.

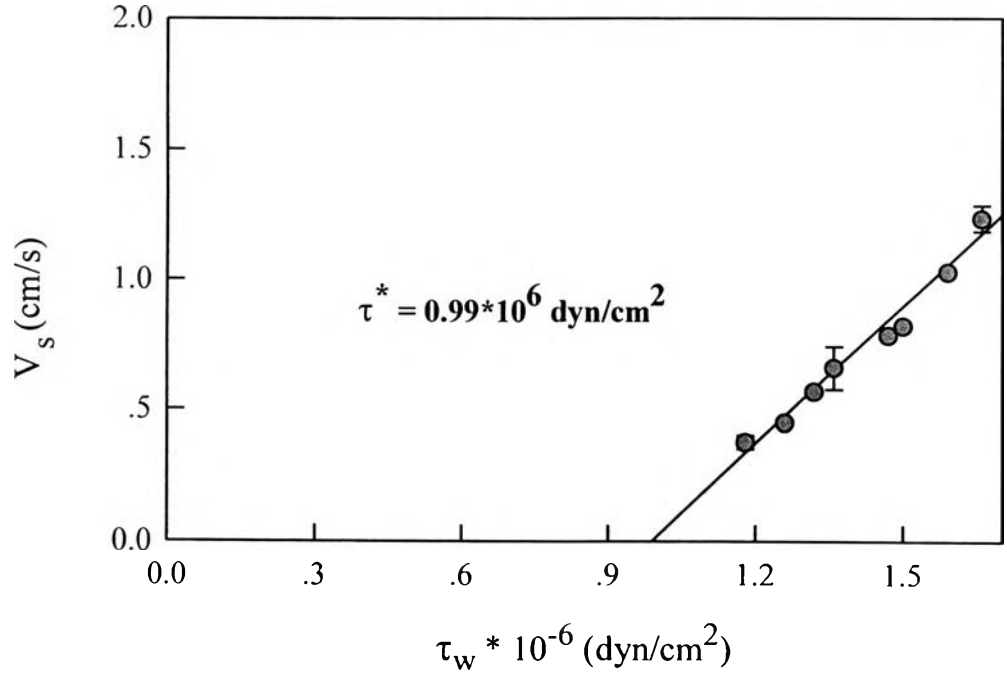

Figure 3.63 The slip velocity, V_S, as a function of the wall shear stress, τ_w, for LLDPE (L2020F) melts at temperature of 210 °C.

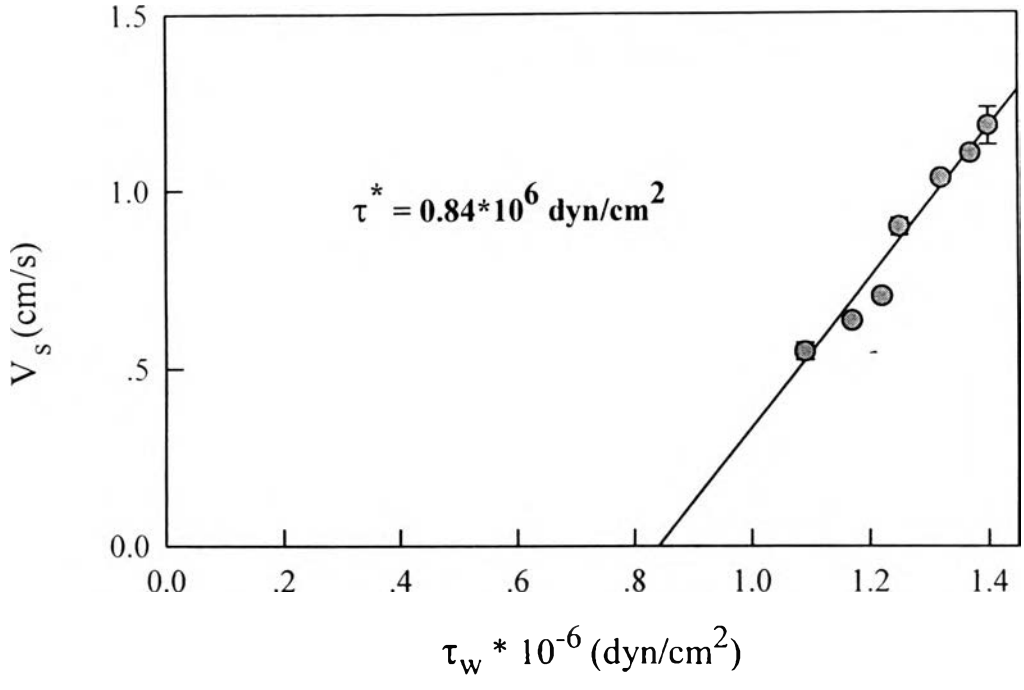

Figure 3.64 The slip velocity, V_S, as a function of the wall shear stress, τ_w, for LLDPE (L2020F) melts at temperature of 230 °C.

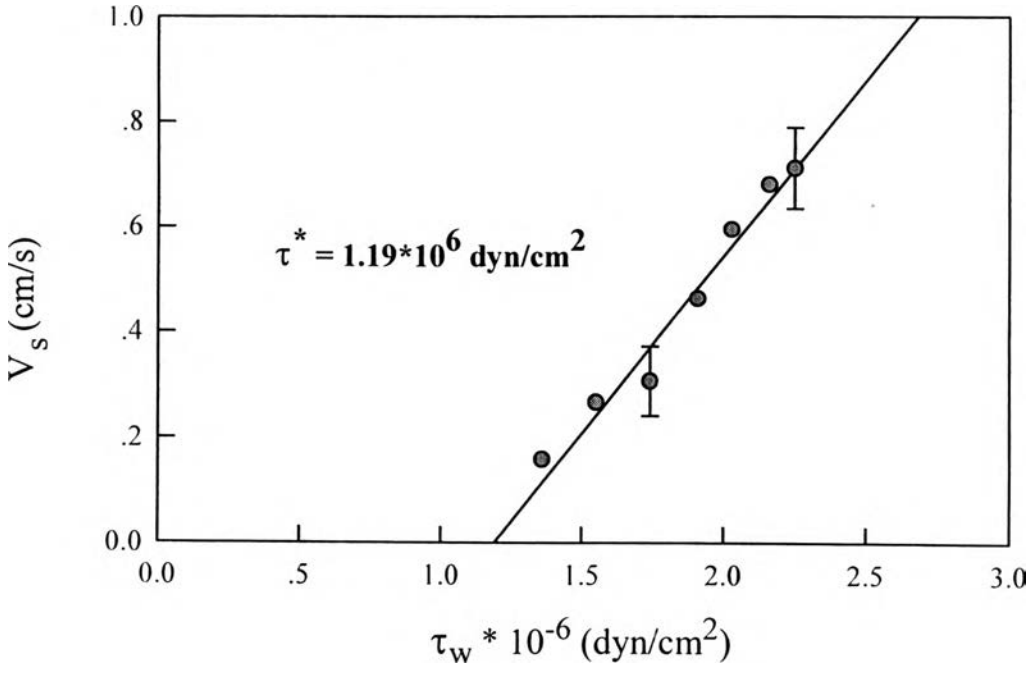

Figure 3.65 The slip velocity, V_S, as a function of the wall shear stress, τ_w, for HDPE (H5690S) melts at temperature of 190 °C.

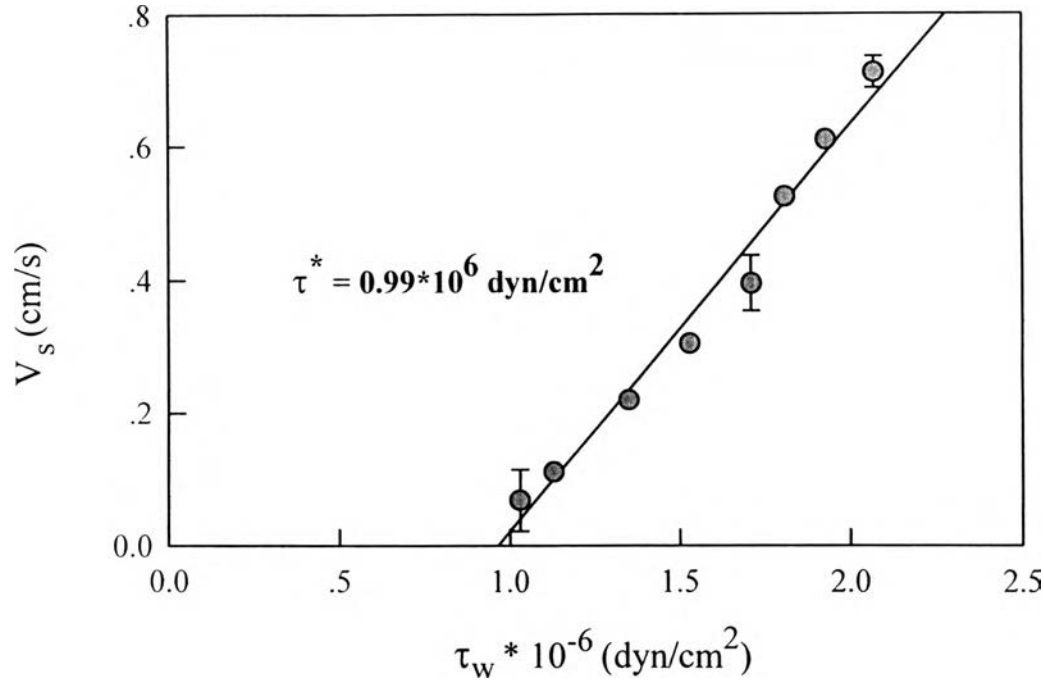

Figure 3.66 The slip velocity, V_S, as a function of the wall shear stress, τ_w, for HDPE (H5690S) melts at temperature of 210 °C.

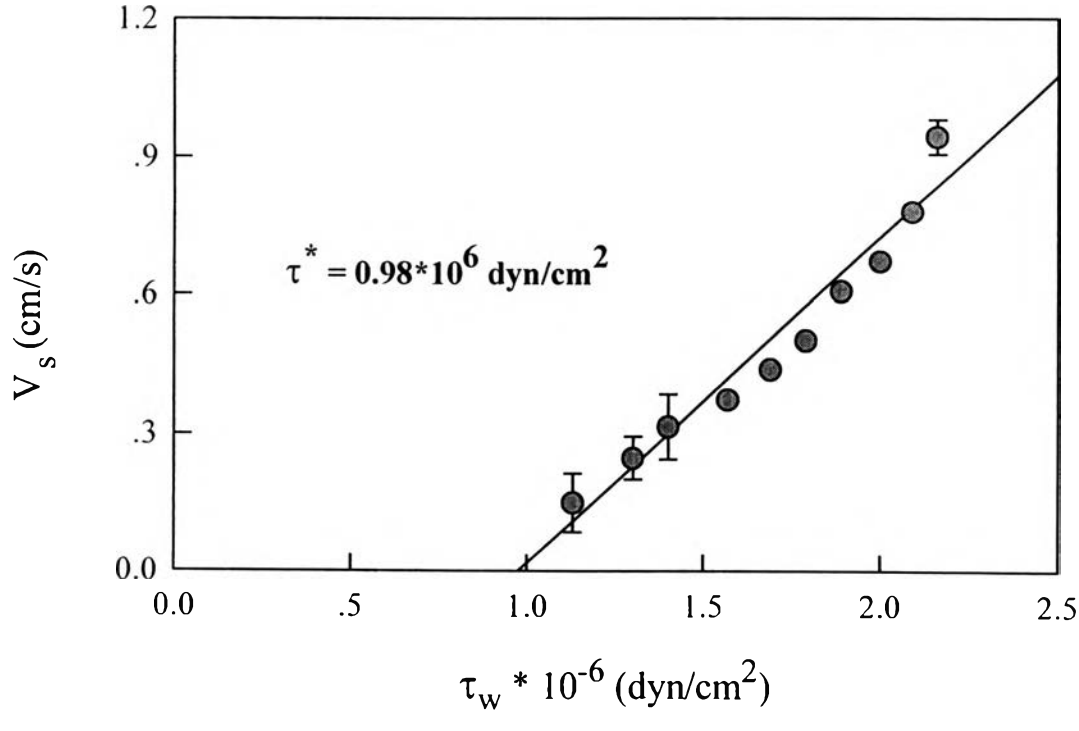

Figure 3.67 The slip velocity, V_S, as a function of the wall shear stress, τ_w, for HDPE (H5690S) melts at temperature of 230 °C.

3.3.5.2 Effect of Molecular Weight. Figures 3.68-3.70 show the stress at the onset of the slip velocity for LLDPE (L2009F, L2020F and M3204RU) melt at temperature of 190 °C. Figures 3.71-3.73 show the stress at the onset of the slip velocity for HDPE (H5604F, H5690S and H6205JU) melt at temperature of 190 °C. The values of the stress at the onset of the slip velocity of LLDPE (L2009F, L2020F and M3204RU) and HDPE (H5604F, H5690S and H6205JU) are summarized in Table 3.3.3. From this results, the stress at the onset of the slip velocity decreases with molecular weight.

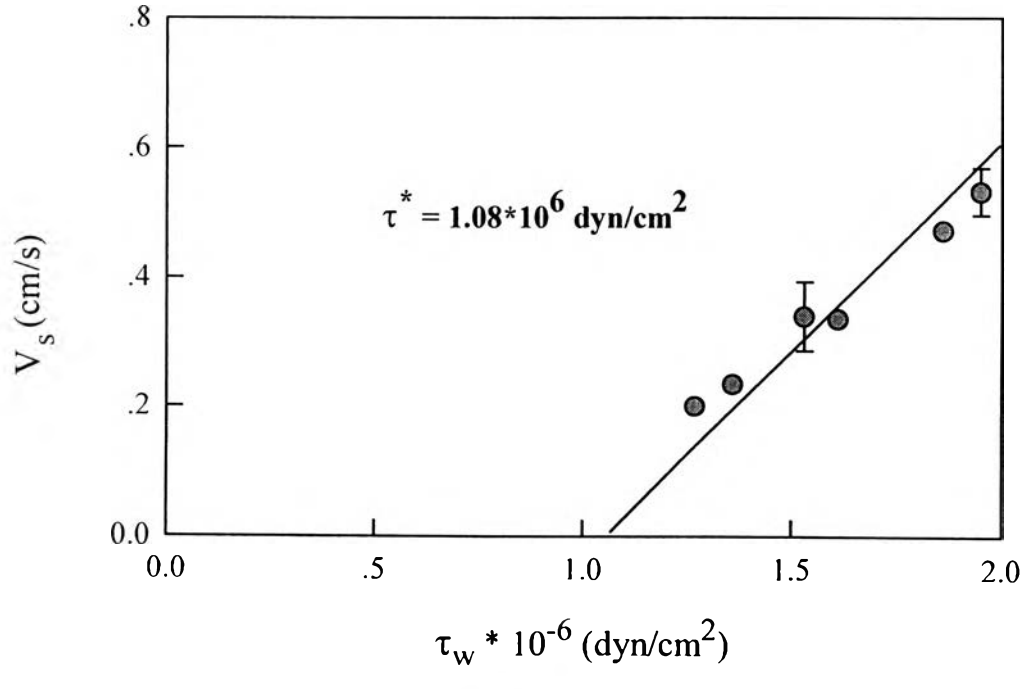

Figure 3.68 The slip velocity, V_S, as a function of the wall shear stress, τ_w, for LLDPE (L2009F) melts at temperature of 190 °C.

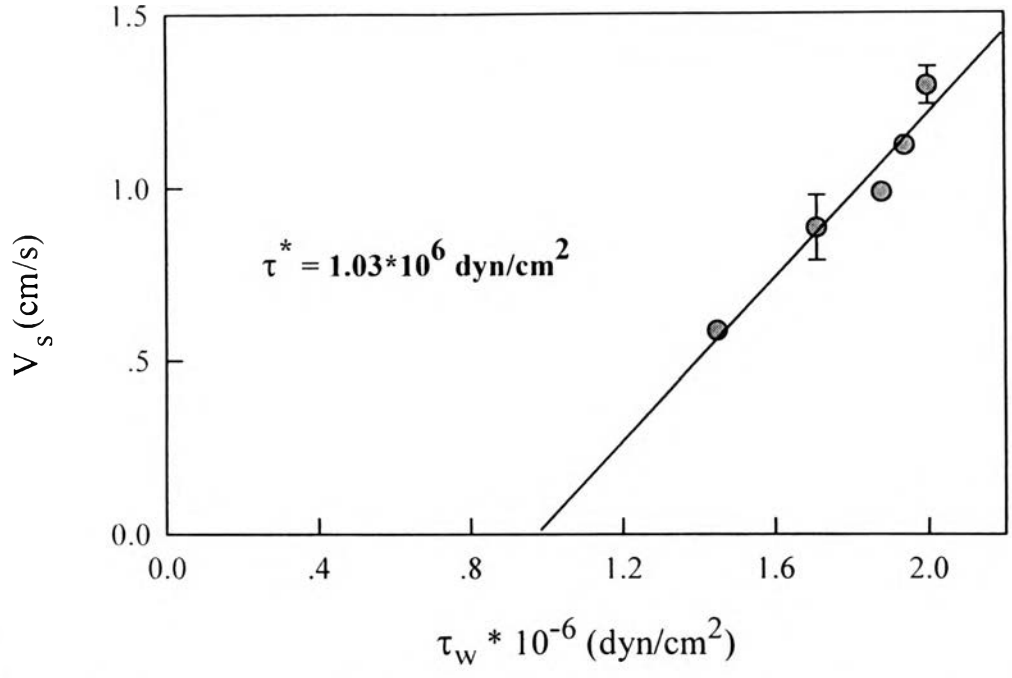

Figure 3.69 The slip velocity, V_S, as a function of the wall shear stress, τ_w, for LLDPE (L2020F) melts at temperature of 190 °C.

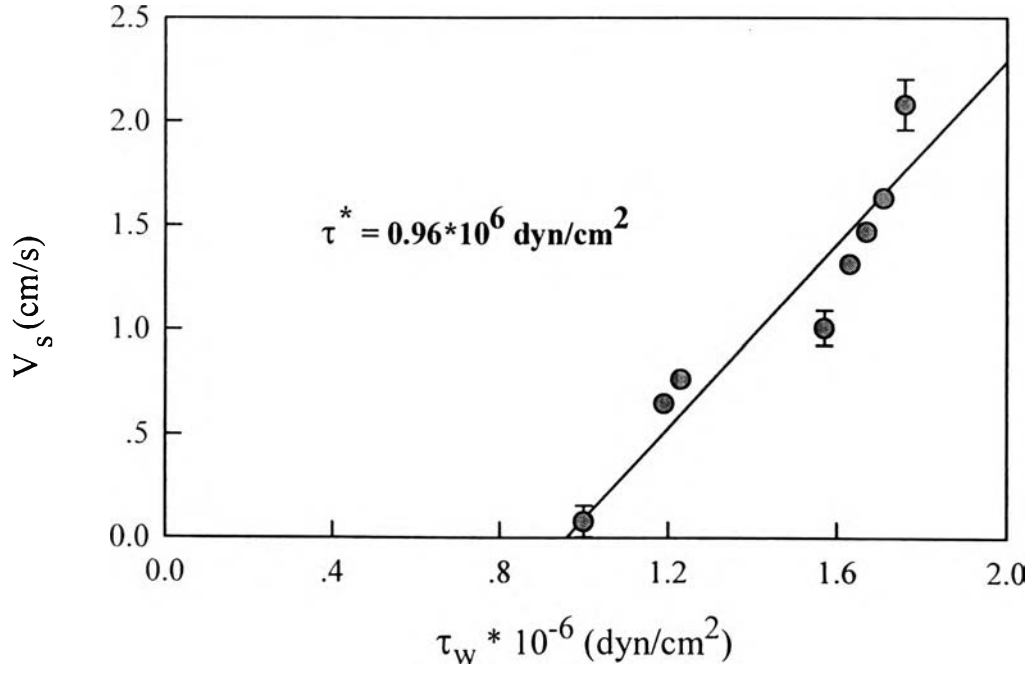

Figure 3.70 The slip velocity, V_S, as a function of the wall shear stress, τ_w, for LLDPE (M3204RU) melts at temperature of 190 °C.

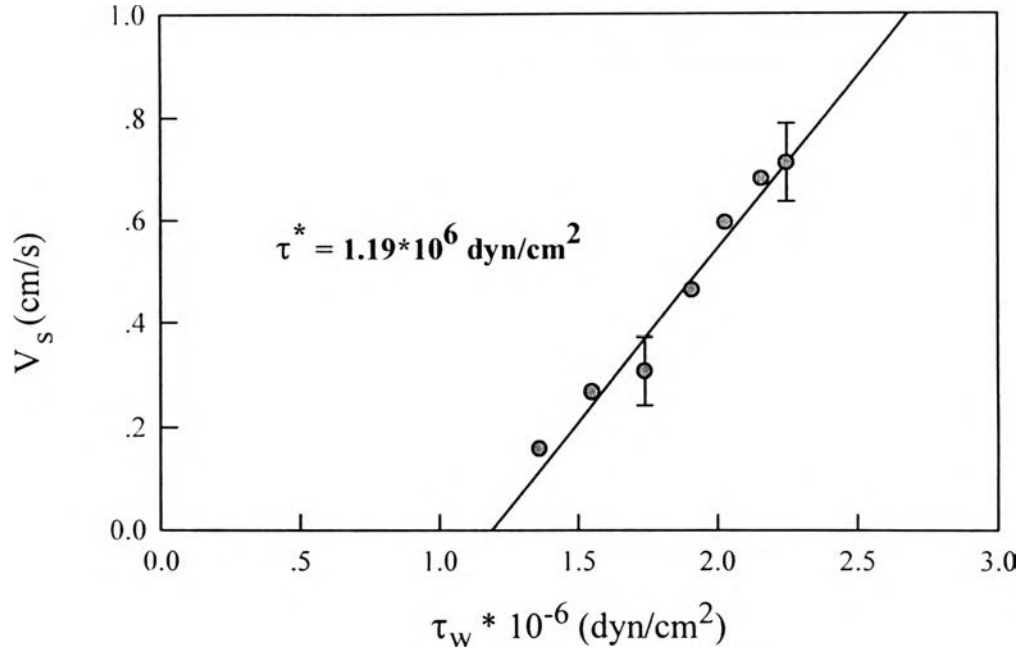

Figure 3.71 The slip velocity, V_S, as a function of the wall shear stress, τ_w, for HDPE (H5690S) melts at temperature of 190 °C.

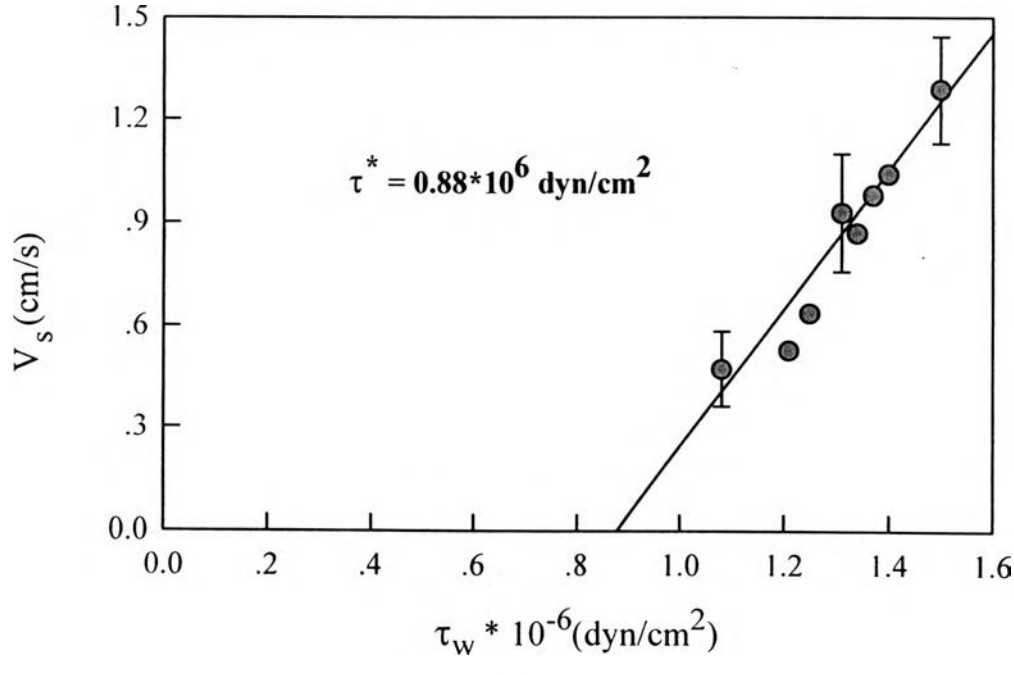

Figure 3.72 The slip velocity, V_S, as a function of the wall shear stress, τ_w, for HDPE (H6205JU) melts at temperature of 190 °C.

Table 3.3.2 The values of G^o_N , the zero complex viscosity, η^*_o, the zero shear viscosity, η'_o, and the stress at the onset of the slip velocity, τ^*, for LLDPE (L2020F) and HDPE (H5690S) at temperatures between 150-230 °C

Materials	T (°C)	G^o_N (dyn/cm^2)	η^*_o (P)	η'_o (P)	τ^* (dyn/cm^2)
L2020F	230	1.95E+07	6.31E+06	3.16E+05	0.84E+06
	210	1.88E+07	7.94E+06	6.31E+05	0.99E+06
	190	1.8E+07	1.00E+07	7.94E+05	1.03E+06
	170	1.72E+07	2.51E+07	1.00E+06	1.14E+06
	150	1.64E+07	3.98E+07	1.26E+06	*
H5690S	230	3.58E+07	1.26E+07	1.00E+06	0.98E+06
	210	3.44E+07	2.00E+07	1.58E+06	0.99E+06
	190	3.3E+07	2.51E+07	3.16E+06	1.19E+06
	170	3.16E+07	3.16E+07	5.01E+06	*
	150	3.01E+07	3.98E+07	6.31E+06	*

* entanglement regime

Table 3.3.3 The values of G^{o}_{N} , the zero complex viscosity, η^{*}_{o}, the zero shear viscosity, η_{o},and the stress at the onset of the slip velocity, τ^{*}, for LLDPE (L2009F, L2020F and M3204RU) and HDPE (H5604F, H5690S and H6205JU) at temperature of 190 °C of different molecular weights

Materials	MFI (g/10min)	M_w (g/mol)	G^{o}_{N} (dyn/cm^2)	η^{*}_{o} (P)	η_{o} (P)	τ^{*} (dyn/cm^2)
L2009F	0.9	87,000	1.7E+07	-	1.26E+06	1.08E+06
L2020F	2.0	60,700	1.8E+07	1.00E+07	7.94E+05	1.03E+06
M3204RU	5.0	33,000	1.7E+07	7.94E+06	2.51E+05	0.96E+06
H5604F	0.04	133,000	2.3E+07	6.31E+07	1.00E+07	*
H5690S	0.9	107,000	3.3E+07	2.51E+07	3.16E+06	1.19E+06
H6205JU	5.0	98,000	3.2E+07	-	1.58E+05	0.88E+06

- cannot be extrapolated

* entanglement regime

3.4 Effect of Temperature on Slip

3.4.1 Slip velocity

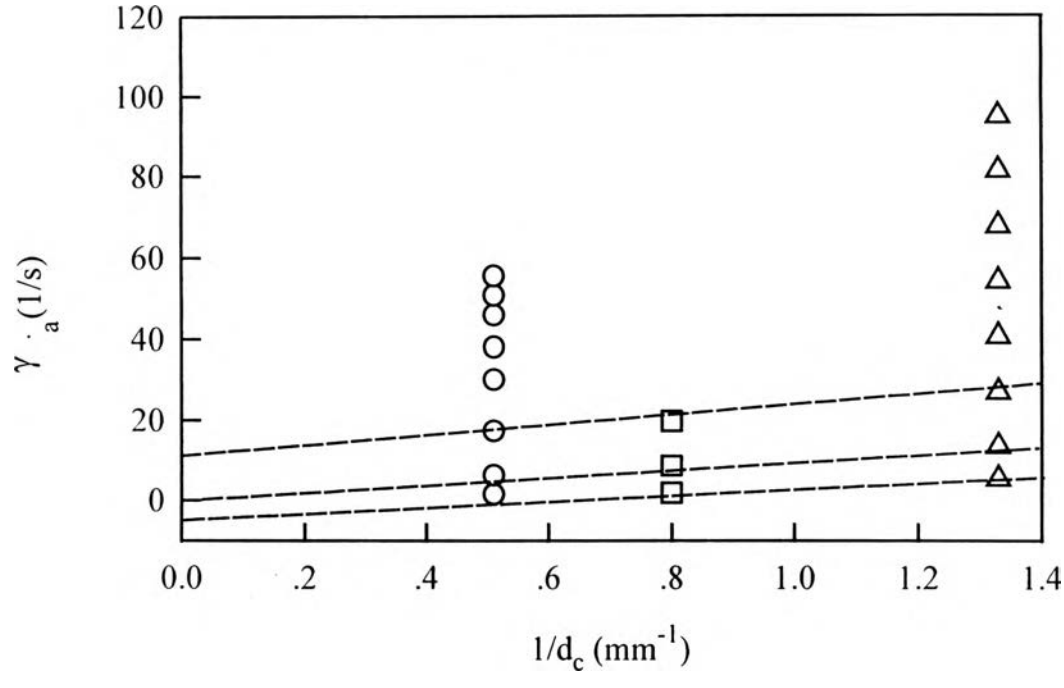

Figure 3.73 The apparent strain rate, $\gamma \cdot_a$, as a function of one over diameter of a capillary, $1/d_c$, for HDPE (H5690S) at temperature of 190 ^oC.

Figure 3.73 shows the determination of slip velocity by using the Mooney equation according to equation (2.16). Figure 3.73, shows the apparent strain rate, $\gamma \cdot_a$, as a function of the inverse of diameter of a capillary, $1/d_c$, of fixed wall shear stresses for HDPE (H5690S) at temperature of 190 ^oC. For each wall shear stress, a straight line can be drawn through the data points. We can obtain the slip velocity, V_S, from the slope and the apparent strain rate without slip, $\gamma \cdot_{a,S}$, from the intercept. The slip velocity as a function of the wall shear stress was determined for LLDPE (L2020F) and HDPE (H5690S) respectively. Figures 3.74 and 3.75 show the slip velocity, V_S, as a function of

the wall shear stress, τ_W, for LLDPE (L2020F) and HDPE (H5690S) at temperatures between 150-230 ^oC respectively. In Figures 3.74 and 3.45, we find that the values of slip fall in the range of 0.1-1.3 cm/s and the values of the wall shear stress, τ_W, fall in the range of $1.0*10^{-6}$ - $2.3*10^{-6}$ dyn/cm^2 . These values are in the same ranges of the wall slip for high density polyethylene melts in a capillary rheometer obtained by Hatzikiriakos and Dealy (1992) and the wall slip in viscous fluids and influence of materials of construction obtained by Ramamurthy (1986). Hatzikiriakos and Dealy (1992) found the values of the wall shear stress , τ_W, fall in the range of $1.0*10^{-6}$ - $3.0*10^{-6}$ dyn/cm^2 and the values of slip velocity fall in the range of 0.1-2.0 cm/s. From Figures 3.74-3.75, the slip velocity increases with temperature at a given wall shear stress (τ_W). This is because at high temperature the viscosity of the polymer melt is reduced, therefore a lower friction between entangled chains and adsorbed chains possibly occurs resulting in an ease of slippage.

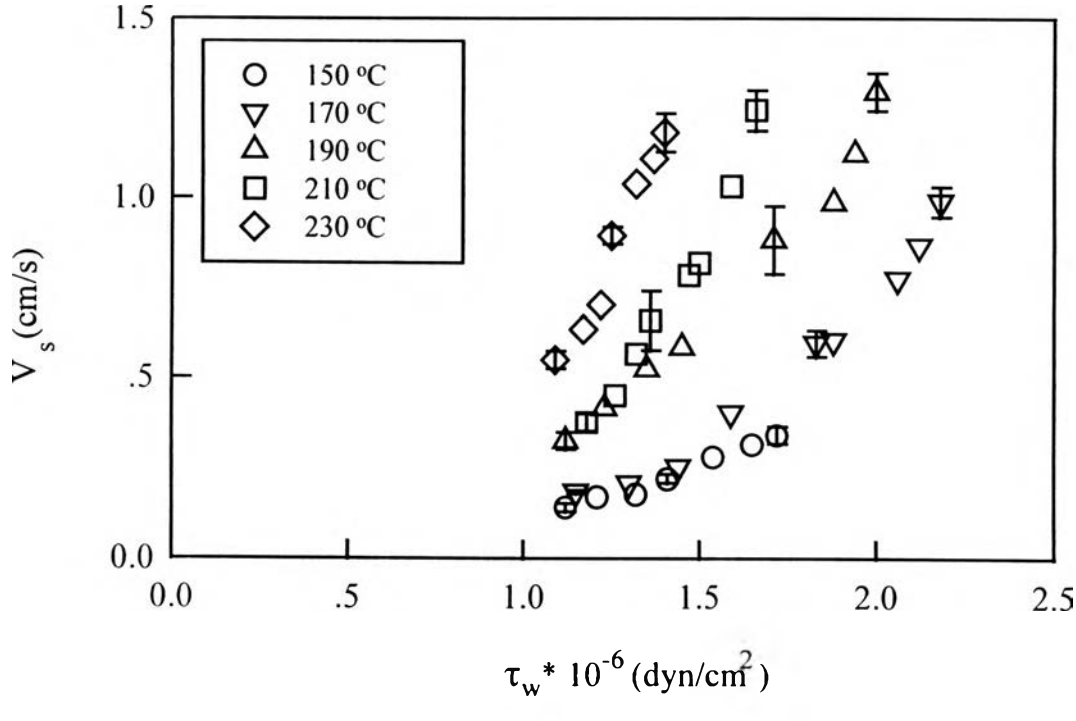

Figure 3.74 The slip velocity, V_S, as a function of the wall shear stress, τ_W, of LLDPE (L2020F) at temperatures of 150-230 ^oC.

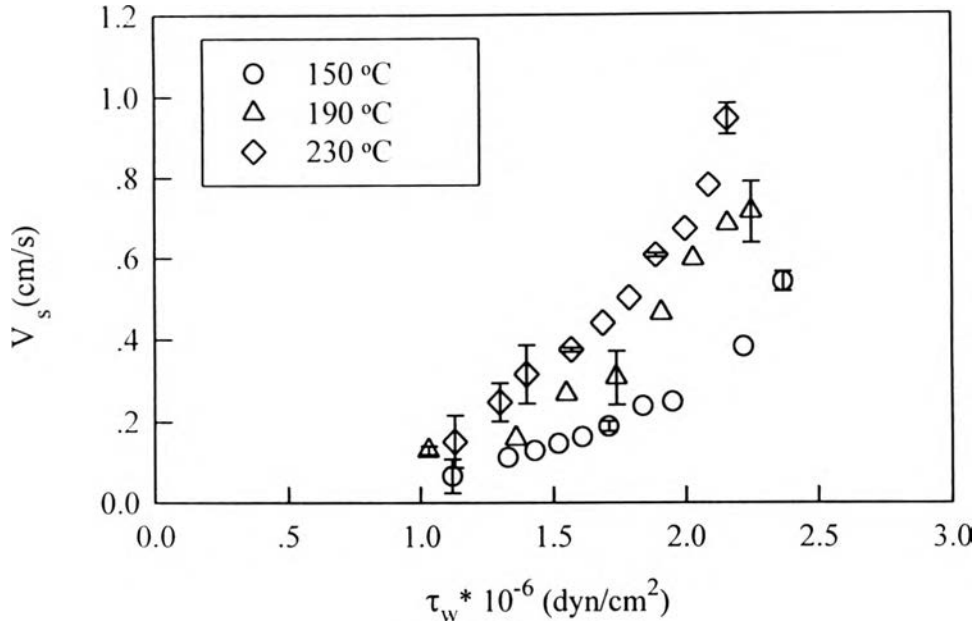

Figure 3.75 (a) The slip velocity, V_S, as a function of the wall shear stress, τ_W, of HDPE (H5690S) at temperatures of 150 °C, 190 °C and 230 °C.

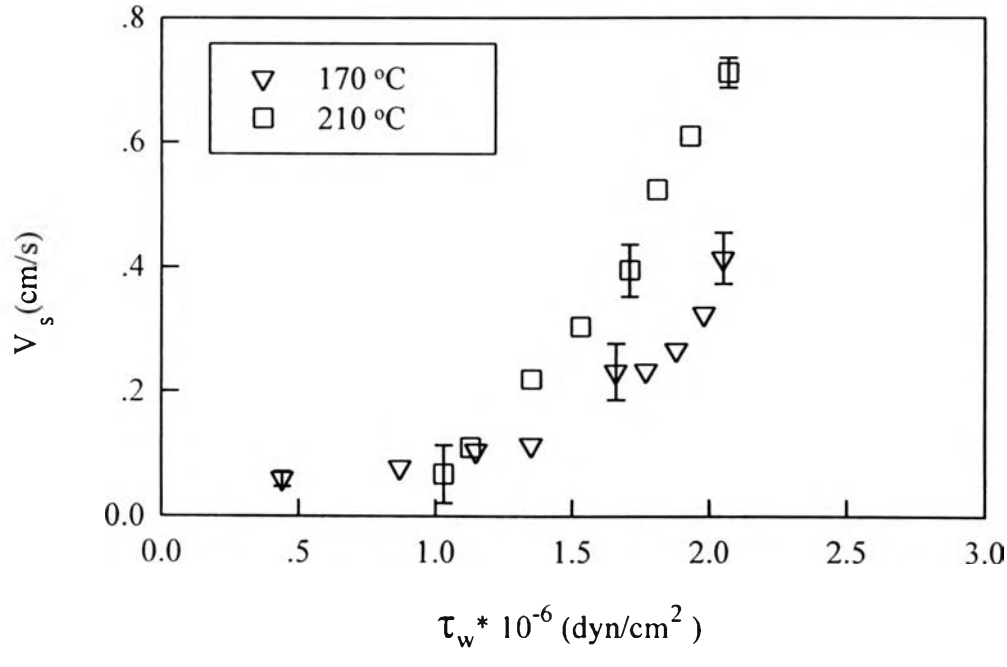

Figure 3.75 (b) The slip velocity, V_S, as a function of the wall shear stress, τ_W, of HDPE (H5690S) at temperatures of 170 °C and 210 °C.

For the quantitative analysis of the slip velocity, we can assume a power law model:

$$V_S = A\tau_W^m, \qquad (3.1)$$

where A is the slip coefficient, m is the exponent and τ_W is the wall shear stress. Figures 3.76 and 3.77 show the slip velocity, V_S, as a function of the wall shear stress, τ_W, on log-log plot for LLDPE (L2020F) and HDPE (H5690S) respectively. From Table 3.3.1, we find that the slip coefficient, A, increases strongly with temperature while the exponent, m, is practically independent on temperature. These results are in good agreement with the work of Hatzikiriakos and Dealy (1992). They investigated the effect of temperature on the slip velocity for high density polyethylene melts by assuming the power law model. They found that at several temperatures, the exponent m is practically constant, equal to 3.0; whereas the slip coefficient, A, is a function of temperature. The calculated values of the slip coefficient, A, and the exponent m for several temperatures and the critical wall shear stress, $\tau_{W,C}$, of LLDPE (L2020F) and HDPE (H5690S) are summarized in Table 3.3.1

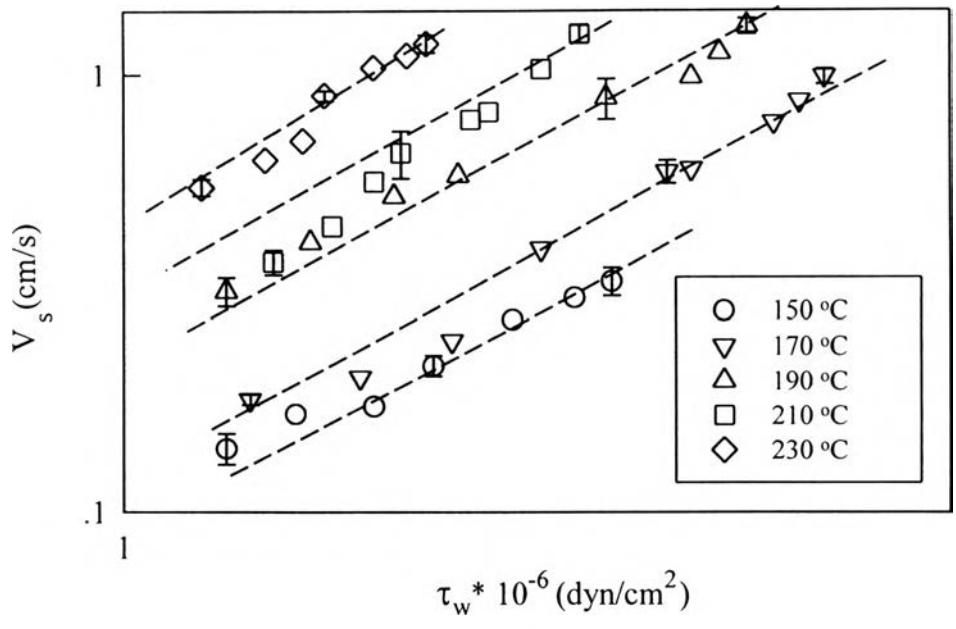

Figure 3.76 The slip velocity, V_S, as a function of the wall shear stress, τ_W, on log-log plot of LLDPE (L2020F) at temperatures of 150-230 ^{o}C.

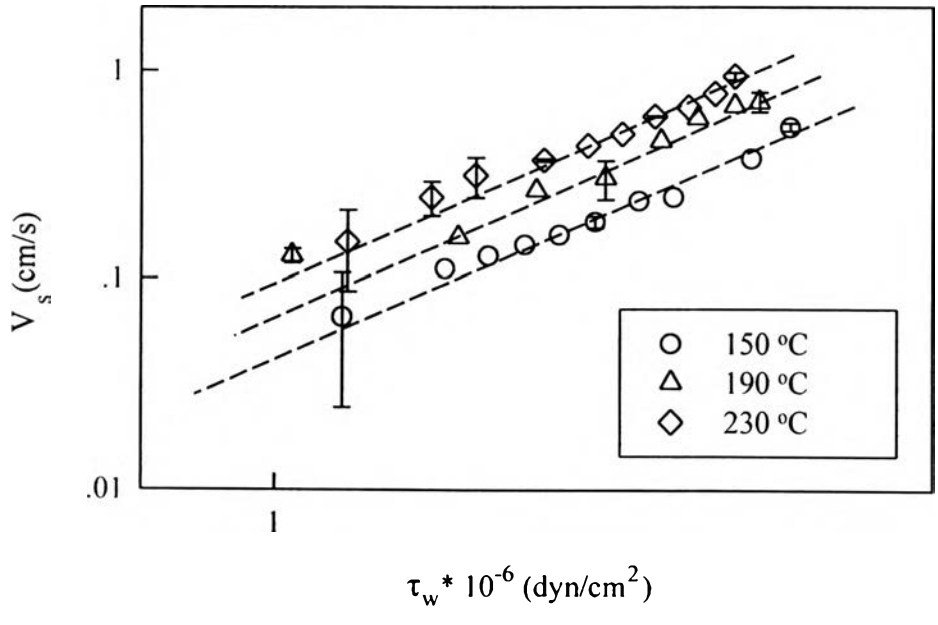

Figure 3.77 (a) The slip velocity, V_S, as a function of the wall shear stress, τ_W, log-log plot of HDPE(H5690S) at temperatures of 150 ^{o}C, 190 ^{o}C and 230 ^{o}C.

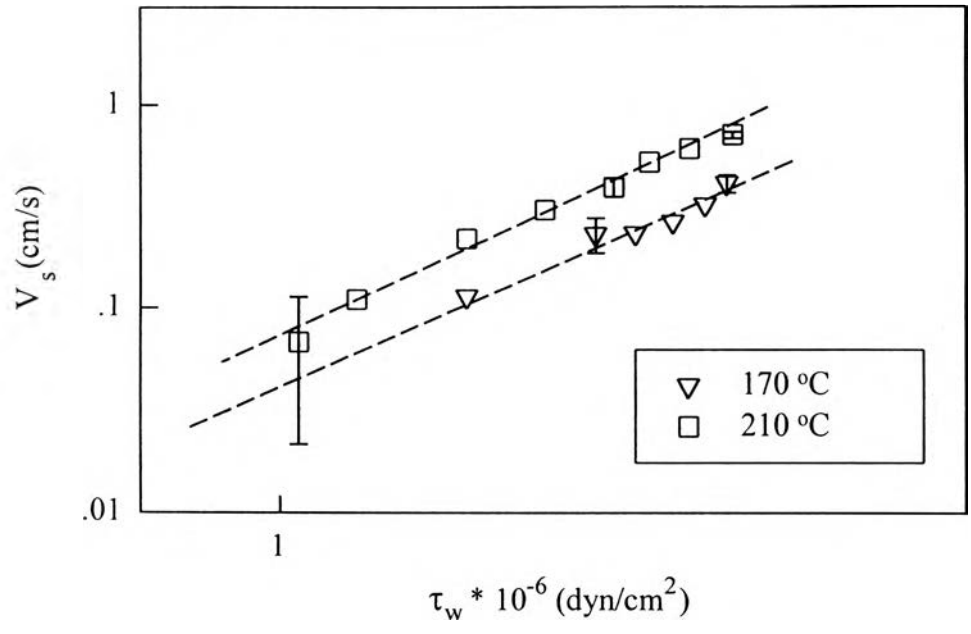

Figure 3.77 (b) The slip velocity, V_S, as a function of the wall shear stress, τ_W, on log-log plot of HDPE (H5690S) at temperatures of 170 °C and 210 °C.

Table 3.4.1 The values of power law parameters A, m and the onset of wall shear stress, τ^*, at temperatures between 150-230 ^oC for LLDPE (L2020F) and HDPE (H5690S)

Materials	Temperature (^oC)	$\tau^* \times 10^{-6}$ (dyn/cm^2)	A $(dyn.cm^{-2})^{-m}.cm/s$	m
LLDPE (L2020F)	150	-	0.08	3.00
	170	1.14	0.09	3.00
	190	1.03	0.20	3.00
	210	0.99	0.22	3.00
	230	0.84	0.40	3.00
HDPE (H5690S)	150	-	0.036	3.06
	170	-	0.042	3.00
	190	1.19	0.067	3.00
	210	0.99	0.800	3.02
	230	0.98	0.810	3.09

- entanglement regime

3.4.2 Extrapolation Length

Figures 3.78-3.82 show the extrapolation length, b, as a function of the slip velocity, V_S, at temperatures between 150-230 ^oC for LLDPE (L2020F) melts. Figures 3.83-3.86 show the extrapolation, b, as a function of the slip velocity, V_S, at temperatures between 170-230 ^oC of HDPE (H5690S) melts. The extrapolation length was calculated from equation (2.22). From these figures, we find that the values of the extrapolation length, b, fall in the range of 0.005-0.02 cm. This result is in qualitative agreement with the study of stick-slip transition at polymer melt/solid interfaces by Drda and Wang (1995). They found that the values of the extrapolation length, b, for high density polyethylene were approximately 0.02 cm. Our results are also in good agreement with the study of the role of attached polymer molecules in wall slip by L. L'eger and coworker (1997); they found that the values of the extrapolation length, b, fall in the range of 0.0002-0.05 cm. In the present results, we find that at low temperature the entanglement state in which the adsorbed chains are weakly elongated, occurs. At high temperature, the marginal state in which the adsorbed chains have been fully extended or disentangled, occurs as predicted by Brochard and de Gennes (1992). This is because at low temperature, there are many adsorbed chains attached to the surface assuming random coil configuration or they are weakly elongated; due to a relatively large friction coefficient they strongly reduce the slip velocity. But at high temperature, the adsorbed chains have been fully extended or disentangled; due to a lower friction coefficient, the extrapolation length increases linearly with the slip velocity.

The extrapolation length in marginal regime is predicted (Brochard and de Gennes 1992) to be

$$b = CV_S , \qquad (3.2)$$

where V_S is the slip velocity. The parameter C can be determined from the relation (3.3)

$$C = (\eta/\tau^*) . \qquad (3.3)$$

where η is the zero shear rate viscosity and τ^* is the stress at the onset of the slip velocity.

We find that the parameter C is slightly dependent on temperature. This is because the parameter C depends on the viscosity of the polymer melt. At high temperature the viscosity of the polymer melt is reduced therefore a lower friction between entangled chains and adsorbed chains occurs and therefore the decrease in the parameter C. The calculated values of the parameter C for several temperatures of LLDPE (L2020F) and HDPE (H5690S) are summarized in Table 3.3.2.

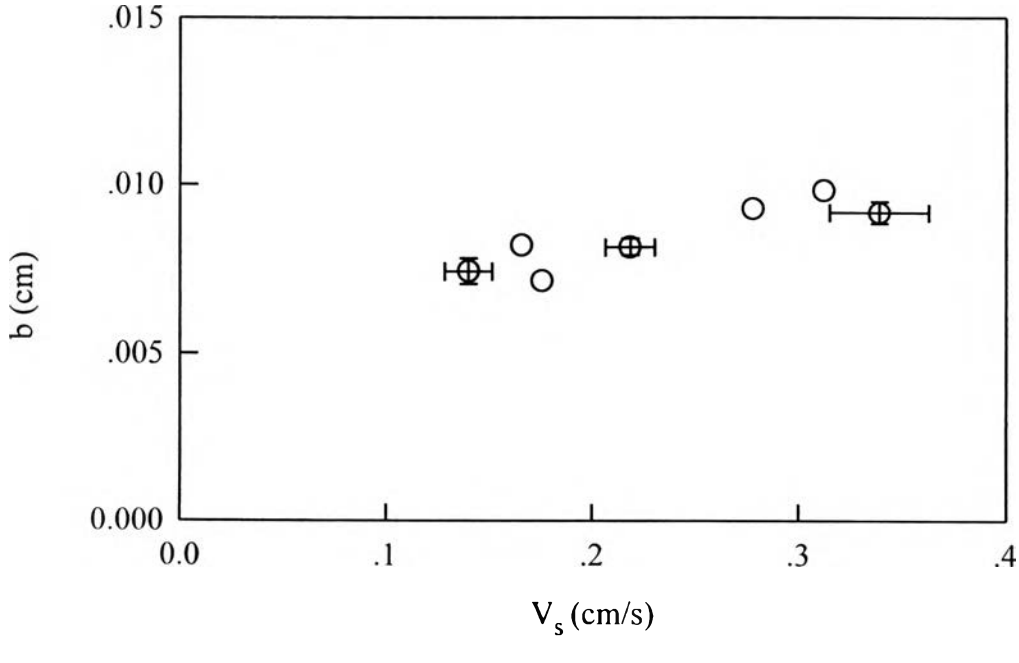

Figure 3.78 The extrapolation length, b, as a function of the slip velocity, V_S, of LLDPE (L2020F) at temperature of 150 ^oC.

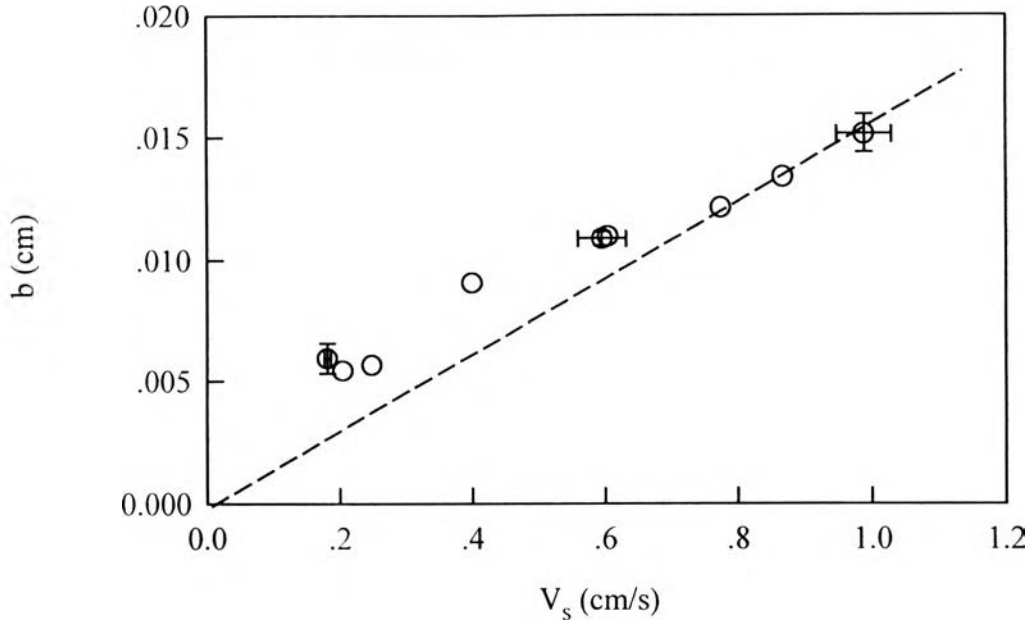

Figure 3.79 The extrapolation length, b, as a function of the slip velocity, V_S, of LLDPE (L2020F) at temperature of 170 ^oC.

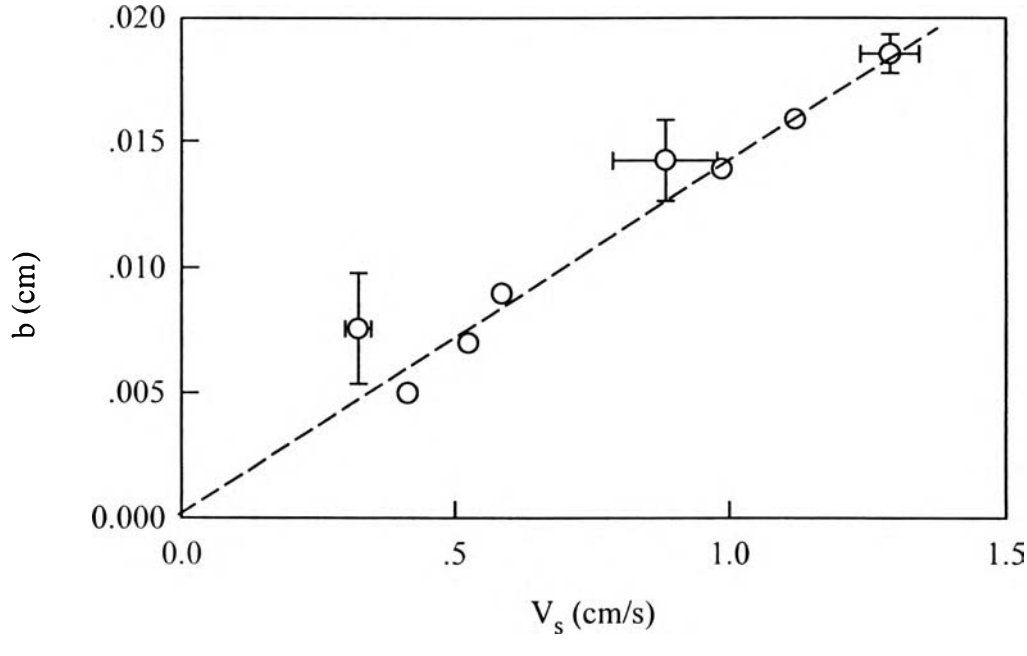

Figure 3.80 The extrapolation length, b, as a function of the slip velocity, V_S, of LLDPE (L2020F) at temperature of 190 ^oC.

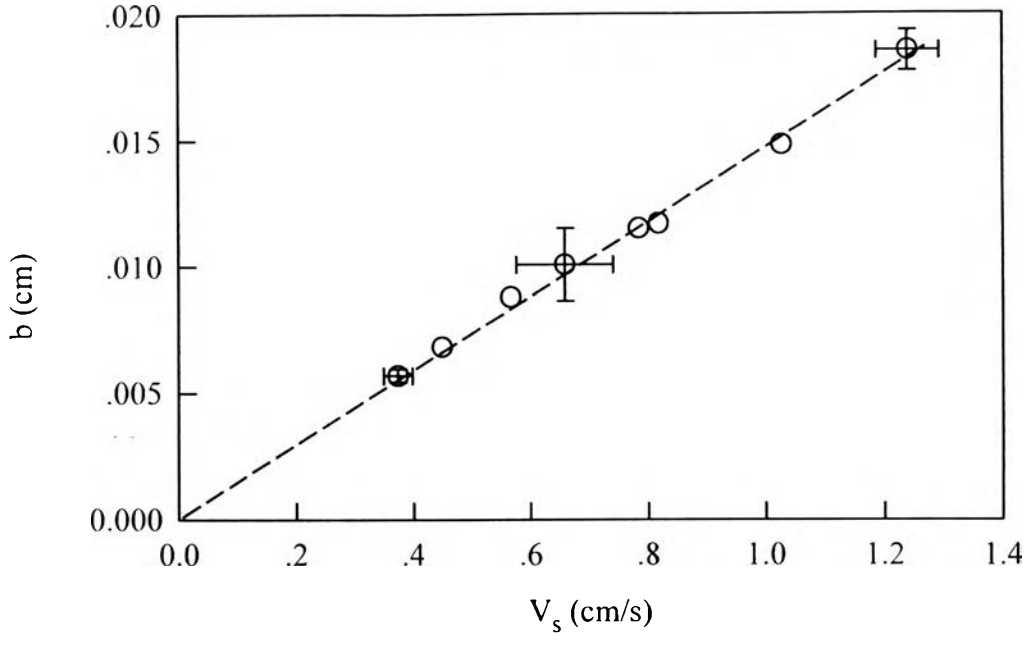

Figure 3.81 The extrapolation length, b, as a function of the slip velocity, V_S, of LLDPE (L2020F) at temperature of 210 ^oC.

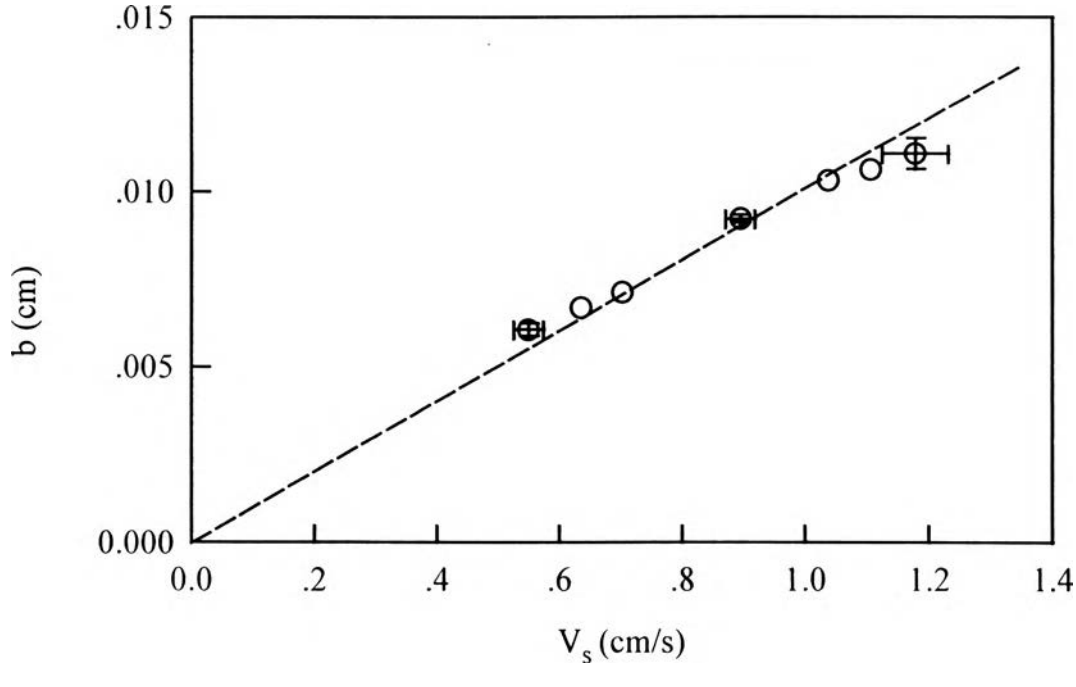

Figure 3.82 The extrapolation length, b, as a function of the slip velocity, V_S, of LLDPE (L2020F) at temperature of 230 ^oC.

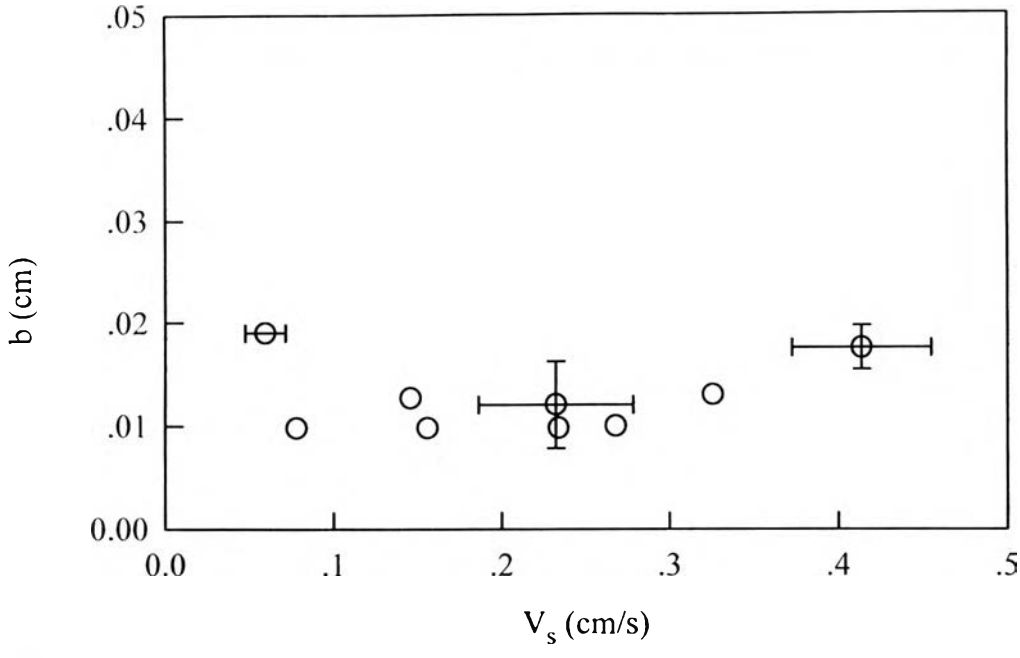

Figure 3.83 The extrapolation length, b, as a function of the slip velocity, V_S, of HDPE (H5690S) at temperature of 170 ^oC.

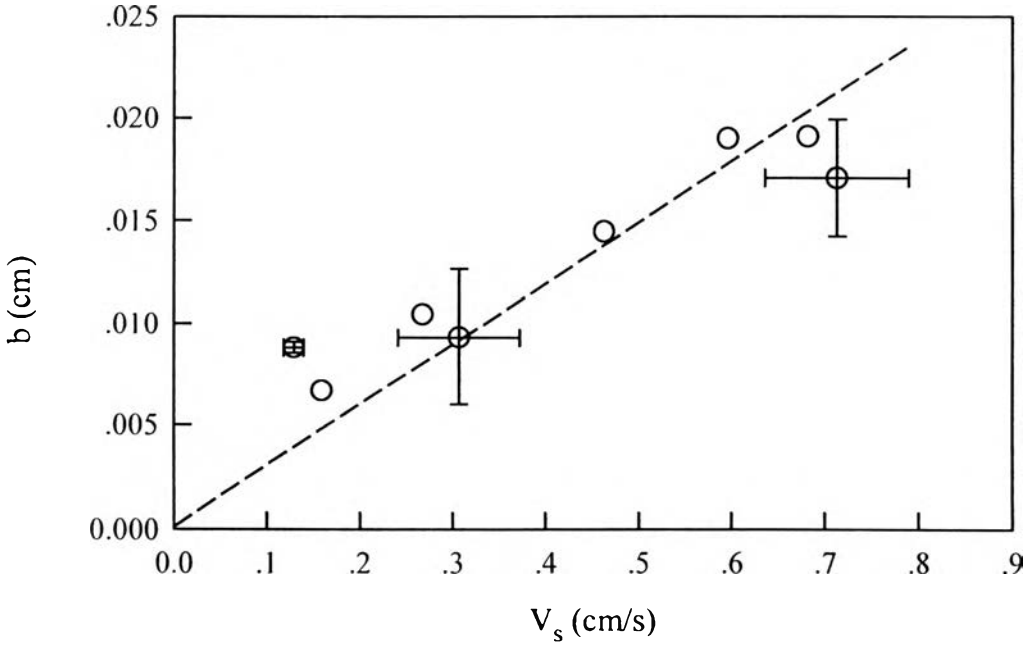

Figure 3.84 The extrapolation length, b, as a function of the slip velocity, V_S, of HDPE (H5690S) at temperature of 190 ^oC.

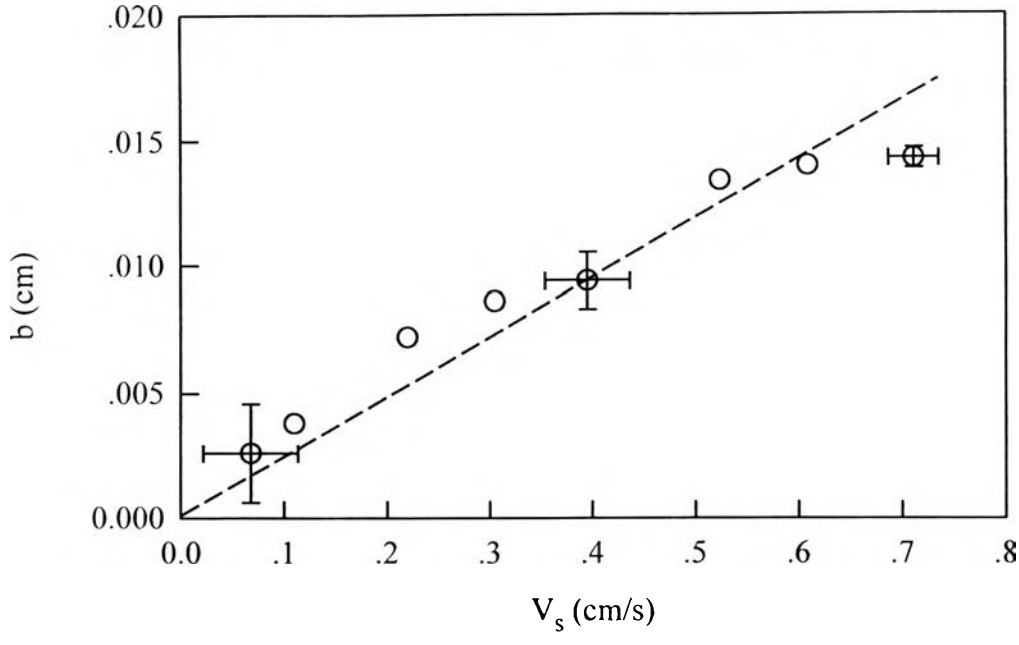

Figure 3.85 The extrapolation length, b, as a function of the slip velocity, V_S, of HDPE (H5690S) at temperature of 210 ^oC.

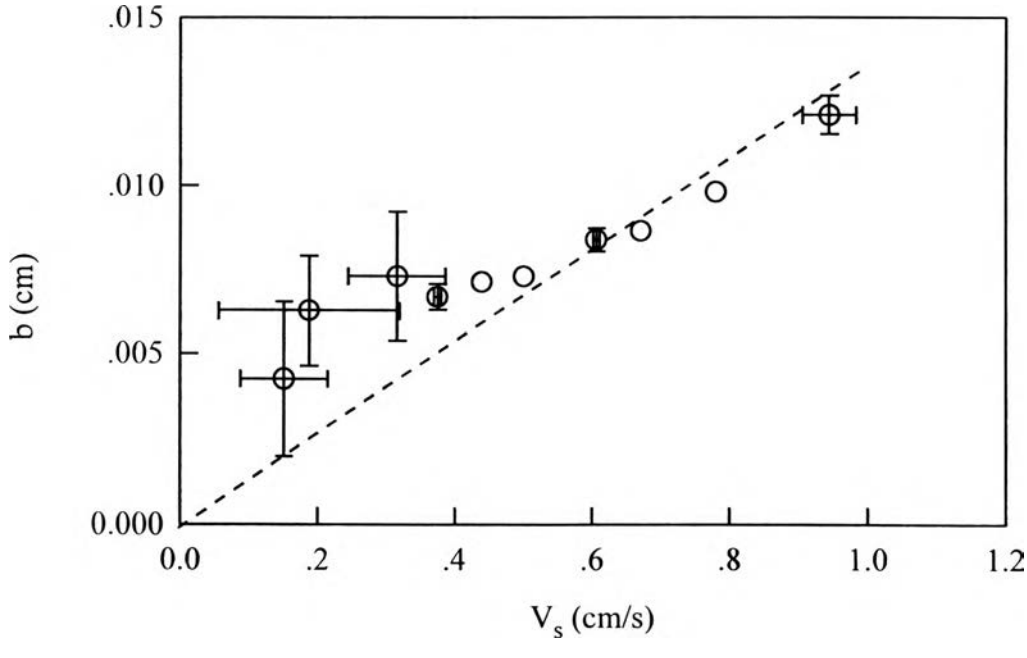

Figure 3.86 The extrapolation length, b, as a function of the slip velocity, V_S, of HDPE (H5690S) at temperature of 230 ^oC.

Table 3.4.2 The values of the parameter C, at different temperatures for LLDPE (L2020F) and HDPE (H5690S)

Materials	Temperature (^{o}C)	Parameter C
LLDPE (L2020F)	170	0.016
	190	0.016
	210	0.015
	230	0.014
HDPE (H5690S)	190	0.025
	210	0.022
	230	0.020

3.5 Effect of Molecular Weight on Slip

3.5.1 Slip velocity

Figures 3.87 and 3.88 show the slip velocity, V_S, as a function of wall shear stress, τ_W, for LLDPE (L2009F, L2020F and M3204RU) and HDPE (H5604F, H5690S and H6205JU) of different molecular weights respectively. We find that the slip velocity decreases with molecular weight. This is because the polymer chains of a higher molecular weight are longer and there are more entanglement loci and therefore slip decreases with molecular weight. A similar effect occurs in the study of molecular characteristics of wall slip for high density polyethylene by Hatzikiriakos and Dealy (1992).

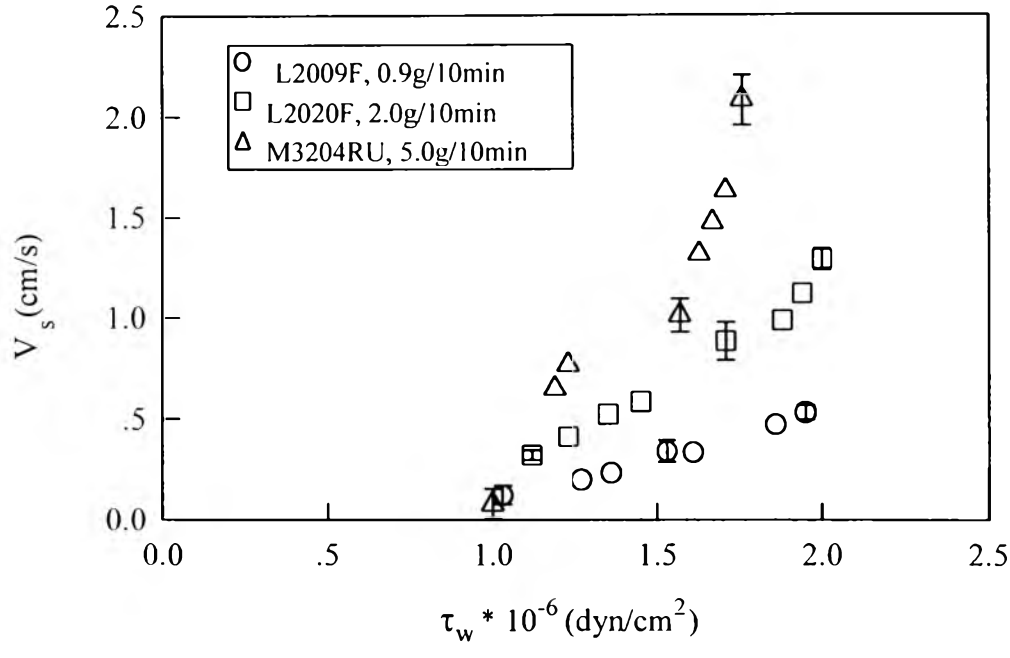

Figure 3.87 The slip velocity, V_S, as a function of the wall shear stress, τ_W, of LLDPE of different molecular weights.

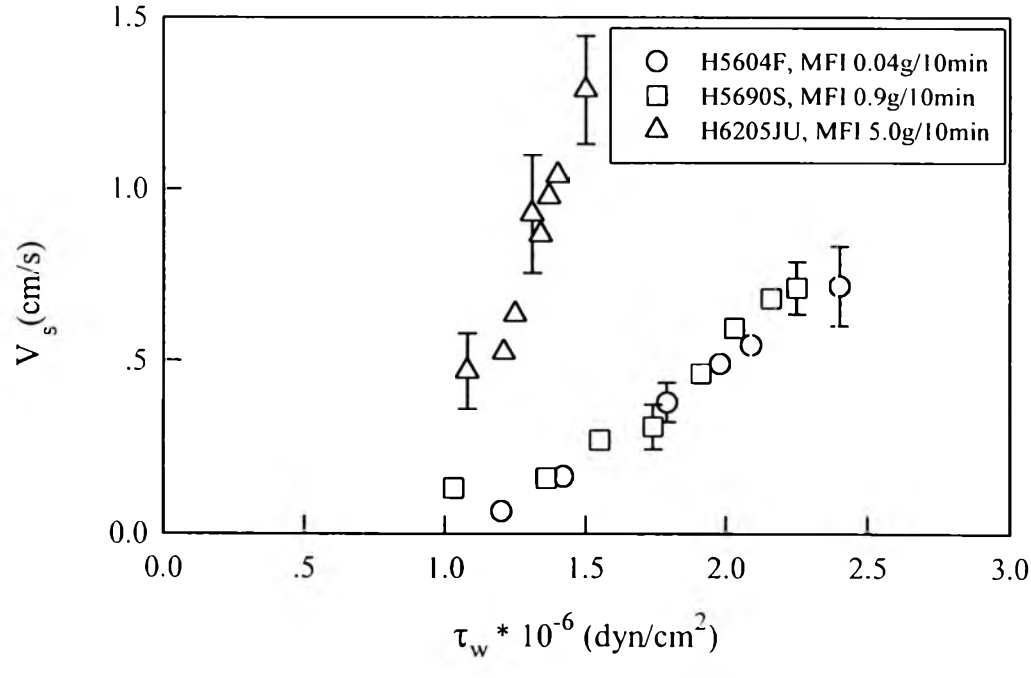

Figure 3.88 The slip velocity, V_S, as a function of the wall shear stress, τ_W, of HDPE of different molecular weights.

The slip velocity can be assumed to follow a power law according to equation (3.1). Figures 3.89 and 3.90 show the slip velocity, V_S, as a function of the wall shear stress, τ_W, on log-log plot for LLDPE (L2009F, L2020F and M3204RU) and HDPE (H5604F, H5690S and H6205JU) respectively. We find that the slip coefficient, A, and the exponent m increase with molecular weight and depends on molecular structure. This is because a branched polymer will have a larger friction coefficient between the entanglement loci than a linear polymer chain. Therefore slip is easier to occur for the linear chain. The calculated values of slip coefficient, A, and the exponent, m, of different molecular weights of LLDPE and HDPE are summarized in Table 3.4.1.

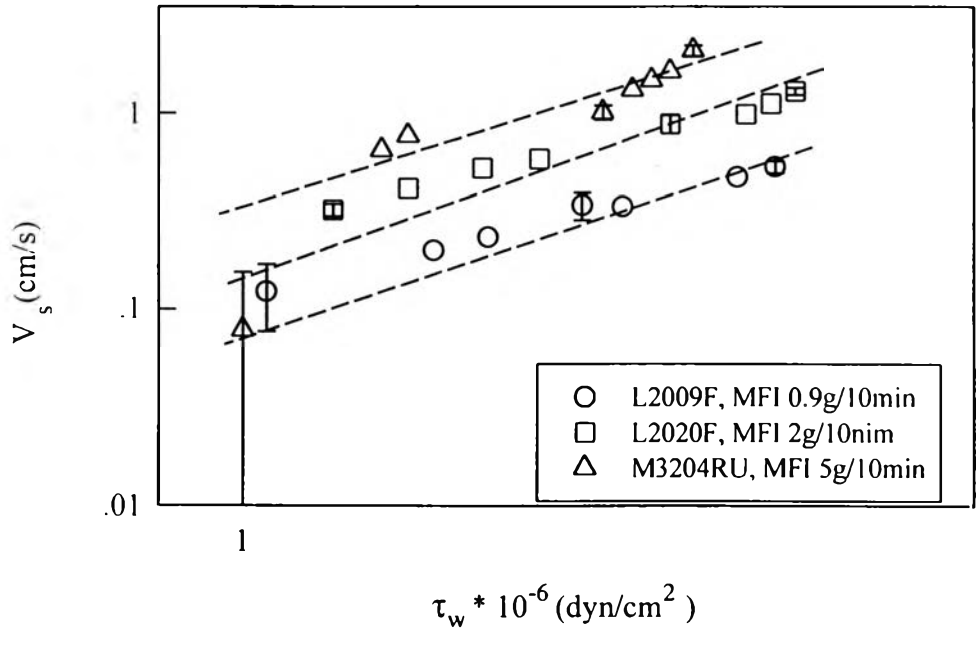

Figure 3.89 The slip velocity, V_S, as a function of the wall shear stress, τ_W, on log-log plot of LLDPE of different molecular weights.

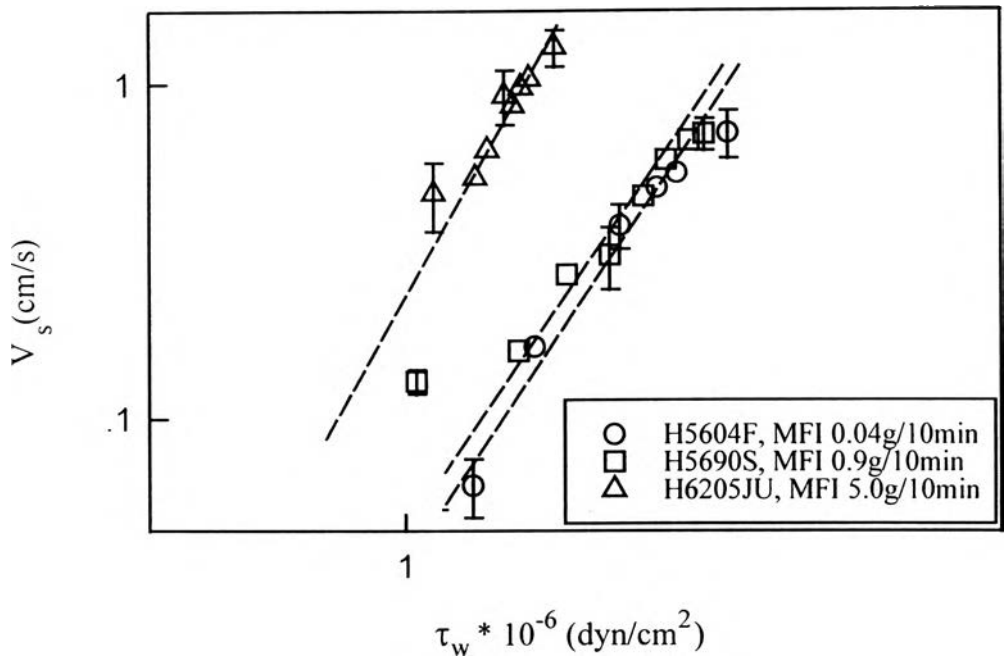

Figure 3.90 The slip velocity, V_S, as a function of the wall shear stress, τ_W, on log-log plot of HDPE of different molecular weights.

Table 3.5.1 The values of power law parameters A and m at the temperature of 190 ^oC for LLDPE and HDPE of different molecular weights

Materials	M_W (g/mol)	m	A $(dyn.cm^{-2})^{-m}.cm/s$
L2009F	87,000	2.20	0.12
L2020F	60,700	3.00	0.20
M3204RU	33,000	3.80	0.22
H5604F	133,000	3.05	0.057
H5690S	18,000	3.15	0.062
H6205JU	10,700	3.49	0.295

3.5.2 Extrapolation Length

Figures 3.90-3.92 show the extrapolation length, b. as a function of the slip velocity, V_S, at the temperature of 190 ^oC for HDPE (H5604F, H5690S and H6205JU) melts of different molecular weights. Figures 3.93-3.95 show the extrapolation length, b, as a function of the slip velocity, V_S, at the temperature of 190 ^oC for LLDPE (L2009F, L2020F and M3204RU) melts of different molecular weights. We find that at a high molecular weight the entanglement state is more likely and is seen to occur because there are many entanglement loci in high molecular weight and a larger friction coefficient between the entangled chains.

The extrapolation length in marginal state was calculated from equation (3.2). We find that the parameter C depends critically on molecular weight. This is because for high molecular weight, there are more entanglement loci due to large viscosity between the entangled chains therefore the parameter C increases with molecular weight. The calculated values of the parameter C of different molecular weights are summarized in Table 3.4.2

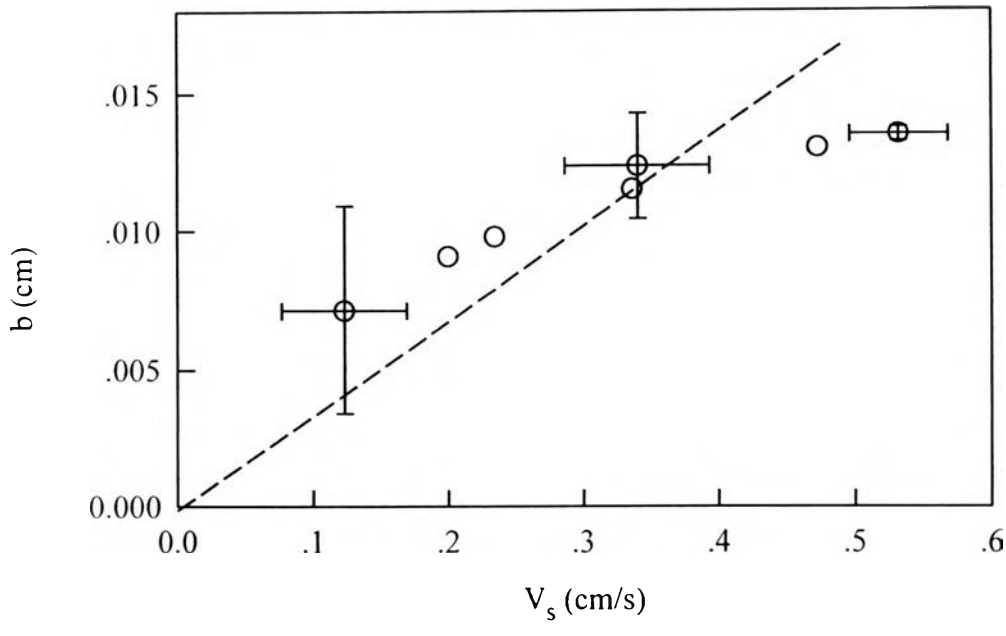

Figure 3.91 The extrapolation length, b, as a function of the slip velocity, V_S, at temperature of 190 ^oC for LLDPE (L2009F).

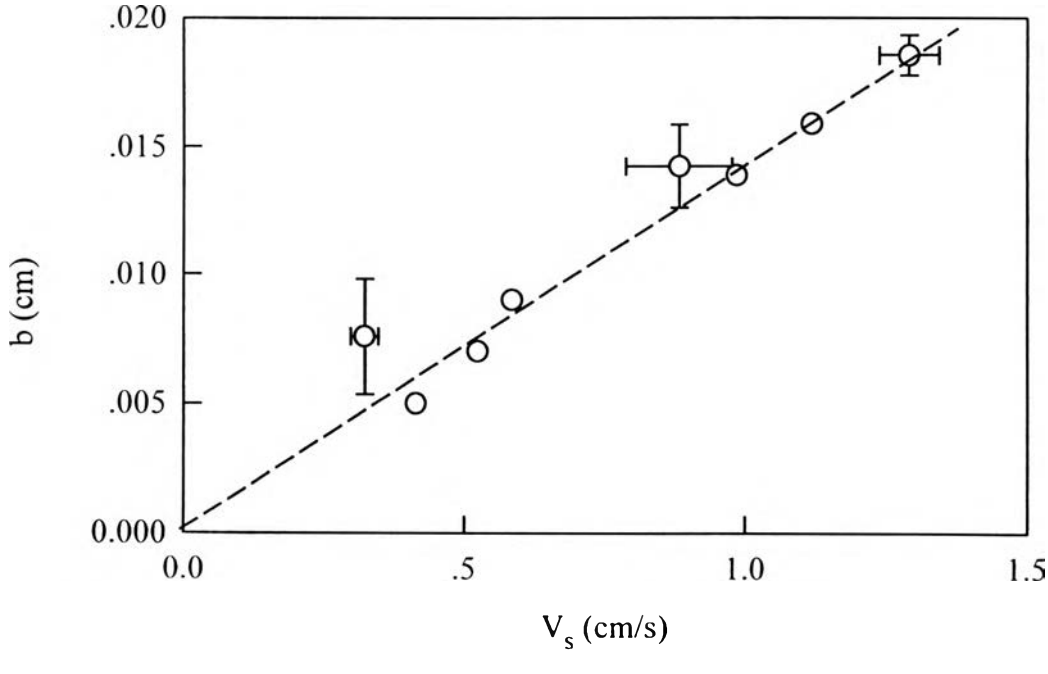

Figure 3.92 The extrapolation length, b, as a function of the slip velocity, V_S, at temperature of 190 ^oC for LLDPE (L2020F).

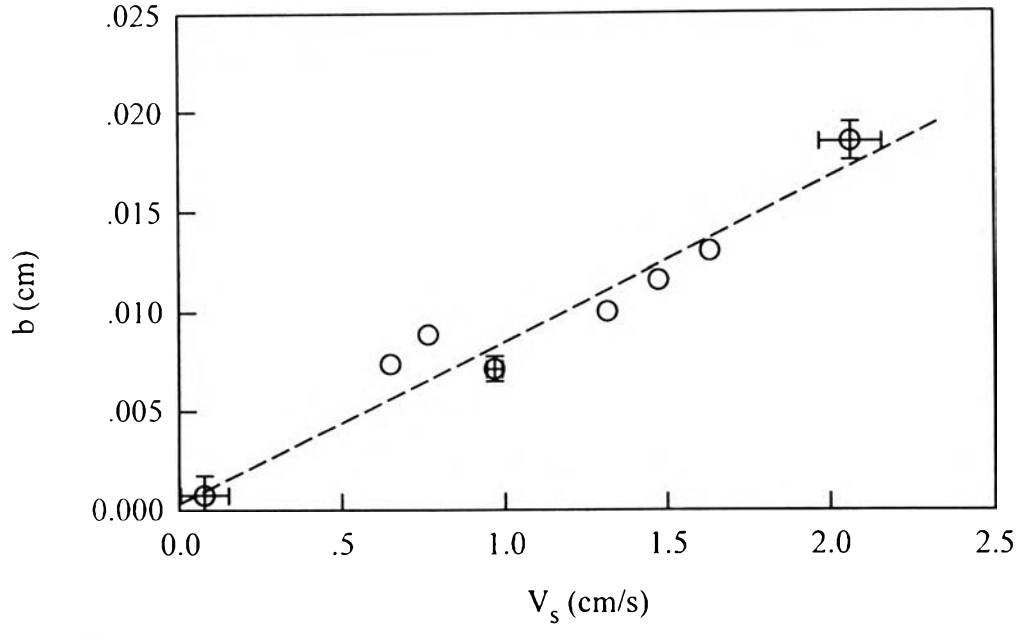

Figure 3.93 The extrapolation length, b, as a function of the slip velocity, V_S, at temperature of 190 ^oC for LLDPE (M3204RU).

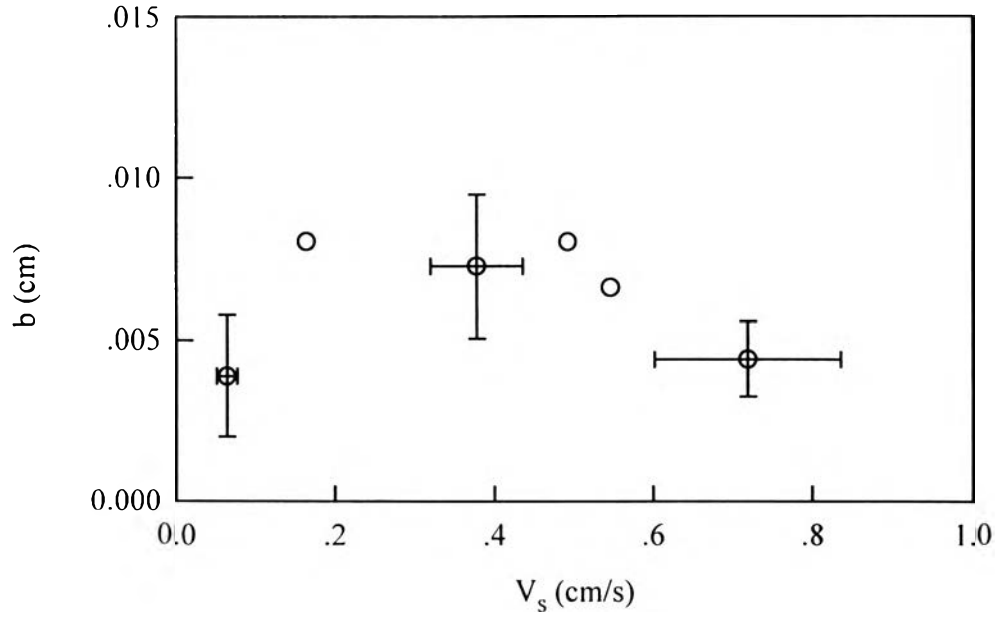

Figure 3.94 The extrapolation length, b, as a function of the slip velocity, V_S, at temperature of 190 ^oC for HDPE (H5604F).

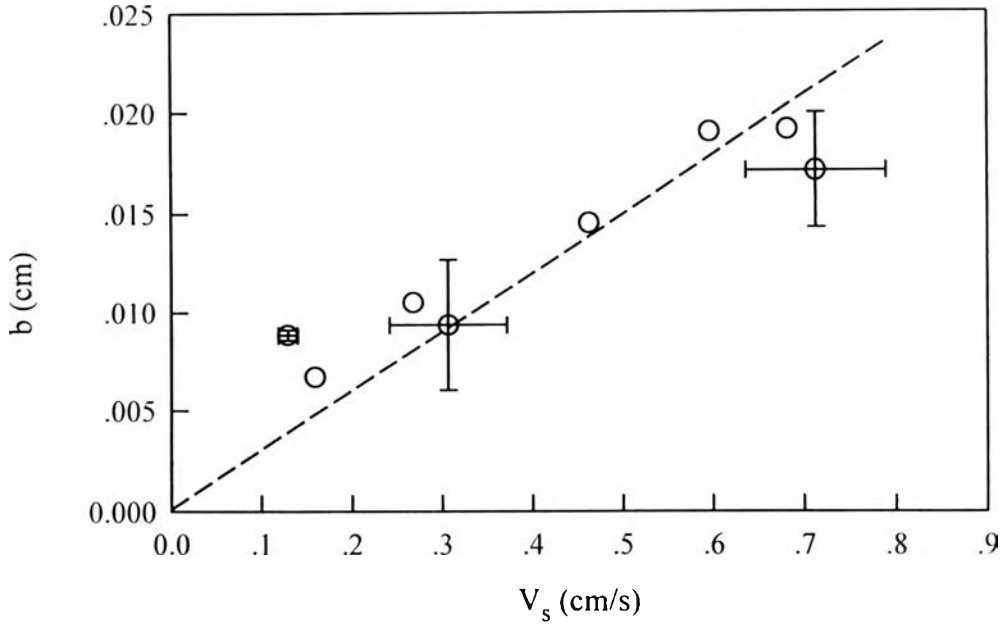

Figure 3.95 The extrapolation length, b, as a function of the slip velocity, V_S, at temperature of 190 ^oC for HDPE (H5690S).

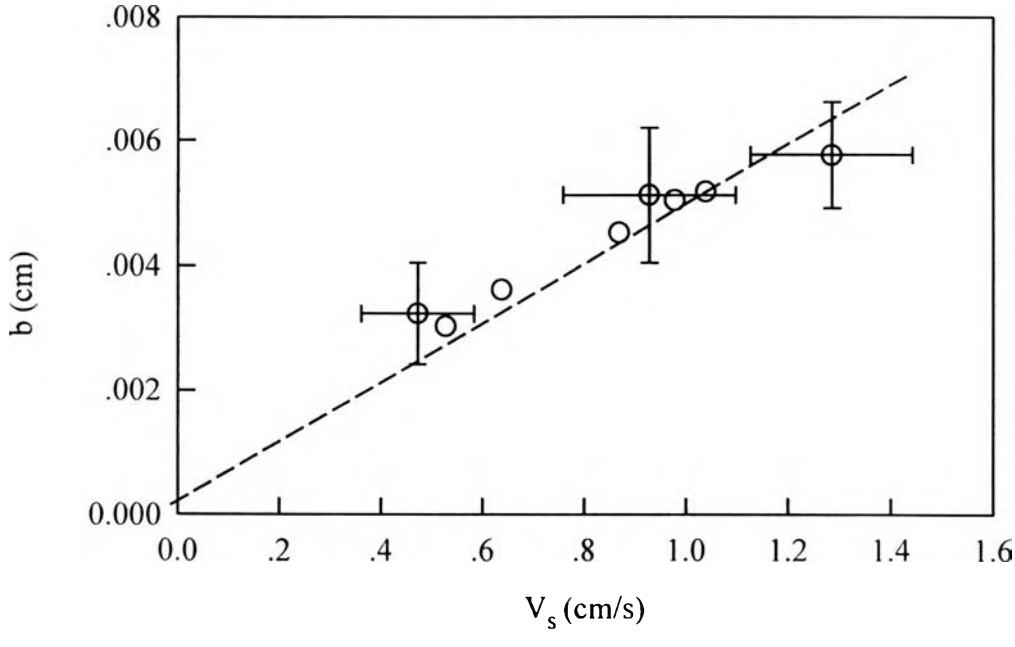

Figure 3.96 The extrapolation length, b, as a function of the slip velocity, V_S, at temperature of 190 ^oC for HDPE (H6205JU).

Table 3.5.2 The values of the parameter C for LLDPE and HDPE of different molecular weights.

Materials	M_W (g/mol)	Parameter C
L2009F	87,000	0.031
L2020F	60,700	0.016
M3204RU	33,000	0.007
H5690S	18,000	0.030
H6205JU	10,700	0.005

3.6 Scaling

Brochard and de Gennes (1992) predicted the extrapolation length in the marginal regime to be

$$b = CV_s . \qquad (3.2)$$

The parameter C was predicted to be

$$C = \eta / \tau^* , \qquad (3.3)$$

where η is the viscosity and τ^* is the wall shear stress at the onset of slip.

3.6.1 Effect of Temperature

Figures 3.97 and 3.98 show the extrapolation length, b, vs. $(\eta_o' V_s)/\tau^*$ for LLDPE (L2020F) melts and HDPE (H5690S) melts at temperatures between 170-230 °C. From these figures, we found that the data of b vs.V_S in Figures 3.17-3.20 and Figures 3.22-3.24 can be brought into a single straight line as in Equation 3.2, as suggested by Brochard and de Gennes (1992). However, our results do not agree with the results of studied of the slip

transition at the polymer-solid interface by Migler (1993); he found that the extrapolation length, b α V_S^n where the exponent n was 0.87 ± 0.05. The discrepency between the present results and Migler result may be due to the fact that the latter study covered many orders of magnitude of b and V_S.

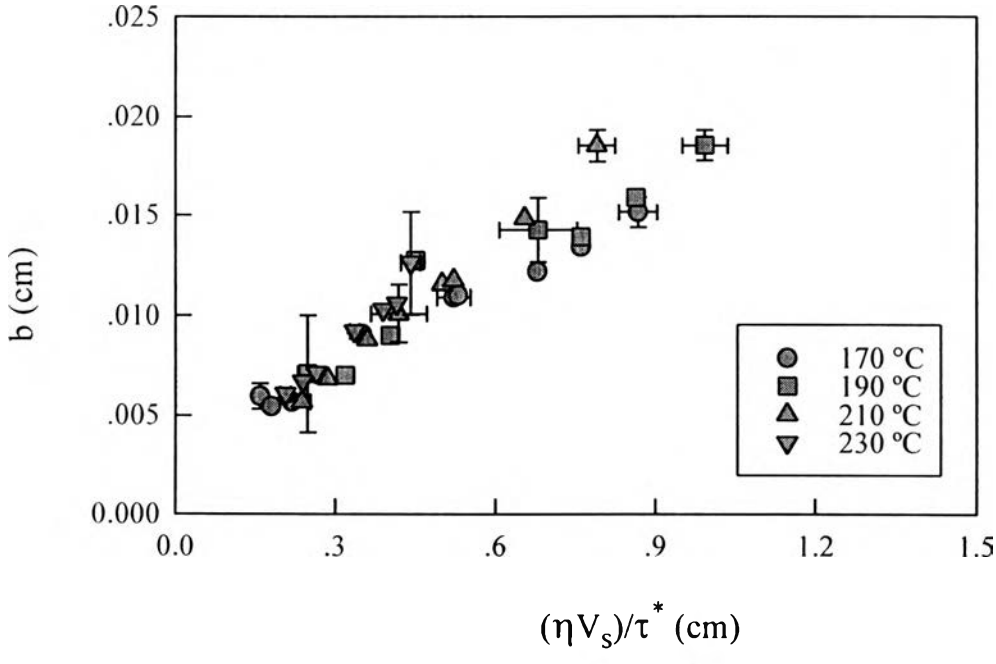

Figure 3.97 The extrapolation length, b, vs.$(\eta_o' V_s)/\tau^*$ for LLDPE (L2020F) melts at temperatures between 170-230 °C.

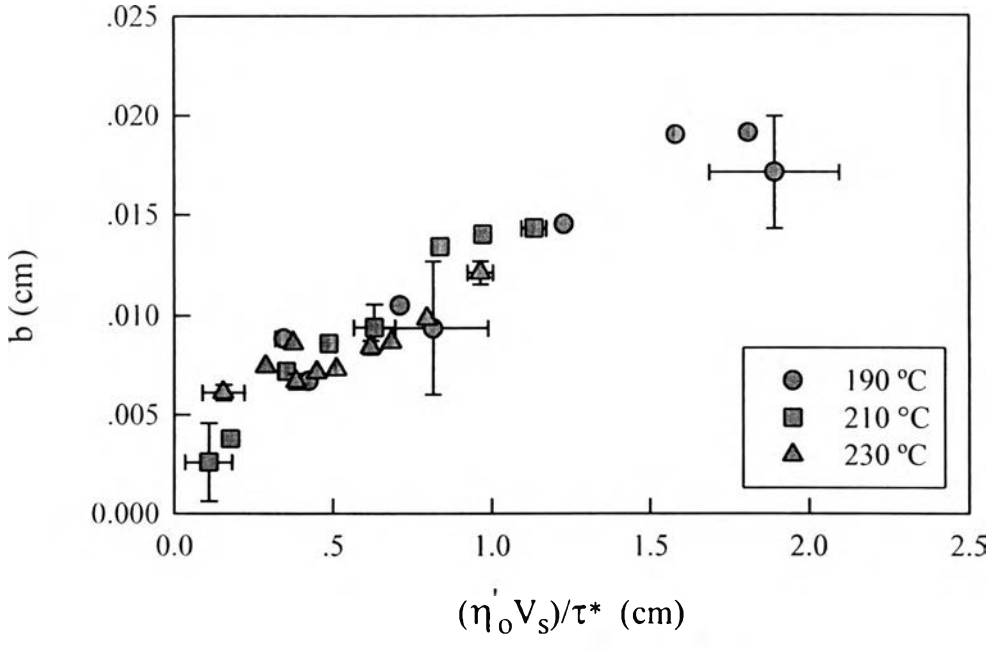

Figure 3.98 The extrapolation length, b, vs.$(\eta'_o V_s)/\tau^*$ for HDPE (H5690S) melts at temperatures between 190-230 °C.

3.6.2 Effect of Molecular Weight

Figures 3.99-3.100 show the extrapolation length, b, vs. $(\eta'_o V_s)/\tau^*$ for LLDPE (L2009F, L2020F and M3204RU) and HDPE (H5690S and H6205JU) melt at temperature of 190 °C. From these figures, we also found that b is approximately equal to $(\eta'_o V_s)/\tau^*$, as suggested in the theory of Brochard and de Gennes (1992).

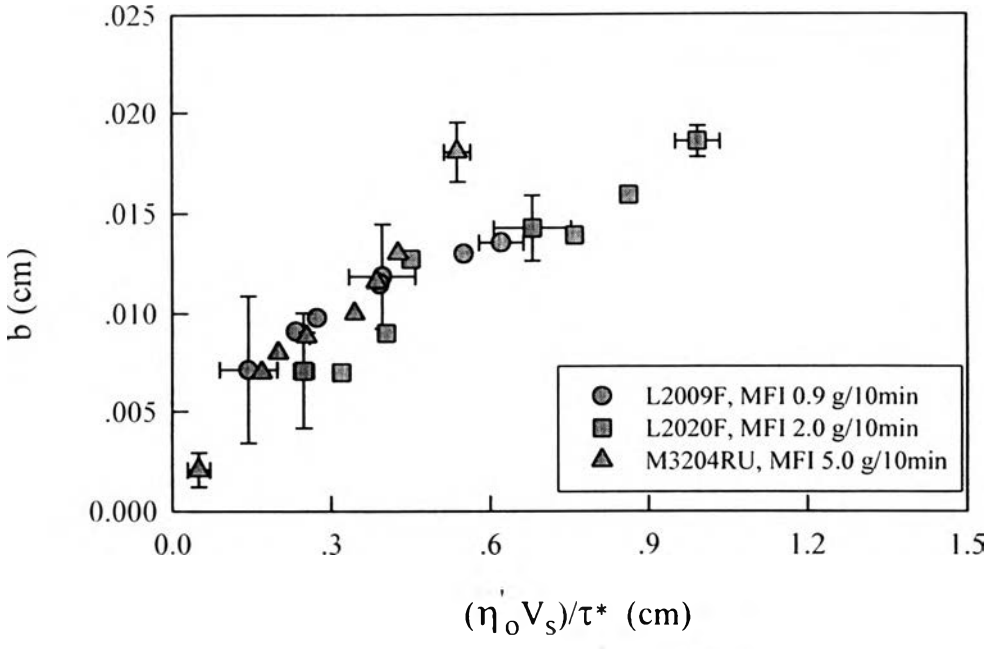

Figure 3.99 The extrapolation length, b, vs.$(\eta'_o V_s)/\tau^*$ for LLDPE (L2009F, L2020F and M3204RU) at temperature of 190 °C.

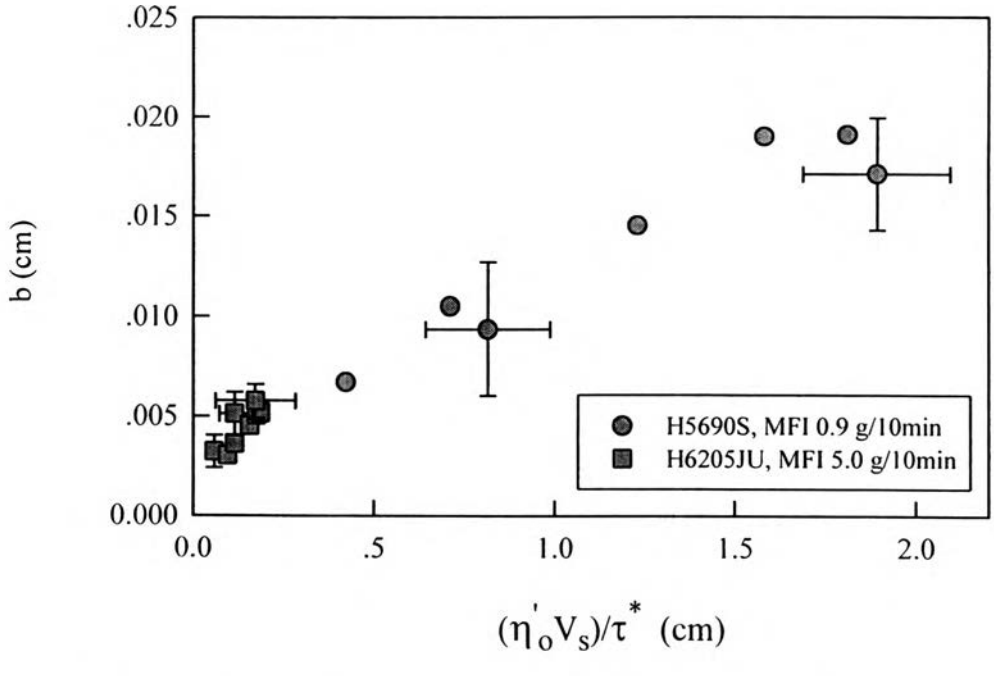

Figure 3.100 The extrapolation length, b, vs.$(\eta'_o V_s)/\tau^*$ for HDPE (H5690S and H6205JU) at temperature of 190 °C.